Development of UV Pulsed Laser Induced Breakdown using Spectroscopy (LIBS) for Assessment of Toxic elements and Plasma Parameters in Food Products

BY

HABIBULLAH YUSUF BABANAGAIRI

A Thesis Presented to the
DEANSHIP OF GRADUATE STUDIES

KING FAHD UNIVERSITY OF PETROLEUM & MINERALS

DHAHRAN, SAUDI ARABIA

In Partial Fulfillment of the
Requirements for the Degree of

MASTER OF SCIENCE

In

PHYSICS

APRIL, 2016

KING FAHD UNIVERSITY OF PETROLEUM & MINERALS

DHAHRAN- 31261, SAUDI ARABIA

DEANSHIP OF GRADUATE STUDIES

This thesis, written by **HABIBULLAH YUSUF BABANAGAIRI** Under the direction his thesis advisor and approved by his thesis committee, has been presented and accepted by the Dean of Graduate Studies, in partial fulfillment of the requirements for the degree of **MASTER OF SCIENCE IN PHYSICS.**

M. A. Gondal

Dr. M.A Gondal
(Advisor)

Dr. Fida F. Al-Adel
(Member)

Dr. Abdullah A. Al-Sunaidi
Department Chairman

Dr. Watheq Ahmed Al-Basheer
(Member)

Dr. Salam A. Zummo
Dean of Graduate Studies

12/4/16

Date

DEDICATED TO

My Parents & My Wife

ACKNOLEDGEMENT

First and foremost, I would like give my sincere gratitude to my Supervisor, professor Mohammed Ashraf Gondal for his guidance and support throughout this research work. His patience and encouragement has been very helpful in overcoming all hurdle throughout the research period. Many thanks to every member of Laser research Group, King Fahd University of petroleum and Minerals for their support and contribution in this research work. Thanks to Physics department KFUPM for providing me all I need to complete my master program.

Thank to Centre of Research Excellence in Nanotechnology (CENT) for their financial support, their support has being very helpful to me and my family here in the Kingdom. My special gratitude also goes to my thesis committee Prof Fida F. Al- Adel and Dr. Watheq Ahmed Al Basheer for their contribution toward the completion of this research work, may Almighty Allah reward them abundantly.

Finally, my most sincere thanks go to my parent, their spiritual and financial support is most appreciated, may you eat the fruit of your labor.

Table of Contents

LIST OF TABLES

LIST OF FIGURES

LIST OF ABBREVIATION

LIBS: Laser Induced Breakdown Spectroscopy

LTE: Local Thermodynamic Equilibrium

ICP: Inductively Coupled Plasma

ICP-MS: - Inductively Coupled Plasma Mass spectroscopy

GI: Gingival Index

PI: Plaque Index

CAL: Clinical Attachment Loss

PD: Pocket Depth

IUPAC: International Union of Pure and Applied Chemistry

ICP-OES: Inductively Coupled Plasma Optical Emission Spectroscopy

TRLIBS: Time Resolve Laser Induced Breakdown Spectroscopy

LAS: Laser Ablation Spectroscopy

LSS: Laser Spark spectroscopy

UV: Ultra-Violet

Nd-YAG: Neodymium Yttrium Aluminum Garnet

KBr: Potassium Bromide

LA-ICP-MS: Laser Ablation Inductively Coupled Mass Spectroscopy

ICCD: Intensified Coupled Charged Device

NIST: National Institute of Standard and Technology

eV: Electron Volt

LIP: Laser induced plasma

ppm : Part Per Million

LOD: Limit of Detection

AAS: Atomic Absorption Spectrometry

HPLC: High-Performance Liquid Chromatography

HPCE: High-Performance Capillary Electrophoresis

PMT: Photomultiplier Tube

RF: Radio Frequency

NAA: Neutron Activation Analysis

SFDA: Saudi Food and Drug Authority

ABSTRACT

Full Name : Habibullah Yusuf. B

Thesis Title : Development of UV Pulsed Laser Induced Breakdown using Spectroscopy (LIBS) for Assessment of Toxic elements and Plasma Parameters in Food Products.

Major Field : Physics

Date of Degree : April 2016

In this study, we assembled a highly sensitive Laser Induced breakdown spectrometer for the detection of nutritional and toxic elements in commercially available food products which are often consumed by the population around the world and most especially in the kingdom of Saudi Arabia. Some of the toxic element are highly carcinogenic and life threatening even at low concentrations causing dangerous diseases. In light of this, there is an increase in demand to device a suitable and effective technique to detect and quantify the level of nutritional and toxic

elements in them. Laser Induced Breakdown spectroscopy (LIBS) were used for spectroscopic analysis of tea, cigarette, smokers & non-smoker's teeth, and date fruit. The LIBS sensitivity was improved by finding the LIBS signal intensity dependence on time delay and laser fluence under ambient conditions. Plasma parameters such as electron temperature T_e and electron number density N_e were estimated for the different samples using Boltzmann plot and Stark broadening profile respectively. With the aid of estimated plasma parameters we were able to validate if our plasma was in local thermodynamic equilibrium (LTE). For tea analysis, LIBS spectra for six brands of tea samples in the wavelength range of 200-900 nm region was recorded and all elements present in Tea were identified as well their spectral transition assignment was also conducted. Prior to determination of concentration, calibration curves were drawn for each element using standard samples prepared in known concentration in the tea matrix. The concentrations of iron, chromium, potassium and bromine detected in all tea samples were between 378-656, 96-124, 1421-6785 and 99-1476 ppm, respectively. To further confirm the accuracy of our LIBS results, we determined the concentration of each element present in tea samples by using standard analytical technique like ICP-MS. The concentrations detected with our LIBS system are in excellent agreement with ICP-MS results. In order to achieve the high sensitivity required for the determination of trace amounts of fluoride in cigarettes and eventually the best limit of detection, the experimental parameters (influence of incident laser energy on libs signal intensity and time response of plasma emission) were optimized. In

addition, the plasma parameters like electron temperature and electron density were evaluated using Boltzman's plot for cigarettes tobacco for the first time. Along with the detection of flourine, other trace metals like Ba, Ca, Ni, Cu and Na were also detected in cigarettes. The concentration of fluorine in different cigarettes tobacco samples was 234 ppm, 317ppm, 341 ppm and 360 ppm respectively, which is considered to be much higher than the safe permissible limits. As for the detection of toxic elements in smokers and non-smokers's teeth, LIBS was assembled and optimized to detect the level of toxic elements such as lead, cadmium and arsenic present in the roots of extracted teeth of smokers and nonsmokers. The Pb, Cd and As concentrations in smoker group were 34 - 55, 0.33 - 0.51 and 0.91-1.5 ppm respectively, compared to the same for non-smoker group, which was 23 - 29, 0.26 – 0. 31, and 0.64 - 11 ppm range and 0.17- 0.31, 0.01- 0.05 and 0.05 -0.09 ppm range for control group. In order to substantiate the LIBS results standard Inductively Coupled Plasma (ICP) was carried out and found to be in good agreement with LIBS data.

ملخص الرسالة

في هذا العمل البحثي طورنا مقياس طيفي للتكسير بالليزر حساس للغاية للكشف عن العناصر السامة في المنتجات الغذائية المتاحة تجاريًا في جميع أنحاء العالم وعلى وجه الخصوص في المملكة العربية السعودية. بعض العناصر السامة تسبب أمراض خطيرة وتعتبر مسرطن للغاية ومهددة للحياة حتى عند تركيزات منخفضة. على ضوء ما تم ذكره، هناك حاجة ماسة لتقنية مناسبة وفعالة لكشف وتحديد مستوى العناصر السامة في المنتجات الغذائية.تم تطبيق مطياف التكسير بالليزر على الشاي، والسجائر، التمور واسنان المدخنين وغير المدخنين لتحديد مستوى العناصر السامة.

تم تطوير حساسية مطياف التكسير بالليزر عن طريق دراسة العلاقة بين شدة الطيف وكلا من زمن التاخير و فيض الشعاع الليزري في الظروف المحيطة. بمعرفة معلمات البلازما مثل درجة الحرارة وكثافة الإلكترونات للعينات المختلفة تم التحقق من حالة التوازن الحراري للبلازما.

تم تحليل ست اطياف لست علامات تجارية من عينات الشاي في نطاق الطول الموجي من 200-900 نانومتر باستخدام منحنيات المعايرة لكل عنصر لعينات شاي قياسية. كانت تركيزات الحديد والكروم والبوتاسيوم والبرومين في جميع عينات الشاي بين 378-656، 96-124، 1421-6785 و99-1476 جزء في المليون، على التوالي. لمزيد من تأكيد دقة نتائج تحليل عينات الشاي تم استخدام تقنية تحليلية قياسية مثل ICP-MS والتي اظهرت نفس النتائج.

باستخدام مطياف التكسير بالليزر تم الكشف عن وجود الفلور، الكالسيوم، النيكل، النحاس والصوديوم في السجائر. كان تركيز الفلور في اربع عينات سجائر مختلفة هى 234 جزء في المليون، 317 جزء في المليون و 341 جزء في المليون و 360 جزء في المليون على التوالي، والذي يعتبر أعلى بكثير من الحد الامن المسموح به. استخدم مطياف التكسير بالليزر للكشف عن مستوى العناصر السامة مثل الرصاص والكادميوم والزرنيخ الموجودة في جذور الأسنان المستخرجة من المدخنين وغير المدخنين. كانت تركيزات الرصاص،الكادميوم والزرنيخ في مجموعة المدخن 34-55، 0.33-0.51 و0.91-1.5 جزء في المليون على التوالي، مقارنة مع مجموعة غير المدخن، والتي كانت 23 - 29، 0.26 - 0. 31، و0.64 - 11 جزء في

المليون. كانت تركيزات هذه العناصر في مجموعة المراقبة كالتالي 0.17- 0.31، 0.01- 0.05 و 0.05 -0.09 جزء في المليون. من أجل التاكد من دقة النتائج تم استخدام تقنية حث البلازما المزدوج (ICP) والتي اظهرت نفس النتائج.

CHAPTER ONE

INTRODUCTION

1.1 Laser Induced Breakdown Spectroscopy (LIBS)

Laser induced breakdown spectroscopy (LIBS) is an optical diagnostic technique that has gained a tremendous success and popularity in analysis of various materials such as solid, liquid and gas. This analytical method has being developing over last decade. This technique provides a multi-elemental analysis that is helpful for quick measurement of small amount of analyte (< ng). This technique involves low energy laser focused on target with the aid of a lens having an appropriate focal length, whereby small amount of analyte is ablated from the target with the generated plasma. Plasma are generated when laser pulse interact with solid target. The light emitted by ionic and atomic species in the plasma emission was collected by an optical fiber supported by miniature lens placed at angle with respect to the normal of the test sample, a high resolution 500mm spectrograph (Andor SR 500i-A) with grating groove density of 1200 lines / mm was used to collect the generated LIBS signal from the fibre optics. Ablation of our target material is said to occur when the power of the laser irradiance is more than the breakdown threshold of the material target. The ablated material is in form of free electron, particles, atoms, ionized atoms, which expands at the rate of supersonic speed forming shock waves in the surrounding atmosphere. After several microsecond, the plasma plume slows down through collision with the species in surrounding ambient gas, then the shock waves separates itself from the plasma front, and continues propagating at a speed approximately the speed of sound. The electron number density varies in order ranging from 10^{15} to 10^{19} and electron temperature ranging from 10^{4} to 10^{5} K [1,2]. The origin of LIBS information comes from the evolution of material ejected by surface of the target. The main idea of LIBS is that by exciting and vaporizing with intense laser pulse on absorbing material (solid, liquid and gas), one can use the

resulting emission spectra to infer the composition and relative concentration of its constituent elements present in the specimen. This is why the name Laser induced breakdown spectroscopy or Laser induced plasma spectroscopy is given to the technique. The core aim of LIBS technique is to search for an optimum plasma conditions for the deduction of quantitative analytical characterization of a test sample in suitable environment [3-7].

In order to determine the concentration of any element present in the test sample, calibration curves are usually drawn. The slope of such curve tells us the sensitivity of our method according to IUPAC (International Union of Pure and Applied Chemistry) definition. Other conventional methods such as inductively coupled plasma optical emission spectroscopy (ICP-OES), ICP- Mass spectroscopy (ICP-MS) and ion chromatography have highly acceptable analytical performance, but the only disadvantages in their sample preparation are the time consuming pretreatment procedure which require the use of acid digestion under high temperature and pressure, also the usage and disposal of hazardous chemical which are detrimental to our environment. In contrast, with LIBS all these disadvantages are overcome due to its simplicity, rapidness, versatility, flexibility of its experimental set up and capability of multi-elemental analysis with little or no sample preparation. All state of matter can be analyzed, be it conductive or non-conductive. It is also capable of remote analysis in harsh surroundings. Due to this uniqueness, LIBS have been applied for both quantitative and qualitative analysis in areas such space exploration,[8,9] medical and forensic field,[10-13]industrial application ,[14] and cultural heritage [12,15,16].

1.2 LIBS THEORY

1.2.1 Introduction

LIBS is an atomic emission spectroscopy technique which can provoke sample excitation with its highly energetic laser pulse. LIBS can provide a fast and easy multi-elemental analysis of samples in solid, liquid and gas with a reasonable precision, limit of detection and cost. Other acronyms for this analytical technique are Time resolve laser induced breakdown spectroscopy (TRLIBS), Laser Ablation Spectroscopy (LAS), Laser Induced plasma Spectroscopy (LIPS) and Laser Spark spectroscopy (LSS). The interaction between laser and mater are govern by laws of quantum mechanics explaining how photons are emitted or absorbed by atoms. For instance when an electron captures an photon, the electron excites to higher energy quantum mechanical state. Since electron prefers to be lower energy level, the electron de-excite by emitting a photon. The LIBS spectral emission lines are as a results of the emissions coming from de-excitation of atoms with well-known associated energy levels for each atoms [17]. An excitation source is needed to excite and produce the needed free atoms from the target. The fundamental of LIBS system is the recording of the plasma spectrum that contain all the qualitative and quantitative analytical information about the elemental composition and identification of the sample material, by using the finger print wavelengths, spectral intensities and relative intensities of the analyte. [18,19]

1.2.2 Main principles of LIBS

When laser energy applied to an atom is higher than its ionization potential, the ionization potential is overcome, electron and positive ions are detached from the atom[20]. Firstly, the external electron (the furthest from the nucleus) is first detached because it has the smallest ionization potential, but when the energy supplied is increased, it is possible to overcome inner

electron with second ionization potential, the third ionization potential and so on[21,22]. The emitted ions can also emit photons during recombination process in a process called free-bound transition or through de-excitation process when cation and electron lose energy due to kinetic energy in a process called free-free transition. This emission is usually a continuum coming from the fact that the ions are having different energies and energy transitions, while on the other hand, the de-excitation of cations has a discrete set of energy levels with characteristics emissions lines for each types of species, which allows its easy identification.

When plasma is irradiated on sample, interaction occurs between pulsed laser and sample, leading to emission of light consisting of discrete lines, bands, and an overlying continuum. The discrete lines which characterize the material are being identified with three main features namely, wavelength, intensity and shape. For average plasma densities, the natural broadening is due to Heisenberg's uncertainty principle and Doppler broadening is due to thermal motion. Each particle emit light which can be slightly red or blue shifted resulting into broadening that dominate the linear shape. For highly dense plasma, atom in the plasma are affected by electric fields due to electron moving very fast and slow moving ions, causing the electric field to split and shifting atomic energy levels. Due to the consequences of these perturbation of atomic energy level, the emission lines are broadened, thereby changing intensity and shape. This effect often dominate the emission line of a dense plasma and is known as stark effects[23]. The broadening, continuum radiation features, spectral line intensity and shapes are different parameters used in estimating plasma parameters such as electron temperature, electron density and pressure [24,25].

1.2.3 Development of LIBS for Analytical Analysis

LIBS technique, since its introduction has been applied for analysis of different material in solid, liquid, and gaseous state. Over the past four Decades, there has been remarkable increase in the use and development of LIBS. This is due to the several attractive features in LIBS. One of most attractive features is that it only needs optical access to a sample, this allow LIBS to be applied for remote sensing and process monitoring. This one of the unique features which distinguish it from other conventional plasma emission spectroscopy, where sample needs to be transferred to a plasma source. In LIBS plasma is formed within the sample or at the surface of the sample. Taking a look at LIBS technique from the spectrochemical analysis point of view, another feature of the technique is that it provide multi- elemental analysis with minimal or no sample preparation. LIBS can analyze all states of matter, be it conductive or non-conductive. It can also easy analyze refractory material such ceramics. Micro-analysis is achievable in LIBS with spatial resolution of 1-10 μm regardless of harshness of the environment. However, there are some setbacks that are yet to be overcome in this technique, some of the problems are variable amount of mass ablates leading to inconsistency in elemental quantification of heterogeneous sample, poor precision between 5-10 %, self-absorption, difficulty in making matrix matching, and spectral interference. The reason for the complexity is due to large number variable that affect the ablation process. These variables are pressure coming from the surrounding environment [26,27], laser wavelength[28-30], chemical and physical properties of targeted species[31][32] [31-33], laser energy [34-36], laser pulse temporal duration & shape[27] and effect of magnetic field[37,38].

1.2.4 LIBS and its laser configuration

There are many devices that made up LIBS system, but the main device is laser. The laser is meant to generate energy that induce plasma and determines the plasma features. The most important parameters related to laser are energy per pulse, the wavelength, pulse time, the number of pulses per burst. Application of LIBS is based on combination of all these parameters. The most common laser used for is nanosecond-pulsed laser.

Laser wavelength has influence on LIBS, such influence can be explained from two different point of views: laser-material interaction and plasma properties and development (plasma-matter interaction). When photon energy exceed the bond energy, photon ionization occurs. Due to this reason, plasma behavior is a function of wavelength in a nanoseconds LIBS set-up. Optical penetration is short length in Ultra-Violet (UV) laser, leading to higher laser energy per unit per unit volume of materials. Generally, shorter laser wavelength (i.e. 157 and 266 nm) usually have higher ablation rate and lower elemental fractionation as compared to other (i.e. 532 and 1064 nm)[39].

The ignition of plasma and its properties is a function of its wavelength. The initiation of plasma with nanosecond laser is achieved by two processes; the first is inverse bremsstrahlung in which free electrons gain energy from the laser during the process of atoms and ions collision. The second is the excitation of ground atom with very high energy and photoionization of excited species. Coupling of laser is better with shorter wavelength, but the threshold for formation of plasma is higher, this is due to the fact that bremsstrahlung is more favorable in infra-red region[40].

On the other hand, short wavelength (between 157 and 266 nm) the photoionization process is more significant. In light of this, the shorter the wavelength, the lower the energy per area

(fluence) needed to initiate ablation process[41]. Additionally, after the occurrence of inverse Bremsstrahlung, some part of nanosecond laser beam reheats the plasma, thereby increasing the plasma lifetime and intensity but increasing the background simultaneously. Longer wavelength increases the shielding of inverse bremsstrahlung but it reduces the rate of ablation and increases elemental fractionation (elemental fractionation is the redistribution of elements between solid and liquid phases which modifies plasma emission)[42].

The commonest laser used for LIBS is pulsed Nd:YAG [43]. This type of laser gives a compact, easy and reliable way to generate plasma in LIBS experiments. The fundamental mode of pulsed Nd: YAG laser is 1064 and its pulsed width is between 6 and 15 ns. This laser has the ability to provide harmonics at 532, 355, and 266 nm. They are less powerful and have shorter time pulse between 4 and 8 ns [44,45]. Other types of laser used for LIBS are CO_2 or excimer laser which in IR or UV wavelength region respectively.

Laser energy parameters that have to do with laser-material interaction are laser irradiance (energy per unit area and time, W/cm^2) and laser fluence (energy per unit area per unit time). The processes of ablation such as melting, sublimation, erosion, and explosion and so on, have different fluence thresholds[46]. The effect in change of energy has a relationship with laser wavelength and pulse time. This is why it is difficult to analyze the effect energy alone. In general, the rate ablation and ablated masses increases with increase in laser energy. The typical fluence threshold for solids. Liquids, and aerosol is 10^{10} W/cm^2 and 10^{11} W/cm^2 for gasses[44].

Acquisition time and time delay are also very important parameters to be discussed. The first stage of LIBS-induced plasma is dominated by continuum emission[47]. This is because background signal delays at a faster rate than the emission signal. The gate time delay of this continuum radiation is susceptible to change with some range experimental parameters such as

pulse time, laser wavelength, sample features and ambient pressure. Laser wavelength can influence the time delay and integration time (gate window), of which both parameters are necessary for the optimization of signal to background ratio. In LIBS when the sample is excited with a high power pulsed laser source of high fluence, a plasma plume predominantly consists of electrons, and atomic and molecular ions of multiple ionization species are generated. This multi-component plasma undergoes a temporal evolution, where in one of the channels, the ionized atomic species undergo the recombination with electrons and become neutral atoms and further comes down to the ground state by emitting the characteristic line spectrum. There are different approaches to optimize delay time, this is as a result of different experimental parameters involved in plasma evolution, which makes it difficult to recommend a particular delay time for an experimental set-up. The optimum delay time should be determined case by case in order to achieve a compromise between high line intensity and low background. For Nd: YAG laser both time delay and gate window are in order of microseconds[47].

1.2.5 Relationship between laser plasma and properties of material target.

The size and shape of laser induced plasma plume is a function of physical, mechanical and thermal properties of the material target. The ablated mass from the target does not only depends on the laser intensity but also the target material properties. The relationship between ablated mass m(t) and heat conduction mechanism is as given in the equation.

$$m(t) = A(aIt) + B(AI)^2 \tau^{3/2} \qquad (1)$$

Where a is the energy coupling factor, A and B are proportional to the material target thermal properties, τ is the laser pulse duration and I is the laser Intensity. In order for plasma to be formed, the laser fluence must exceed a threshold value usually of the order of several Jcm^{-2} for nanosecond laser pulses. The first step in plasma formation is the vaporization of the material

target and vaporization occurs when the energy deposited on sample exceed the latent heat of vaporization of the target $L_{v.}$ The threshold fluence (F_{th}) below which no evaporation will occur is given by

$$F_{th} = \rho l_v a^{1/2} w^{1/2}, a = K / \rho C_p \quad (2)$$

Where ρ the density of sample, Lv is the latent heat of vaporization of the material target, a is the thermal diffusivity, w is the laser pulse width, C_p is the specific heat per unit mass and K is the thermal conductivity. It is worth mentioning that the threshold fluence for laser induced breakdown of hard tissue (teeth or Bone) is lower than that of soft tissue ablation, and the effect is dependent on the pulse duration. Physical and mechanical properties of a target has some effect on the size and shape of the crater formed on its surface and consequently on the size and shape of the plasma plume. A reflecting surface absorbs laser energy effectively due to change of material at high temperature, of which this is possible only at high laser intensity. The reflectivity of sample surface, specific heat, density, boiling temperature influences the shape and size of the craters and is given by the following relation [34]

$$D = A(1-R) \Big/ \rho C_p T_b \quad (3)$$

Where D is the crater diameter, R is the reflectivity of the surface, A is the proportionality constant, and T_b is the boiling temperature.

1.2.6 Geometry of Set-up

The geometry of plasma and spatial emission intensity profile are largely a dependent on the density of laser power, optical alignment for laser focusing, and emission collection from plasma plume for spectrum acquisition. Hence, it is quite important to understand the LIBS signal

dependence on the optical alignment and the collection of emission for the recording of spectrum. A lot of effort has been put forth in an attempt to compare the effectiveness of spherical and cylindrical lens by focusing a laser pulse on soil sample, it was found that cylindrical lens showed a more precise results. In the case of LIBS analysis of solids sample, laser pulse is usually focused perpendicular to the target surface[48]. The high intensity laser often produce a breakdown in air before the focus at the surface, with dust particles been irradiated occasionally. This problem can be contained by setting a suitable distance between focusing lens and the target, such that it is shorter than the focal length and consequently producing a stable breakdown [49,50]. The collection plasma emission and detection is normally performed along the direction normal to the target surface due to it reproducibility and simplicity. There are other certain types of changes, which are occur in plasma emission, i.e those produced by time evolution of the plasma plume as the plasma plume evolution is govern by strong explosion law. Assuming a one-dimensional model, where the plasma expansion is along x-direction and the surface target is at x = 0, the distance x (t) reached at time t is given by

$$x(t) = K\left(\frac{E_l}{\rho_o}\right)^{m/2} t^m \qquad (4)$$

Where E_L is the deposited energy by the laser during ablation process, ρ is the ambient gas density. The coefficient m depends on plasma expansion geometry which is equal to 2/3 for planar propagation and 2/5 spherical symmetry. Eq. (4) Indicates that the plasma is moving fast at the initial stage, and slows down at a later time. One of the important technique in collecting emission from plasma plume is placing optical fiber near the plume, at a distance of a few millimeters, this is to avoid damage from excessive heating. The placing of optical fiber at angle allows the gathering of light from broad volume of plasma plume. Various configuration had

been proposed, one of it is the use of two optical fibers, where one is for delivering laser beam, and one for collecting the plasma plume emission, the other configuration is the use of single fiber for both purposes. After optimization of different LIBS parameters, nearly similar limit of detection was achieved for both cases from spectral emission of some elements[51].

1.2.7 Laser ablation

Laser Ablation has been studied extensively for over 50 years, since laser discovery. Laser ablation is defined as the removal of material from a target material by direct absorption of laser energy. Plasma is said to occur, when high powered pulsed laser is focused on a target such that the applied energy density superseded the ablation threshold of the material. This is because the thermal properties and constants no longer play a major role. The physics between laser-plasma generation and subsequent evolution is very complex, which involves processes like heating, melting, vaporization, ejection of particles, and plasma creation and expansion. The laser ablation crater and plasma produced are dependent on laser beam parameter such as wavelength, energy, pulse duration, target properties and surrounding conditions. Two of the well-known analytical applications of laser ablation, are LIBS and laser ablation inductively coupled mass spectroscopy (LA-ICP-MS). In LIBS high laser power is used to for ablation, typically of nanosecond (ns) Q-switched lasers, and the resulting light emission is collected and dispersed using spectrograph. The detection is done using either time-integrated CCD or intensified CCD (ICCD). LA-ICP-MS is a technique where the ablated mass is analyzed for isotope detection. For long pulsed ns laser ablation, the dissipation of absorption energy in target material and material removal take place during laser pulsed duration. Important phenomena in ablation are minimum power density to start vaporization, the effect of long or shorter pulsed length, the rate

at which the ablation proceeds, and the goal of retaining the composition of the sample after the plasma ablation. The minimum laser power density required to produce vaporization is given by

$$I_{\min} = \left(\frac{L_v \rho \kappa^{1/2}}{\triangle t^{1/2}} \right) w / cm^2 \qquad (5)$$

Where, L_v is the latent heat of vaporization, ρ is the density of target material, κ is the thermal diffusivity of the target, and $\triangle t^{1/2}$ is laser pulsed length [9,56,57]. Material ablated by plasma can take form of particle, atom, and molecules, this is due to different volatilities of elements and their compounds.

1.2.8 Influence of binding materials on Laser – solid interaction.

Binding materials is of great importance in LIBS sample preparation. Most of sample are been prepared for bulk analysis and hence there is need for proper processing to obtain compact target prior to analysis using LIBS technique[35]. The process of making and binding sample into a specific shape is called palletization. The sample is expected to have strong mechanical strength for LIBS analysis, this is because of the high power pulsed laser beam interacts with the sample, which make the sample crumble into original particulate material. For a homogeneous target sample preparation, it is mandatory for this sample to be processed into homogeneous pellet, by first grinding the sample into extremely fine powder, then palletization using proper binding material[47,39]. In order to attain higher sensitivity and accuracy with LIBS system, appropriate binding material should be selected. This can be achieved by thorough mixing of actual powdery material with suitable powder. The common suitable binding material are Al, Ag, Potassium bromide (KBr), and starch. One of the most important parameters of binding material is called bond strength, which is the measure of strength between particle that bind a sample together and

ablation resist. Also, the uniformity of particle bond strength throughout the pallet is quite necessary for accurate analysis of different LIBS samples [52,53]. M. A. Gondal et al studied various binding material using LIBS system, it was found that Potassium bromide was better as a binder for LIBS study of powder samples[54].

1.2.9 Influence of ambient condition on LIBS plasma

The size and shape of plasma depends on the ambient conditions such as background gas, presence of particles, pressure and humidity. Yalcin et al investigated the sensitivity of laser spark produced by Nd: YAG laser to ambient condition such as variation in humidity, background gas, and presence of particles. It was found that the electron temperature and electron number density of the plasma remains constant with the variation in ambient conditions [55]. Usually the emission intensity of plasma rises with increment in pressure, this is as a result of confinement of the plasma plume which produces a hotter and denser plasma.

However at moderate pressure ($50 < p < 500$ torr in air), the effect of absorption become notable due to increase in the concentration of the absorbing species around the hot plasma, making it thin and expanding rapidly, and consequently decreasing the emission intensity.

1.2.10 Qualitative Analysis

The main goal of LIBS is to achieve chemical analysis at atomic level, either qualitatively (i.e to assess the presence of a particular element) or quantitatively. Quantitative analysis of constituent element of a sample by LIBS is simply the spectroscopic identification of persistent, strong and weak emission lines from a LIBS spectrum. There are lot of data base where finger print wavelength and relative intensity chemical elements are been identified, but the common and

more acceptable is National institute of Standard and technology (NIST). If the composition of a sample is known appropriately, the set up can turned to an optimal spectral range, where there are expected emission lines of the element of interest, of which any other unexpected lines can be discarded. Persistent, strong, and weak emission lines are all compiled in NIST data base for more than 100 elements, using various atomic emission line spectroscopy references. The recommended wavelength resolution are 0.03 to 0.2 nm for identification of emission line.

1.2.11 Plasma Opacity

Plasma is a local assembly of electron, atoms, and ions overly electrically neutral. They are characterized by a number of parameters but the most basic is the degree of ionization. There are three stages in plasma life time. The first one is the ignition process, which include bond breaking and plasma shielding during the in the process of laser pulse, this depends on the irradiance, laser type and pulsed duration. The next step is critical optimization of LIBS spectra collection because the plasma causes atomic emission during the cooling process. After ignition process, the plasma will continue expanding and cooling, during which simultaneously the electron temperature and electron density will change. The last stage in plasma life is not favorable to LIBS measurements. A quantity of ablated mass is not excited as in the case of vapor and plasma, therefore this quantity of material is ablated as particles, and such particles create condensed vapor, sample ejection, liquid, and solid sample exfoliation, which unfortunately are shot of emitted radiation. During the temporal evolution of plasma, the spectral lines of LIBS spectrum are observed to be superimposed on the continuum (background) however it decays faster than the spectral lines. Since the core motive for LIBS is to produce an optically thin plasma in local thermodynamic equilibrium with composition the same as the

sample. Plasma is said to be optically thin when the emitted light traverses and escapes from significant absorption or scattering. The intensity of radiation emitted by plasma is given by

$$I(\lambda) = \left(\frac{\varepsilon(\lambda)}{\alpha(\lambda)} \right) \left(1 - \exp[1 - \alpha(\lambda) L]\right) \tag{6}$$

Where $\varepsilon(\lambda)$ is the emissivity, $\alpha(\lambda)$ is the absorption coefficient in cm^{-1}, L is the plasma length along the line sight of the observer. Where α is small, because it is the condition to have an optically thin plasma, then Eq. (6) can the written as

$$I(\lambda) = \left(\frac{\varepsilon(\lambda)}{\alpha(\lambda)} \right) \left(\alpha(\lambda) L]\right) \sim \varepsilon(\lambda) L \tag{7}$$

Different test have been developed to ascertain if thermodynamic equilibrium exist in the plasma. One of the easiest way is to confirm it, is to determine the relative intensities of atomic spectral lines from closely spaced upper level in the same multiplet agrees with the prediction from basic theory (i.e Kuhn 1963). The draw backs of this approach is the self-absorption and interference from neighboring lines which can limit the success of this approach. Another approach is McWhirter approach, where electron density in the plasma must be high enough for collision to dominate the population of levels. This criterion is called McWhirter criterion and is given as:

$$n_e > 1.6 \times 10^{12} T^{1/2} (\Delta E)^3 \tag{8}$$

Where the electron density is in cm^{-3}, T is in kelvin (K), ΔE is in electron volt (eV). Here ΔE is the energy of the first level above the ground state.

If it is confirmed experimentally that LTE exist, the distribution of different quantities such as population of energy levels or ions stages and electron speeds, are all dependent on a single plasma quantity, temperature. The classical Maxwell velocity distribution function F_m is given as

$$f_m(v)dv = \left(\frac{m}{2\pi kT_e}\right)^{3/2} \exp\left[-\frac{mv^2}{2kT_e}\right] 4\pi v^2 dv \qquad (9)$$

Where m is the electron mass, and *v* is the electron speed. Relative population of energy levels, whether atomic or molecular in origin, are given by the Boltzmann distribution.

$$\frac{N_j}{N_o} = \left(\frac{g_i}{Z}\right)\exp\left[-\frac{E_j}{KT}\right] \quad \text{with respect to the ground state} \quad (10)$$

$$\frac{N_j}{N_o} = \left(\frac{g_i}{g_i}\right)\exp\left[-\frac{(E_j - E_i)}{KT}\right] \text{ for relative populations} \qquad (11)$$

Where *i* and *j* refers to two energy levels, N_o is the total specie population*;* N_{ij} is the population are the population of energy level $E_{ij,}$ g_{ij} is the statistical weights of the levels $(2J_{ij} + 1)$*; J* is the total angular momentum quantum number of the term; and Z is the partition function. However, this can be inaccurate sometimes. For example when the ground state is closely spaced multiplet, then the statistical weight of the lowest lying level needs to be added.

1.2.12 Laser induced plasma (LIP) parameters (electron temperature and electron density) and Local Thermodynamic Equilibrium (LTE).

The light emitted from laser induced plasma (LIP) is an important asset that give both the qualitative and quantitative information of the test sample and the plasma properties as well. The fundamental properties of plasma determining the light emitting from sample are plasma temperature, electron density, and the number density of the emitting species[19]. The information about the LIP temperature is important because it allows the understanding of the process occurring in whole complicated processes such as atomization, dissociation, and excitation and also improves the LIBS Sensitivity [58-62]. LIP is characterized with occurrence of the following processes, namely photo-ionization, collision ionization, collisional excitation,

radiative and three-body recombination, radiative decay, de-excitation process and Bremsstrahlung process. Spectral line intensities of a LIBS system can be used to detect and quantify the elements present in the test sample with the condition that the laser induced plasma are optically thin and in local thermodynamic equilibrium (LTE). The elemental composition of the optically thin plasma are the same as that of the sample. In an optical system like the plasma generated by pulsed laser ablation, LTE condition holds if the electron-ion and electron- atoms collision processes are very fast and prevail the radiative process. As the plasma is in Local Thermodynamic Equilibrium (LTE), the entire plasma plume volume consist of all kinds of species which can be described by series of equilibrium distribution law [47] namely, Maxwell distribution which describes the plasma particle, Boltzmann's statistic which describes the distribution of population in the energy level, Saha's equation which describes the ionization process, and the radiation density obeys the Planck's law [47, 63-65] In order to ascertain if LTE is reached, the electron density must sufficiently be high enough for collision to dominate the population of levels. This criterion was originally formulated by McWhirter and is now called McWhirter criterion [66,67]. One of the form of this criterion is given in Eq. (8).

In order for plasma temperature to be suitable for spectroscopic analysis, laser induced plasma is expected to be optically thin and in LTE condition. For plasma in these condition, the population of energy level of the species in such plasma is describe by the Bolzmann distribution law given as:

$$\frac{N_{k,z}}{N_z} = \frac{g_{k,z}}{p} \exp\left[\frac{-E_{k,z}}{K_b T}\right] \qquad (12)$$

Where $N_{k,z}$, $E_{k,z}$, $g_{k,z}$ are the population, energy and degeneracy of upper energy level K respectively, N_z and p_z are the number density and partition function of the species in the ionization stage z, K_b is Boltzmann constant, T is the electron temperature. The integrated intensity I_z of atomic emission lines occurring between the upper energy level K and the lower energy level I is the species in the ionization stage z in an optically thin plasma is given as:

$$I_z = \frac{hc}{4\pi\lambda_{kl,z}} A_{kl,} N_{k,z} L \tag{13}$$

Where h is plank's constant, c is the speed of light; L is the characteristics length of the plasma, $A_{kI,Z}$ is the transition probability and and $\lambda_{kl,z}$ is the spectral line wavelength. By substituting Eq. (12) in Eq. (13), we have:

$$I_z = \frac{hc}{4\pi\lambda_{kl,z}} A_{kl,} L \frac{N_z g_{k,z}}{P_z} \exp\left(-\frac{E_{k,z}}{K_b T}\right) \tag{14}$$

Taking the natural logarithm of the both side of Eq. (14), we have:

$$In\left[\frac{\lambda_{KI,Z} I_z}{A_{KI} g_{KZ}}\right] = \frac{E_{kz}}{K_b T} - In\left[\frac{4\pi Z}{hcN_z}\right] \tag{15}$$

where ln is the natural logarithm, I_z is the integrated signal intensity of the spectral line occurring between upper level k and the lower level I of the species in the ionization stages z in an optically thin plasma, K_b is the Boltzmann constant, T is the plasma temperature $A_{ki,z}$ is the transition probability , $\lambda_{KI,Z}$ is the transition line wavelength, $g_{K,Z}$ is the degeneracy of the upper level k, P_Z is the partition function of the species in ionization stage z, L is the characteristic

length of the plasma and all other symbol carry their usual meaning[68]. This equation is always a straight line with a slope of –1/kT. Hence if one plots the quantity on the left hand side of Eq. (2) against E (of the upper state emission), then a straight line is expected to be obtained if there is a Boltzmann distribution. Some of the crucial factors in obtaining a good Boltzmann plot are the accurate line intensities, accurate transition probabilities, and well-spaced upper levels [66,67,70,71].

Spectral line in an optical spectrum is characterized with a non-zero line width and its central line usually shift from its nominal central wavelength. This broadening and shift is as a result of Doppler, instrumental, natural and stark broadening[25,72]. Stark broadening in spectral lines are basically from collisions between ions and electrons. Stark broadening can also introduce shift of energy levels, which results in shift of wavelength positions of spectral lines[56].

The line profile for Stark broadening is described by a Lorentzian function with full width at half maximum $\Delta\lambda_{1/2}$ and electron density is related by the expression.

$$\Delta\lambda_{1/2} = 2w\left[\frac{n_e}{10^6}\right] + 3.5\left[\frac{n_e}{10^6}\right]^{1/4} + \left[1 - \frac{3}{4}N_D^{-1/3}\right]w\left[\frac{n_e}{10^{16}}\right]A^0 \qquad (16)$$

where w is the electron impact factor, n_e is the electron density, A is the ion broadening parameters and N_D is the number of particle in Debye sphere[25,72,73]. The first term on the right hand side of Eq. (3) represents the broadening due to electron contribution and second term is due to ions contribution. For non-hydrogenic ions, stark broadening is mainly due to electron impact, since the perturbation by ions are negligible compared to that of electron. Therefore the equation reduces to the form:

$$\Delta\lambda_{1/2} = 2w\left[\frac{n_e}{10^{16}}\right] \quad (17)$$

where W is an electron impact parameter which is a function of the temperature and only changes by a factor of two over the temperature range of 10,000- 80,000K. The Stark broadened profile of an isolated atomic or singly charged ionic line is one of the most powerful spectroscopic techniques used in the calculation of electron density to a very reasonable accuracy.

1.2.13 Quantitative Analysis

In quantitative LIBS analysis, ionic and atomic emission line intensities can be used for quantification of different species in the sample (e.g. in parts-pert-million)[73-75]. The quantification usually is conducted by constructing a calibration curve based on some set of samples (usually above three) with different known concentration of a specific analyte. The calibration curve provide a means to estimate the concentration of a specific species in an unknown sample. A plot of emission line intensities of a particular specie versus its concentration gives the calibration curve. The preparation of these standard sample allows the correlation between the spectral line intensity and the corresponding concentration of element in question. The emission line intensity of plasma is given by equation below:

$$I = \left[\frac{h\nu_{ji} N A_{ji} g_i}{Q}\right] \exp^{\left(-E_j/KT\right)} \quad (18)$$

h= plank's constant

V_{ji} = Transition frequency from state j⟶ i

A_{ji}= Einstein's coefficient for spontaneous emission between state j and i

N= Population density of atom exited by plasma in the ground state.

E_j = energy of the upper level of the atom

g_i = Statistical weight of upper level

Q= Partition function

T= electron temperature

K= Boltzmann's constant

1.2.14 Limit of Detection

Detection limit is defined as the smallest amount of an analyte which a system (i.e. laser induced breakdown spectroscopy) can reliably detect. The estimation of limit of detection (LOD) is very important for any analytical instrument because it tells us the limit of concentration of particular element it can detect. The limit of detection is estimated as 3σ divided by slope ($\Delta c / \Delta x; x = signal$) of the calibration curve.. The limit of detection is given as:

$$LOD = 3\left[\frac{\sigma}{S}\right] \tag{19}$$

where σ is the standard error of the experimental calibration data, and S is the sensitivity which is given by the ratio of intensity to the concentration.

1.2.15 Accuracy

The accuracy of an analytical method is defined as the degree to which the measured experimental value to close to the measured value from standard technique like ICP-MS. There are numbers of ways to estimate the relative accuracy of a calibrated technique. The relative accuracy is calculated as follows

$$Error = \frac{\left|x_m - x_{atv}\right| + SD \times t_{0.975} / \sqrt{n}}{x_{atv}} \qquad (20)$$

Where $\left|x_m - x_{atv}\right|$ is the difference between the measured value x_m and the acceptable value (x_{atv}), SD is the standard deviation of LIBS measurement, x_{atv} is the acceptable value, n is the number of measurement, $t_{0.975}$ is the t value at 2.5 % error confidence.

1.2.16 MOTIVATION

The presence of toxic element in the raw material (plant and animal) or supplement use in making food product which are consumed in Kingdom of Saudi Arabia is of great concerned. Since diet is the main source of exposure to toxic element for the population who are not occupationally exposed. The intake of these toxic element over a long period time could be carcinogenic, allergic and eczematous when they are above the permissible limit. Some of the life threating ailment in the kingdom are chronic liver diseases, chronic renal failure, kidney damages, and cancer, which are all as result of excess toxic element intake. Thus, developing an analytical technique for detection and quantification of these toxic element in food products so as ascertain if they above the permissible limit are worthwhile.

1.2.17 OBJECTIVES

A. To assemble a UV pulse laser induced breakdown spectrometer for detection and elemental analyses of toxic element in food products.

B. To optimize the LIBS system by studying the LIBS signal intensity dependence on delay time and laser energy.

C. To estimate the concentration level of toxic element present in the food products

D. To study the theory LIBS system and estimation of plasma parameters (electron density and plasma temperature) for different sample matrix.

CHAPTER TWO

LITERATURE REVIEW

2.1 General overview of LIBS

The early origin of LIBS was in the 60s when first experiment was performed by producing vapor from solid target using laser beam irradiance and then exciting the ablated plasma plume by electrical sparks.[76] These experimental achievement has shown a huge potential for an effective fast multi-elemental analytical technique. In the 1980s and afterward, tremendous achievement have been put forth in laser and detector technology, which are reliable and relatively cheap for analysis in research laboratories. Due to these facts, the technique is fast developing for quantitative and qualitative analysis of wide range of variety of samples [54,78-80].

Over the past decades, there has been constant interest on how to improve the LIBS technique, this is due to its uniqueness in terms of simplicity, rapidness, versatility, extremely flexible set-up and multi-elemental analysis of any type of solid sample in different mediums with little or no pretreatment procedure. Also the sample analysis can be achieved in air, vacuum, in fluids and even under extreme conditions such as high temperature and pressure environments [81-87].

2.2 LIBS Applications

Below are some of the experimental application of LIBS technique for detection and analysis of toxic element and other contaminant in solid and fluids:-

G. Kim et al [88] collected heavy metal contaminated soil sample from two different site in Korea (Deawon and Manjang respectively), additionally oil contaminated soil sample was also collected from army camp in Korea, which is reported to be contaminates with oil residue. The

soil samples were pressed into pallet to form a homogeneous surface for laser ablation process. Simple pretreatment of pelletizing and sieving was carried out for all samples to achieve a uniform water content and grain size in all samples. The effect of grain size and water content was investigated after pelletization and sieving process using laser induced breakdown spectroscopy (LIBS). The LIBS spectra lines reduced by a factor of 59-75 % whens water content increased from 1.2 to 7.8 % and soil sample having grain size of 75μm shows higher LIBS emission lines intensity with lower relative standard deviation than those with grain size of 2mm. Conclusively, the effect of water content on LIBS emission lines is far greater than the grain size. The data suggest that LIBS with the chemometric method is a very good tool for rapid analysis of soil sample contaminated oil and heavy metals.

Some orange fruit with less Cr concentration were investigated by Mingyin Yao et al [89]. Toxic Cr contained in Gannan Navel orange fruits from XingGuo Country, GanZhou municipality and Jiangxi Province in china were treated using contaminant in controlled lab condition, and then analyzed using laser induced breakdown spectroscopy (LIBS) and atomic absorption spectrometry (AAS). The goal of the work was to access the performance of LIBS technique in the analysis of natural organic substances by comparing the analytical result to that of AAS. To approve the workability of LIBS the Gannan Navel orange fruits needs to be contaminated prior to analysis. Firstly, 15 known standard concentration of Cr solutions were prepared by dissolving measured concentration of potassium bichromate ($K_2Cr_2O_7$) in DI water and stirring it over a period of several hours to form a homogeneous solution. The 15 Gannan Navel orange fruits with different concentration were analyzed under optimized experimental parameters, where Cr I 425.43nm was selected as the analytical line. The concentration of Cr were also determined using AAS. In a word, the comparative results between LIBS and AAS

demonstrate the capacity of LIBS to determine the Cr concentration in Gannan Navel orange fruits.

Quienly Godoi et al [90] investigated the toxic element in plastic toys which children are exposed to when playing with it, using LIBS as tool. In order to classify different model of plastic toys, 51 different toy sample manufactured with different polymers were selected at informal market in Sãu Paulo Brazil and analyzed using LIBS. LIBS spectra were recorded for these samples after 50 pulse per site in the test sample, the treatment of the LIBS data were based three test portion (n=3). NIST Atomic Database, ESAWIN software, and routine developed at MATLAB® version 7.0 software were used for data acquisition and treatment. Conclusively, some of the toy sample were found to contain toxic element such as Cr, Cd, and Pb with concentration above that recommended by Brazilian association of technical standard (ABNT NBRNM).

G.S. Senesi et al [91] collected five samples of soil and one sewage sludge sample at Murgia hills in the province of Bari Italy to detect heavy metal with emphasis on chromium, the objective of the work was to demonstrate the use of LIBS technique for quantitative and qualitative detection of heavy metal in soil and comparing the result with conventional ICP spectrometry. In this experiment, second harmonic of Nd: YAG laser of energy 15mJ was used. The emission spectra line was recorded with delay time = 750 ns, gate width 9 µs and 30 accumulation. Plasma temperature (T) and electron density (n_e) was estimated to verify the LTE condition for each sample. In conclusion the linearity existing between the background-normalized LIBS signals and ICP determined concentration of various heavy metal have been established, also the existence of LTE condition for all test sample.

UV nanosecond Laser induced breakdown spectroscopy (LIBS) has been used to analyze trace element contained in fresh vegetable by Vincent Juvé et al [92]. The vegetable are the common root, stem, and fruit vegetable available for consumption in the local market. In this experiment, quadrupled Nd:YAG laser (266 nm) with energy 10 mJ and repetition rate of 10 Hz. The fiber used gives good transmission between 200-850 nm. For the root the spectrum was recorded for the trace element from the center to the outer part. In the case of the stem the spectrum was recorded at different height of the plant from the lower part to upper part, while for the fruit the measurement was carried throughout the whole part of the fruit. A careful line by line identification of the spectra using NIST data base yielded 422 lines, among which 391 lines were emitted by ionic and atomic species, 9 lines by molecules (C_2 and CN), and 22 lines by ghost lines. In a word, UV nanosecond LIBS has been demonstrated to be effective in detection trace element which include organic element, metal, and nonmetals. Finally this shows that LIBS technique is a potential tool for detection and analyses of trace element in fresh vegetable and can be extended to other food stuff.

Josef Kaiser et al [93] used laser induced breakdown spectroscopy (LIBS) to detect trace element in matrix of microbiological, plant and animal samples. The use of LIBS for the analyses of bacterial and animal is still not common which make it cutting edge achievement. For the first time LIBS was used to distinguish between normal and malignant tumor cells from dog histological section, it was found that the concentration level of trace element in normal and tumor cell differs, in order to improve high performance, the analyses was carried out under pressure and the sample were frozen to -196 ^{o}C. Some element detected in tumor are Al, Ca, Cu, Fe, Mg, K and Na. Conclusively in this work, LIBS has demonstrated the capability of detecting trace element in biological samples and diagnoses of some diseases.

Laser induced breakdown spectroscopy was used in the determination of the level of calcium concentration by Edilene C. Ferreira et al [93]. In this work, sixteen different samples of commercially available cereals in Brazil were selected with differences as regards to their grain, sugar and flavor composition. The samples were then grounded to form a homogeneous cereals samples using a cryogenic mill model MA 775 (Marconi). The spectrum for the test sample was captured using Ocean Optics LIBS2500 system, with gate pulse energy of 50 mJ and pulse duration of 8ns. The wavelength range considered for this studies was between 391.4 to 398.4 nm with emphases on finger print wavelength of Ca II at 393.3 nm. Seven known Ca concentration of 16.02, 37.21, 68.62, 124.7, 1288, 3734 ppm were prepared in the breakfast cereals matrix for calibration. The calibration was then done to predict the Ca concentration in all the samples.

Lingling Peng et al [94] used laser induced breakdown spectroscopy as a tool to investigate the rapid analyses of heavy metal in Zn-Mn batteries. In the experimental work, a Nd: YAG laser (DCR-3D, spectral physics) with fundamental wavelength of 1064 nm, repetition rate of 10 Hz, pulse width of 8 ns, was used to generate plasma. The sample selected were spent batteries (6F22 Zn-Mn), with MnO_2 as anode and Zn metal as cathode, other constituents are acetelyne black and starch mixed together to strengthen the conductivity. Two samples were made from this batteries, sample #1 mixture of its anode (MnO_2) with the mixed acetelyne black and starch, sample #2 is its cathode (Zn). After making the pallet of the sample, plasma spectrum were obtained by averaging 10 acquisition. The element identified in sample #1 are Fe, Mn, Zn, V, Cr, Al, Si, Ca, Mg and C, while in sample #2 the element identified are Fe, Zn, Al, Si, Mg, Ca, Pb and C, with all the spectra identification from NIST database. Finally the relative mass

concentration of the identified metal present in spent Zn-Mn batteries were obtained with emphases on heavy metal such as Cr, V, Pb and Mn.

M.A Gondal et al [95] applied laser induced breakdown spectroscopy as a tool to determine the concentration of toxic element in four different brands of locally available lipstick in Saudi Arabia. Since lipstick is always in form of fluid, therefore pretreatment process is needed prior to analyses by LIBS technique. In order to remove the liquid content of the lipstick, it was heated to a temperature of 105 ^{o} C and then frozen in a refrigerator and then cut into a circular shape of 1 cm diameter so as to fit into the LIBS system sample holder. After taking the spectrum of the samples, the toxic element detected in these lipsticks samples are lead, cadmium, zinc and chromium. Afterwards, the calibration curves for lead, cadmium, Zinc and chromium were achieved after preparing standard known concentration of the respective element. Standard conventional ICP analyses was also adopted to affirm the findings from LIBS result, the two result were in agreement with each order. In a word, the continuous use of these cosmetics could result in increase of heavy metal in the ocular system and human body beyond the acceptable limit.

M.A Gondal et al [80] uses fourth harmonic pulsed Nd: YAG laser coupled with spectrograph and gated ICCD camera to detect and quantify the fluoride level in Toothpaste in semi fluid state. Spectral line of fluorine at a fingerprint wavelength of 731.102 nm was used as a marker line for the quantification of the fluoride level in the toothpaste. The LIBS signal as a function of laser fluence and time delay were all investigated, where the optimum laser fluence and time delay were found to be 22J/m^2 and 700 ns respectively. Prior to data acquisition for LIBS spectral analysis of the toothpaste sample, plasma parameters such as electron temperature and electron density were estimated for the validation of LTE condition. The concentration level of

fluoride was found to be between 1300-1750 ppm in all the toothpaste samples. The limit of detection of the setup for the detection fluoride was 156 ppm.

T. Hussain and M.A Gondal et al [59] employ laser induced breakdown spectroscopy for the qualitative and quantitative analysis of solid and liquid samples such as iron slag and open pit ore. Two different samples of iron slag and open pit ore were collected from major steel manufacturing plant located at Jubail, Saudi Arabia. The excitation source wavelength was 1062 nm from an Nd: YAG laser. The various concentration of element of environmental concern such as zinc, iron, copper, cadmium, chromium, magnesium, calcium, titanium, barium and phosphorus were estimated. By construction of calibration curve the various concentration of different element in the samples were determined. The concentration of all these elements were found to be remarkably high in all the test samples.

M.A Gondal et al [54] applied laser induced breakdown spectroscopy to study the role of various binding material on detection of trace element in powder samples. The binding materials studied are Alluminium, starch, KBr, silver and poly (vinyl alcohol). The masses ablated and crater depths were measured for particular spectral line for different binders using the same matrix. From the level of crater depth and masses ablated, KBr was found to be the best binder.

Hideki Horie and Katsunori Kohata [96] et al discussed two newly developed technique for the analysis of low-molecular-weight tea components, which are high-performance liquid chromatography (HPLC) and high-performance capillary electrophoresis (HPCE). Some of tea component analyzed using HPLC and HPCE are different type of amino acid such as theanine, arginine and g-aminobutyric acid, and also derivative of amino acid such as o-phthalaldehyde, phenylthiocarbamoyl (PTC) etc. Other component of tea sample analyzed using HPLC and

HPCE are Polyphenols, Purine alkaloids, purine alkaloids, oxalic acid, Vitamins & photo-pigments, and Cations & anions.

Tanmoy Karak and R.M. Bhagat [97] et al examine the intake of a number of nutritional trace elements and excess non-essential element in human through ingestion tea leaves. Among different trace element detected and quantified in tea infusions in different literature are nickel (Ni), manganese (Mn), fluoride (F), copper (Cu), chromium (Cr), cadmium (Cd), arsenic (As), and aluminum (Al) with their concentrations ranging between BDL-0.16 mg L-1, 0.1–250 mg L-1, 0.2–4.54 mg L-1, 0.02–40.0 mg L-1, below detectable limit-43.2μg L-1, trace-0.79μg L-1, trace-1.53μg and 0.06–16.82 mg L-1 respectively. There were some tea infusions with toxic metal exceeding the maximum permissible limit for different countries.

R.N. Gallaher [98] et al discusses the mineral content of 10 commercially available dry tea (herbal infusion) and their infusion. The herbal infusion studied are red clover, Echinacea, dandelion, red raspberry leaf, Siberian ginseng, blueberry leaf and green tea. It was observed that none of the infusion was good source of Na, Cu, Ca, P, K, Mg, Fe, Mn, or Zn in a single serving. Potassium (k) was found to have the highest extraction rate of 71%, while iron (Fe) had the lowest extraction rate of 6%.

S. Beldjilali [19] et al used laser induced breakdown spectroscopy to study minor element concentration in both flesh and skin of potatoes. The element detected are H, C, Mg, Al, Ca, Fe, Na, Mn, Li, Si, K and Cu. Aluminum and Silicon were found in large mass fraction in the skin whereas not found at all in the flesh.

CHAPTER THREE

EXPERIMENTAL METHO

3.1 Introduction

Before the detection and the quantification of element present in food products, it is required to assemble and optimize the LIBS system in order to have the best limit of detection and to minimize the signal to noise ratio. The experimental set-up, materials, and operating condition were are selected based on adequate literature survey. The details about the LIBS set-up used and the sample preparation methods will be discussed in the following subsection.

3.2 LIBS Experimental Set-up

The main components of LIBS system are depicted in figure (3.1). A pulsed laser with high-energy is focused on a target sample. The energy of the light induces plasma and vaporizes the sample. What the spectrometer does is to diffract the light collected, with the aid of an inbuilt optical system which acquire the spectral signature. Then, the devices such as photomultiplier tube (PMT), photodiode array (PDA) or intensified charged coupled device (ICCD) is used to detect the light. Finally, the acquired LIBS spectrum is processed with the help of a computer system for spectroscopic analysis. An accurate time control mechanism is needed for LIBS system in order to avoid some plasma life stages and to improve spectral emission lines. The choice of laser coupled with spectrometer, time control and environmental condition determines the success or failure of the experiment. The main component includes the Nd: YAG pulsed laser, focusing systems (i.e. mirror and lens), target holder, optical fiber, spectrometer, and computer systems [99-101].

3.2.1 Laser configuration of LIBS

The main device of LIBS system is the laser. It produce the necessary energy needed to induce plasma and also determines the plasma characteristics. The main parameters in LIBS systems are laser energy, pulse time, wavelength and number of pulses per burst. The workability of the LIBS system depends on each of these parameters. Nano-second pulsed laser is the commonest used for LIBS. Thus, most of these section will be expatiating on it [102].

3.2.1.1 Laser properties

3.2.1.1.1 Intensity

Laser intensity also called power density or irradiance is the power per unit area (Wcm^{-2}) and also indicates the peak power of laser per output beam cross section. Since a typical laser allows the generation of a very short duration pulses in order of nanosecond or femtosecond, LIBS intensity as large as billions or trillion of watt per unit cross sectional area is achievable. It should be noted that, in LIBS experiments what is really important is the power per unit area actually hitting the surface target, which also depends on the optical systems used in delivering the laser beam [52,103].

3.2.1.1.2 Directionality

The directionality of the laser beam refers to its very narrow divergence angle (typically of order of milli-ridians for solid state lasers utilized in LIBS studies). With this unique property laser beam can be focused on a very small spot size, which allow the delivering of high irradiance on the target. Spatial coherence is indirectly related to low divergence of laser beam and its ability to produce high irradiance. However, it should be noted that the coherence (spatial and temporal)

is not mandatory in LIBS, in as much as the irradiance does not change, the plasma formation process remain the same, irrespective of whether the laser beam is coherent or not[103]

3.2.1.1.3 Monochromaticity

A laser is characterized with the ability to generate most of it output energy within a very narrow spectral range, unlike conventional light source which is composed of wide range of wavelengths. The monochromaticity of light play a very little role as far as plasma production is concerned, it is the power per unit area that matters irrespective of whether the laser beam is monochromatic or not. In some special cases, highly monochromatic light may be needed to probe plasma using resonance excitation of atomic species[103].

3.2.2 The light collecting system

The light collecting system is an optical device used in LIBS study to collate radiation emitted by plasma and send it to the spectral detection unit**.** In this study, optical fiber is used as the light collecting system, and its position is close to the region occupied by the plasma plume and then directing the collected emitted light to the spectrometer through of fiber collecting port. The optical fiber used in this experiment is supported with miniature lens placed at an angle 45^{o} to collect signals from the plasma spark created on the surface of the sample. The optical fiber is place on a 3-D translator which can be moved in x, y, z directions [104].

3.3.3 LIBS spectrometer

Spectrometer is the spectral detection system used utilized in LIBS experiment to provide the spectral composition of radiation emitted by the plasma, whose analysis would bring identification of fingerprint wavelength of atomic species present in a sample. Due to the

complexity of LIBS spectra and wide range of LIBS spectral ranging from vacuum ultraviolent to near infra-red, an ideal spectrometer should fulfill the following requirement

a) The spectrometer should cover a wide spectral range and have a high spectral resolution (to resolve closely spaced spectral lines).
b) The spectrometer should have a large dynamic range and should exhibit high quantum efficiency over a whole recorded spectrum.
c) The spectrometer should have a short data-acquisition and readout time.

A high resolution 500 mm spectrograph (Andor SR 500i-A) with grating groove density of 1200 lines / mm was used in this study to collect the generated LIBS signal from the fiber optics. This system offers maximum resolution between wavelength range 200-900 nm.

3.2.4 Lens

The irradiance on the point of interaction with sample can be increased by focusing the laser irradiation to a very small spot with the aid of an optical lens system (usually cylindrical or spherical lens). In this way, the threshold for the plasma formation (> 10^7 W/cm^2) can be easily attained and exceeded by a modest fluence of the laser. Ideally, laser beam with a Gaussian intensity profile is focusable provided the lens is free aberration to have a diffraction limited beam waist radius given by

$$w_o = \frac{f\lambda}{\pi D/2} \tag{21}$$

Where f is the focal length of the lens, λ is the wavelength of laser radiation and D is the diameter of the unfocused beam impinging on the lens. From Eq. (21), higher power densities is achievable at focal point by the use larger unfocused beams and lenses with shorter focal length. Lenses with shorter focal length are also preferred because it produces highly localized sparks

for spatially resolved measurements. On other hand, lenses with long focal length provides wider focal volume, but requires higher laser energy to excite the plasma, and are often used when it is difficult to place the focusing lens close to the sample.

3.2.5 Target holder

One of the very vital component of LIBS system is the target holder. The sample holder used in this LIBS system is a 2 D translator which can be manually moved in X and Y directions as depicted in Fig. 3.2 The sample holder is made up of an eye protective polymer to provide a clear view of the sample. Usually the laser pulse has the tendency to create a crater within the sample when it hit the same spot for a long time, and this is due to the high irradiance of laser pulse. When crater is formed on the sample surface the optical fiber loses the signal from the light emission from the plasma plume, and this drastically affect the quality of LIBS spectrum recorded. Hence, there is need for movement of the sample holder during the experiment to avoid the creation of crater within the sample by strong laser shot and also to provide a fresh surface for every laser shot during the analysis.

3.2.6 Inductively coupled plasma mass spectrometry (ICP-MS)

ICP-MS is one the analytical tools used in determination of trace element in a myriad sample**.** It comprises of different components such as nebulizer, plasma touch, spray chamber, interface and a detector**.** The schematic diagram of these components is depicted in Fig. (3.3) This technique is based upon the spontaneous emission of photons from atoms and ions that have been in a radio frequency (RF) discharge. Liquids and gas are directly injected in the system, solid have to be extracted or digested using acid, so that the analyte will be present solution.

The prepared sample is converted into aerosol and links into the central channel of the plasma. In an ideal situation, the inductively coupled plasma operates at approximately 10, 000 K, this makes the aerosol to quickly vaporized, which allow the analyte element to be liberated as free atoms in the gaseous state. The sample in liquid form is pumped into nebulizer at ml/min using peristaltic pump, which is then converted into fine aerosol with the aid of argon gas at 1L/min. Then the spray chamber is used to separate the fine droplet (about 5 μm in diameter) of the aerosol from the large droplet of the sample. The fine droplet is then directed from spray chamber into the plasma torch through the injector[105]. The plasma torch is used to generate positively charged ions which is directed to the mass spectrometer via the interface region having a vacuum pressure of 1-2 torr. The ions are extracted from interface region and then exit into the main vacuum chamber the ion optics (electrostatic lenses). The ion optics direct the ion beam toward the mass separation device and stops the particulates, photons, and neutral species from getting into the detector. Lastly, the ion detector coverts the ions into electrical signal and the data handling systems conventionally process it and convert it into analyte concentration using the calibration set for ICP-MS[105,106]. The ICP-MS equipment is as shown in Fig. (3.4)

3.3 Preparation of Samples

In this study, we intend to analyze food products such as tea, date fruit, cigarette and other biological samples like smokers and non-smoker's tooth. In order to eliminate splashing and to increase laser repetition rate and the efficiency of plasma formation & excitation, all sample were grinded and made into a solid sample via palletization, and this has been reported to have significantly improved the LIBS analysis.

3.3.1 Tea Sample preparation for LIBS Analysis

As part of this experimental study, six different brands of commonly consumed black tea by most of the people was purchased from different food stores in Dammam city Saudi Arabia. The selection was based on price tag ranging from moderately cheap to expensive. The different tea grains were separated from their sachets and placed in labelled petri dish. In order to make pallet from the tea grain, the tea grain was placed in a cylindrical dye (2 cm diameter and 2 mm thickness) and then pressed with aid of hydraulic press into round shaped pallet that will fit well into the system sample holder. The pelletization process is as depicted in Fig. (3.5). The pallet was quite firm enough to withstand laser pulse thrust without adding any binder. In order to avoid contamination, the pallets were stored in desiccator prior to its LIBS analysis.

3.3.2 Tea Sample preparation for ICP-MS Analysis

For the analysis of tea samples using ICP-MS technique, 0.01 g of each tea samples were weighed using an analytical balance and then added into 5 ml of nitric acid (HNO_3) with 99 % purity (Fisher Scientific), which was then heated at 60 ^{0}C until the nitric acid reduces to 2 ml, by this process one to allows the metal to dissolve in the nitric acid solution. After solution cooled down, 40 ml of DI water was then added to resultant solution and further heated at 45 ^{0}C for 2 hours so as to allow complete digestion of the tea sample. After cooling down, the resultant solution was sieved into to 50 ml volumetric flask to remove any remaining undissolved particle and then topped with DI water to get exactly 50 ml solution and then thoroughly mixed by shaking the volumetric flask. The resultant solution was then analyzed using ICP-MS analysis.

3.3.3 Date Fruit Sample preparation for LIBS Analysis

The four dates samples named Sakary, Khas alhasa fakar, Nabut saff, Sakaray al kaseem were obtained from different local market of Kingdom of Saudi Arabia. At first, the seeds were removed from the dates, and then it is placed in a flat sheet of aluminum foil for drying. After 2 hours of drying at 600C (using Binder Heating Oven, Model ED53, 230V, 50/60Hz), the samples were grinded into powder by using standard Mortar & Pestle (see Fig. 3.6). By using the hydraulic press machine the powder of date is converted into the pallets. This pallet was placed on rotary table inside the LIBS chamber to avoid the ablation of the samples from the same spot. The plasma generated from these four date fruit samples was recorded.

3.3.4 Date Fruit Sample preparation for ICP-MS Analysis

For the analysis of date samples using ICPMS technique, standard preparation method as recommended by EPA for ICPMS analysis was adopted. At first, 0.01 g of each date sample was added into 5 ml of nitric acid (HNO3) with 99 % purity (Fisher Scientific), which was then calcined at 60 0C until the nitric acid reduces it to 2 mL, it allows the metal to dissolve in the acid solution. Then this solution was allowed to cool down. After this, deionized water of 40 mL was added to a resultant solution and further calcined at 45 0C for 2 hours, so that it allows complete digestion of the date samples. After cooling down, the resultant solution was sieved into to 50 mL volumetric flask to remove any remaining undissolved particle and then topped with deionized water to get exactly 50 mL solution and then thoroughly mixed by shaking the volumetric flask. The resultant solution was then analyzed using ICP-MS.

3.3.5 Tobacco cigarette Sample preparation for LIBS Analysis

Four different brand of commercially available cigarettes which are common among smokers in Saudi Arabia were purchased. The selection of these brands was based on price tag ranging from lower price to higher price. The tobacco was separated from each brand of the cigarettes by removing the filter, tipping paper and the rolling paper. This tobacco was then hydraulically pressed into pallets with maximum rigidity to withstand the high laser power thrust and to reduce the error for effective LIBS signal analysis. The tobacco under this study were pressed into round pallets shape by applying a pressure of 5.2 bars for 10 minutes while placing the tobacco in a special dye. The cylindrical dye was 2 cm in diameter and 2 mm thickness**. Fig. 3.7** depicts the pictorial view of the pelletization process of tobacco cigarette. There was no need to use any type of binder because the tobacco bonded well on its own. The pallets were preserved in clean petri dish and stored in a desiccator to avoid any absorption of moisture and other contaminants.

3.3.6 Teeth Sample preparation for LIBS Analysis

Various teeth samples of different dimensions were collected after extraction from three famous Hospitals (King Fahd Medical City Riyadh, Central Hospital and Prince Sultan Medical City located in Riyadh). All samples were extracted by dental specialists and were adult male and females. We analysed 90 teeth in three main groups (30 smokes, 30 non-smokers and 30 for control). Here control group are persons having no periodontal disease. A pictorial view of the teeth of three groups is depicted in Fig 3.8.

In this study, out of these ninety teeth samples, sixty extracted teeth were patients having history of chronic periodontitis. They were divided into two groups, thirty teeth were of patients having

smoking habits and 30 having non-smoking habits. Another 30 extracted teeth from non-smoking patients who didn't have history of periodontal disease and their teeth were extracted due to orthodontic reasons. Each sample of extracted teeth were scaled by ultrasonic scaler for calculus removal then washed in distilled water, were dried under ambient air and then kept in a solution of 10% formalin in water to avoid contamination prior palletization. Before the palletization process, the various teeth sample were removed from the formalin water, thoroughly washed and dried under in the sun, then the teeth were grinded into powered form and then hydraulically pressed into pallets with maximum rigidity to withstand the high laser power thrust and to reduce the error for effective LIBS signal analysis. The teeth samples under this study were pressed into round shape pallets by applying a pressure of 6.2 bars for 15 minutes while placing the sample in a special cylindrical dye of 2 cm in diameter and 2 mm thickness**.**

3.3.7 Teeth Sample preparation for ICP-MS Analysis

For ICP-MS analysis, the teeth samples were digested in 5% nitric acid of 99.99% purity. Representative 1 gram (dry weight) of teeth sample was digested with repeated additions of nitric acid (HNO3) and hydrogen peroxide (H_2O_2). The resultant solution was reduced in volume while heating at 95 ^{0}C for 6 hours and then diluted to a final volume. The resulting solution of the sample was analyzed for As, Cd, Pb metal using Inductively Coupled Plasma Spectrometer calibrated using reference standards of three levels of accuracy.

3.4 Preparation of standard concentration of materials

3.4.1 Preparation of standard concentration of Iron (Fe), Chromium (Cr), Potassium (K) and Bromine (Br) for quantitative analysis of different tea samples.

In order to determine the amount of Iron (Fe), Chromium (Cr), Potassium (K) and Bromine (Br) in tea samples (1-6), standard calibration sample were prepared using the tea sample matrix. Sample # 2 was used because the sample matrix are identical. Each sample matrix were prepared by homogeneously mixing the sample matrix with different known concentration of a specific analyte such as iron (III) sulfide, Chromium (II) Sulfate, Potassium bromide (KBr) and Potassium bromide respectively. The calibration standard sample concentrations that were prepared for Iron (Fe) were (a) 500ppm (b) 1500 (c) 2500 (d) 3500 (e) 5000, for Chromium (Cr) were (a) 100 (b) 300 (c) 500 (d) 700 (e) 1000, for Potassium (K) were (a) 500 (b) 700 (c) 900 (d) 1100 (e) 1300, and for Bromine (Br) were (a) 50 (b) 300 (c) 500 (d) 700 (e) 1000. This was achieved by hydraulically pressing the powered sample into pallet using a special cylindrical dye of 2 cm in diameter and 2 mm thickness**.**

3.4.2 Preparation of standard concentration of, Magnesium (Mg), Calcium (Ca), and Chromium (Cr) for quantitative analysis of different Date fruit samples.

In order to determine the concentration of nutritional element such as magnesium & calcium and toxic element such as chromium in the test date sample, 10,000 ppm (parts per million) solution of Mg, Ca and Cr were used to prepare standard sample of known concentration in deionized (DI) water. The standard concentration for Mg, Ca and Cr ranges 5 to 2000 ppm (i.e. a. 5ppm, b. 200 ppm, c. 500 ppm, d. 1000 ppm, e. 1500 ppm, and f. 2000 ppm), 5 to 2400 ppm (i.e. a. 5ppm,

b. 400 ppm, c. 900 ppm, d. 1400 ppm, e. 1900 ppm, and f. 2400 ppm), and 5 to 1200 ppm (i.e. a. 5ppm, b. 100 ppm, c. 300 ppm, d. 600 ppm, e. 900 ppm, and f. 1200 ppm) respectively. The persistent signature lines of Mg, Ca and Cr used in the construction of calibration curve are 277.9, 317.9 and 520.4 nm respectively. Standard calibration sample were prepared using the powered date sample matrix. Since the sample matrix are identical, Sample # 1 was used. The prepared samples were then hydraulically pressed in a cylindrically shaped dye of 2 cm in diameter and 2 mm thickness and the surface of the resulting samples were smooth to allow uniform generation plasma for LIBS analysis.

3.4.3 Preparation of standard concentration of fluoride for quantitative analysis of different Tobacco cigarette samples.

In order to determine the amount of fluoride in cigarette samples (#1, #2, #3, and #4). The calibrated samples were prepared by adding known concentrations of fluoride to the sample matrix (samples #1) and subsequently we used fluorine line 690.20 nm as the marker line for drawing the calibration curve. The added concentrations of sodium fluoride (NaF) were 15 ppm, 30 ppm, 60 ppm, 122 ppm, 231 ppm, 348, 420 ppm and 537 ppm. The resultant mixture were thoroughly mixed and compressed using a pressure of 6 torr from pellet pressing machine. The diameter and thickness of dye used are 20 mm and 2mm, respectively.

3.4.4 Preparation of standard concentration of lead (Pb), Cadmium (Cd) and Arsenic (As), for quantitative analysis of Smokers and non- smoker's teeth samples.

To draw the calibration curves, 5000 µg/ml solution of As, Cd, and Pb was used to prepare standard samples of known concentrations in double distilled water. The standard solutions were

having concentrations varying from 50 ppm (parts per million) to 1200 ppm for As, Cd, and Pb by weight. These solutions with known concentration were utilized, and the wet paste was dried in the Oven (see Fig. 3.9) at 350 K temperature during one day for preparation of standard samples to draw the calibration curves. The dried powdered teeth samples were then hydraulically pressed into smooth surface pallet by placing a cylindrical dye under a hydraulic pressing machine and applying a pressure of 6 torr. The dimension of the cylindrical dye are 20 by 2 mm.

3.5 Precaution taken during the experiments.

(1) All equipment used in experiment were kept clean and dry to avoid contamination of sample.

(2) Equipment such as dye and mortar were kept clean after each use.

(3) All samples were store in desiccator to avoid contamination with atmospheric moisture.

(4) The binding material used were ensured to be in powered form before thoroughly mixing it with the sample, this ensures homogeneity of the prepared pallets.

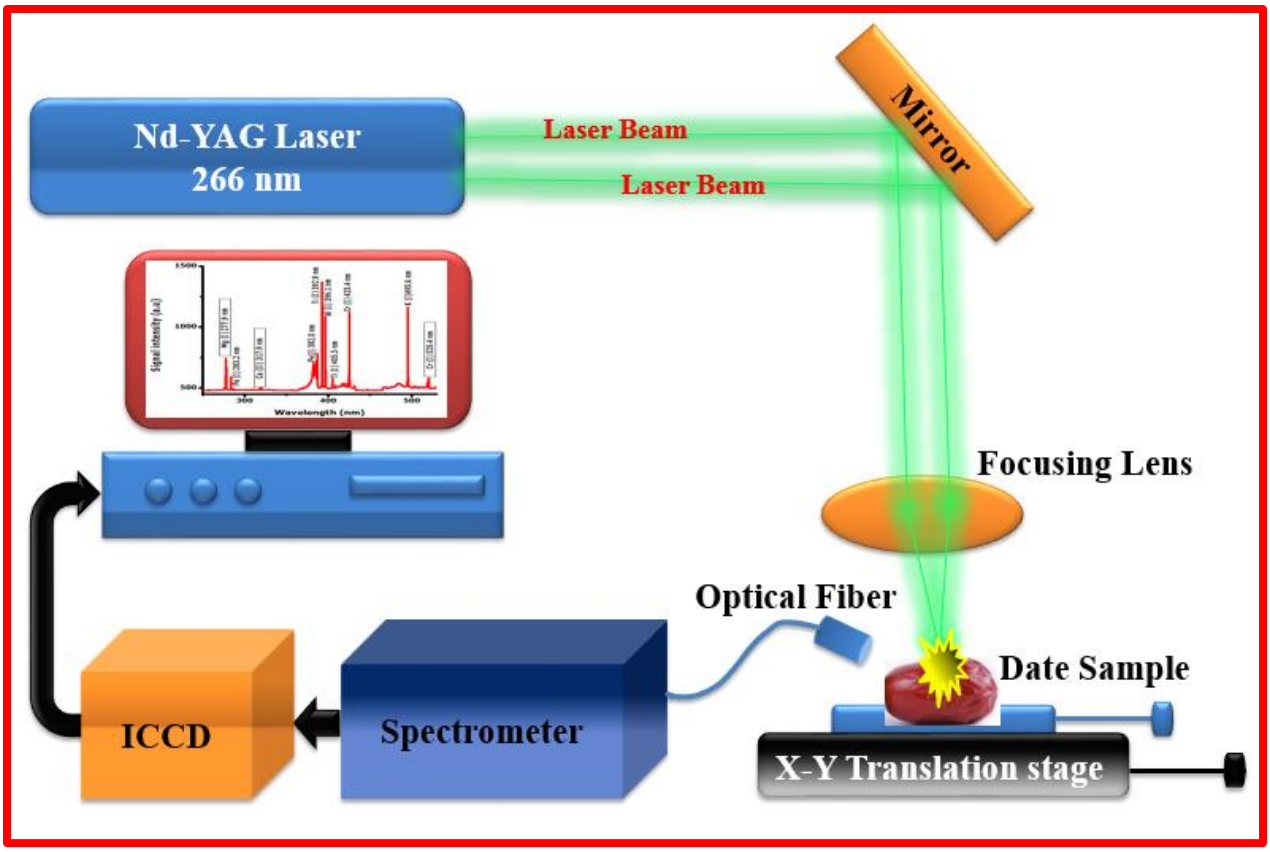

Figure 3.1: Schematic diagram of the LIBS setup.

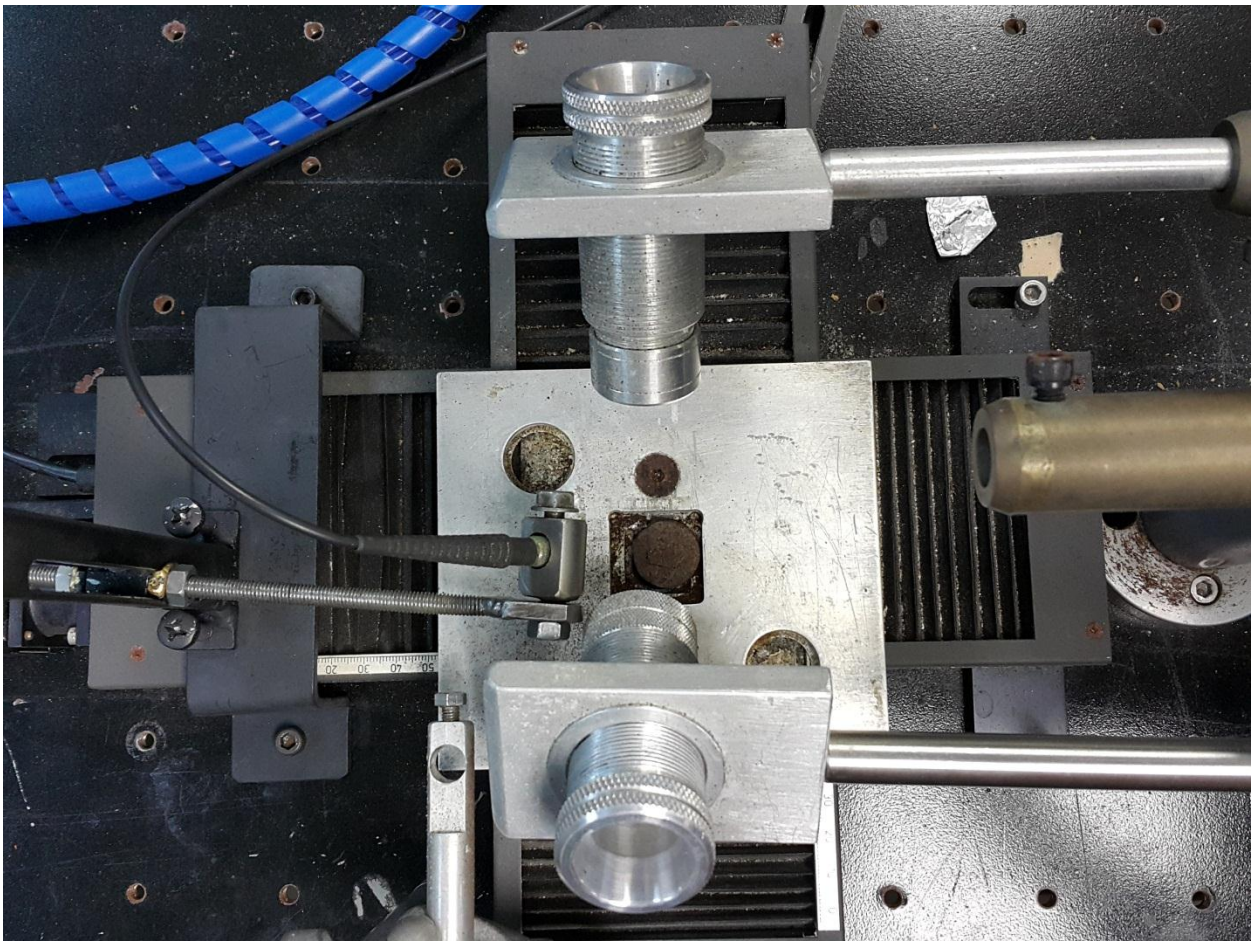

Figure 3.2: Sample Holder in the LIBS Set –up.

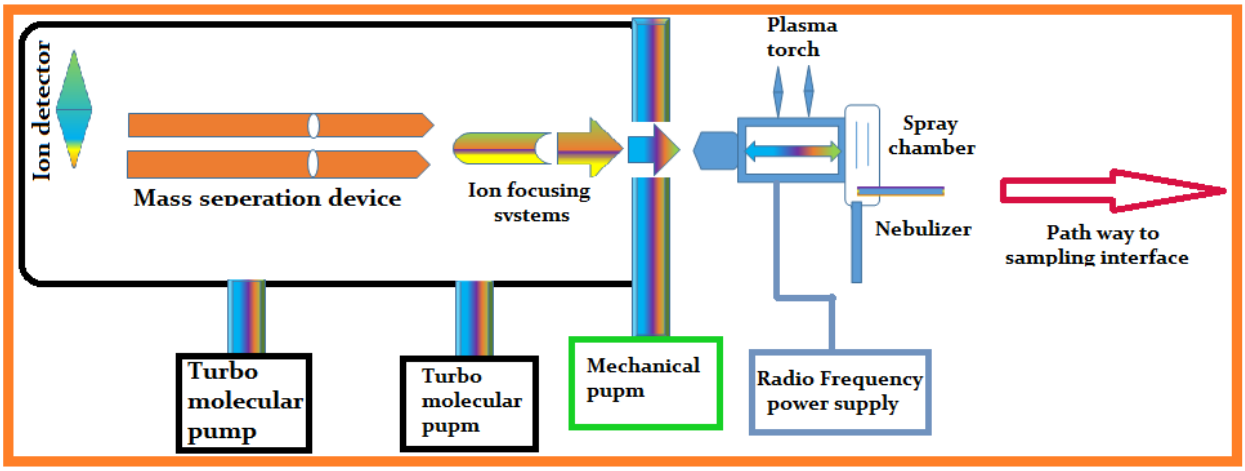

Figure 3.3: Schematic diagram of the ICP-MS setup

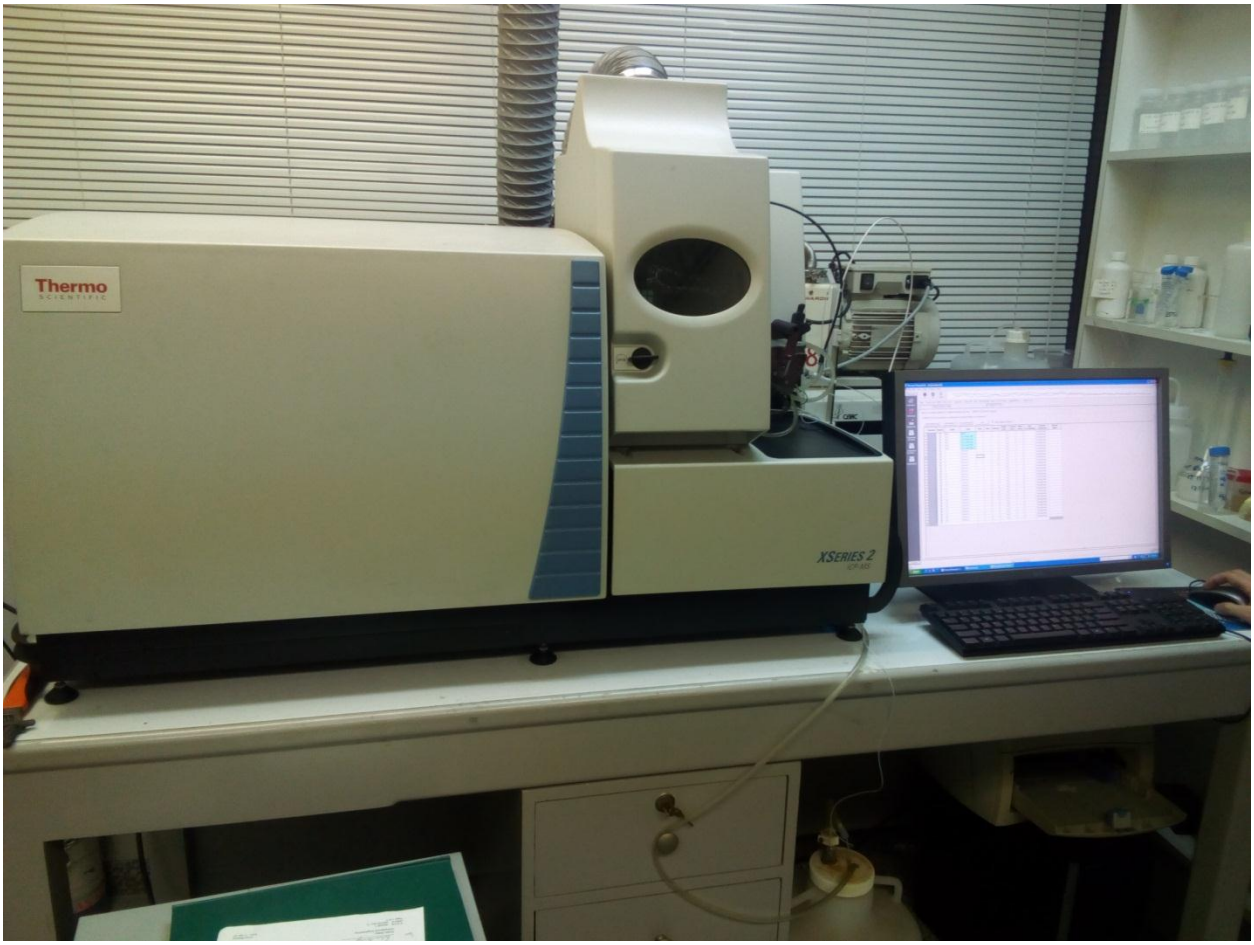

Fig. 3.4 Inductively Coupled Plasma Mass Spectrometry

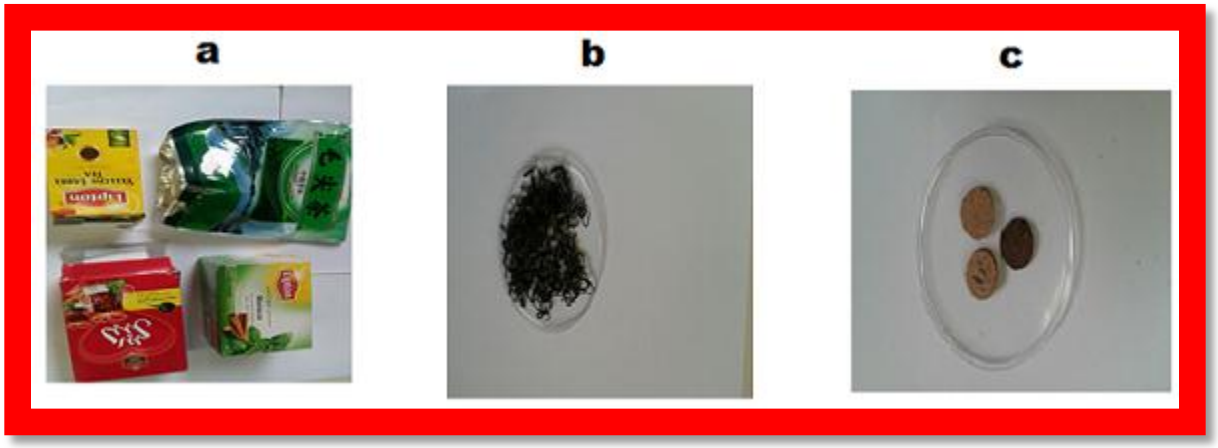

Fig.3.5 Pictorial view of the pelletization of tea samples (a) as purchased tea sachet (b) separated tea grain from a tea sachet (c) pelletized tea sample

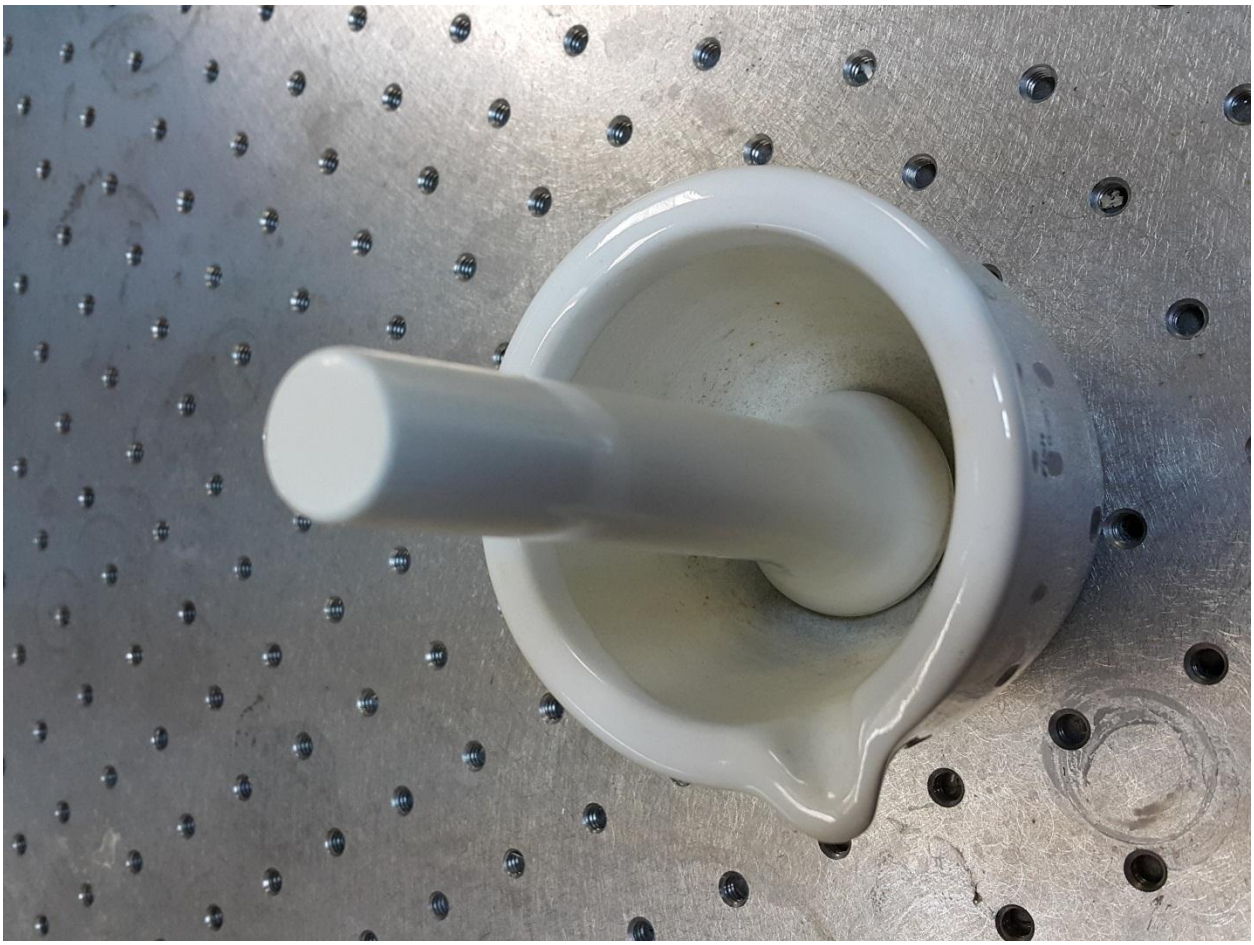

Fig. 3.6 Pestle and Mortar used for grinding LIBS samples.

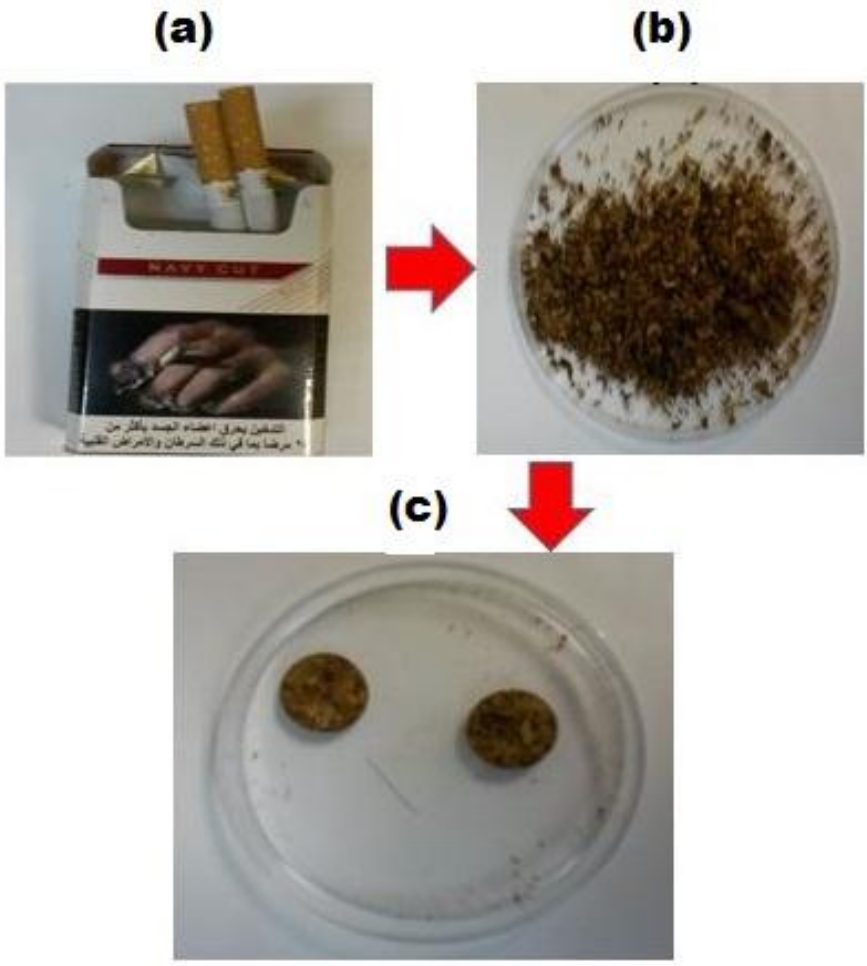

Fig. 3.7 Pictorial view of the pelletization of tobacco cigarette (a) As prepared

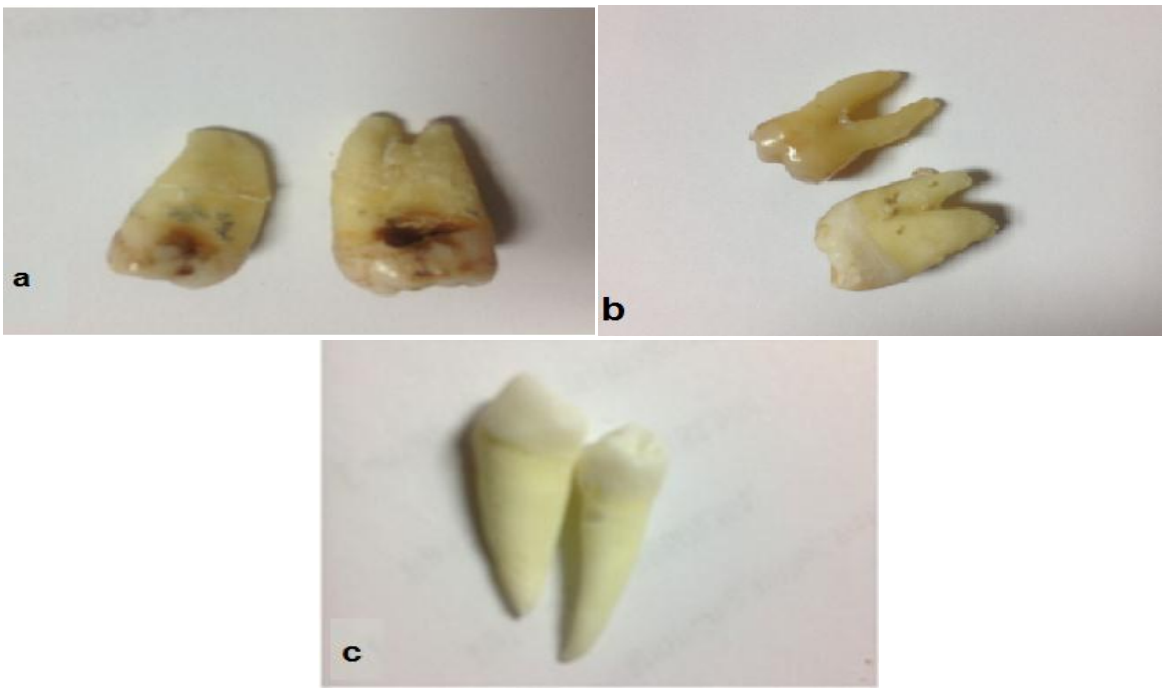

Fig. 3.8: Pictorial view of the teeth samples which were extracted from different groups (a) smokers, (b) non-smokers and (c) control.

Fig.4.9 Oven used in for drying paste samples for LIBS sample preparation.

CHAPTER FOUR

RESULTS AND DISCUSSION

This chapter discusses in details the results from our experimental study, which is as follows**:**

4.1 LIBS spectrometer Application and Evaluation Laser induced plasma (LIP) parameters for verification of local thermodynamic equilibrium (LTE).

In this section, we discusses the application of LIBS in detection of to toxic element such as Arsenic (As), Bromine (Br), Cadmium (Cd), Chromium (Cr), Fluoride (F) and Lead (Pb) and comparatively detection of nutritional element such as Iron (Fe), Magnesium (Mg), Calcium (Ca), and Potassium (K) in food products such as tea, date fruit, cigarette and human tissue like teeth. The plasma parameters for each products were also studied for verification of Local Thermodynamic Equilibrium (LTE).

4.2 Direct Spectral Analysis of Tea Samples using 266 nm UV pulsed Laser-induced Breakdown Spectroscopy and cross validation of LIBS results with ICP-MS.

4.2.1 Introduction

Tea is the second most consumed beverage in the world beside water, with an estimate of 18-20 billion cups consumed daily [96,107,108]. It is commonly cultivated in Southeast Asia, especially in china, and other 45 countries worldwide [97,109]. Tea leave contains many trace elements which are beneficial to human, along with other toxic elements present in the tea leave. The main sources of toxic elements in the tea plant could be from their growth media, agro input, nutrients, soil, and other sources like fertilizers, industrial activities, pollution and pesticides[110]. The common chemical species present in tea leave are, copper, zinc, manganese, iron, magnesium, bromine, titanium, aluminum, potassium, phosphorus, strontium, sodium, iodine and fluorine. Among potentially toxic elements like chromium (Cr), bromine (Br),

cadmium (Cd), manganese (Mn) are the most health threatening substance even at low concentration. These toxic elements have strong tendency to accumulate in food chain and their removal rate probability through excretion is quite low[111]. Some of the ailments which human could experience due to excess intake of these toxic elements above the safe permissible limit are high blood pressure, distortion of mental and central nervous system, fatigue, kidney neurological disorder, liver and kidney dysfunctions [97,98,112,113]. However, the consumption of tea have some benefits to our health, as the very presence of manganese and excessive amount of potassium helps a hypertensive patient, while other health benefits are prevention of Parkinson's diseases[97], myocardial infarction[98], and coronary arteries diseases[114-116]. There are six different types of tea available in the market namely pu-erh, black, oolong, white, green, and yellow, the most popular among them are black, oolong and green tea, which are distinguished on the bases of their degree of fermentation[117]. In this study, we focused on the analysis of different brands of black tea, which are the most consumed tea brands in the Kingdom of Saudi Arabia using laser induced breakdown spectroscopy for the first time.

In this study, we are interested in detection of the nutritional elements with more emphases on iron (Fe) and potassium (K) which are highly beneficial for better health and for the toxic elements our focus is on Bromine (Br) and Chromium (Cr) which are life threating species even at low concentration intake. Iron (Fe) is one of the most important nutritional element which often exist in the blood and it is responsible for oxygen transport and DNA synthesis[118] [118,119]. Iron deficiency can cause anemia, dizziness, itching, eczema and constipation[120-122], while excess iron intake cause health problems and some serious diseases[123]. The estimated world population that suffers from iron deficiency is about 30 % [124], therefore determination of total iron content in tea for the safety of sound public health is very crucial.

Potassium (K) is a nutritional element required for human body, but unfortunately people consume more of Sodium (Na) than Potassium (K), where excessive consumption of Na contribute to hypertension in the population. The more K intake is associated with lowering of the blood pressure of both hypertensive and normotensive people and indirectly reduces the intake of Na which is the main cause of hypertension. It also reduce the tendency of having stroke and it inhibit renal glomerular, vascular and tabular damage[125]. It is therefore necessary to monitor the dietary intake of potassium (K) to optimize the dietary management of blood pressure in the population. As for bromine is concerned, there is no substantial scientific evidence to show the physiological benefit of Br for maintaining good nutrition or healthy human function[126], but rather it combines with hemoglobin causing hematologic disease. Bromine also has a high tendency to displace iodine (I) and thereby reducing iodine accumulation not only in mammary glands but also in thyroid gland[127], hence the analysis of Tea for the detection of Br data is important to consumers. Chromium gets into food chain through environmental media such as air, water and soil, and then cause havoc in human body. It can exist in the body in two oxidation states: toxic Cr (VI) and considerable less toxic Cr (III). Cr (VI) is considered to have more toxicological effect because of its high oxidation tendency and it is known as human carcinogen and mutagen [128-130]. Cr (VI) is the most prevailing oxidation state of chromium in food, and is usually involved in pathogenesis of diseases like lung, kidney, liver and gastrointestinal cancers. Other health issues from chromium (Cr) intake even at low concentration levels are skin allergy, asthma and renal diseases [131,132]. Till date there is little information about the level of chromium and bromine in tea in literatures. Due to this reason, there is a compelling need to determine the level of chromium in tea especially for the safety of people who are drinking tea.

In order to determine the concentration of nutritional and toxic elements present in the tea samples, calibration curves are usually drawn. The slope of such curves can be used to estimate the sensitivity of our LIBS method according to IUPAC (International Union of Pure and Applied Chemistry) definition. The conventional methods used for elemental analysis among which are inductively coupled plasma, optical emission spectroscopy (ICP-OES), ICP- Mass spectroscopy (ICP-MS), neutron activation analysis (NAA) and ion chromatography , but these methods have inherited disadvantages especially in their sample preparation which requires lengthy and tedious pretreatment procedures and use of acid digestion under high temperature & pressure, and also the usage & disposal of hazardous chemicals which are detrimental to our environment[93-95,133-135]. In contrast, in this study, we used laser induced breakdown spectroscopy (LIBS), which is more user friendly because LIBS overcomes the above mentioned disadvantages pertinent to other conventional techniques due to its simplicity, rapidness, versatility, flexibility of its experimental set up and capability of multi-elemental analysis with little or no sample preparation. The fundamental of LIBS system is the recording of the plasma spectrum that contain all the qualitative and quantitative analytical information about the elemental composition and identification of the sample material, by using the finger print wavelengths, spectral intensities and relative intensities of the analyte [19,136]. The generation of plasma for LIBS measurement is achieved by applying high laser irradiance (energy per unit area, W/cm^2) to the surface of the test sample to be analyzed. There are a numbers of parameters which the laser irradiance depend upon, which are the laser pulse width, the laser pulse energy, the laser beam diameter and the quality of beam at the point of interaction with the analyte surface. LIBS measurement is usually performed under ambient atmospheric conditions, with no need for the sophisticated measurement chamber. We also determine the concentration level of

the nutritional and toxic elements using calibrated ICP-MS in order to compare with the results obtained from our calibrated LIBS technique.

4.2.2 Laser induced plasma (LIP) parameters (electron temperature and density): their studies for optimization of LIBS analysis of Tea samples.

The light emitted from laser induced plasma (LIP) is an important asset for the qualitative and quantitative analysis of the test sample and to study the plasma properties as well. The fundamental properties of plasma determining the light emitting from sample are plasma temperature, electron density, and the number density of the emitting species[18]. The plasma parameters (electron density and plasma temperature) determination is very important to satisfy the optically thin plasma and to obtain the Local Thermodynamic Equilibrium (LTE) conditions which are critical for the LIBS quantitative analysis. If the plasma is not in the LTE state, then there will be strong self-absorption and then the quantitative analysis for concentration determination will not be accurate. In addition, the information about the LIP temperature is important because it allows the understanding of the process occurring in the whole complicated plasma generation processes such as atomization, dissociation, and excitation and also improves the LIBS Sensitivity [60-62,137,138]. The LIP is characterized with occurrence of the following processes, namely photo-ionization, collision ionization, collisional excitation, radiative and three-body recombination, radiative decay, de-excitation process and Bremsstrahlung process[61]. As the plasma is in Local Thermodynamic Equilibrium (LTE), the entire plasma plume volume consist of all kinds of species which can be described by series of equilibrium distribution law[62] namely, Maxwell distribution which describes the plasma particles Boltzmann's statistic which describes the distribution of population in different energy levels, Saha's equation which describes the ionization process, and the radiation density which obeys

the Planck's law. The most important criterion that determine if plasma is in LTE state is having the collisional process dominating the radiative process and this could only be partly achieved in a state deviating from complete LTE. In such a state, there exists a certain energy level in which the excitation and de-excitation rate through a collisional process is equal to that through a radiative process, and such state is said to be in partial local thermodynamic equilibrium (PLTE)[139]. The most common used method to estimate LTE are electron energy distribution function (EEDF) and McWhirter criterion. The former holds when electron density (N_e) $>10^{16}$ cm^{-3} and kT < 5 eV, while the later holds when the rate of collisional process is higher than that of the radiative process, and is expressed mathematically by Eq. (17) [58,140-143] where T is the temperature of the plasma and ΔE is the largest energy gap between the upper and lower energy state of the spectroscopic lines used in the analysis, where N_e, T and ΔE are expressed in cm^{-3}, K, and eV respectively. The plasma electronic temperature can be estimated using Boltzmann equation (15).

In order to calibrate our LIBS system and validate our tea results, we recorded the spectrum of a standard mercury xenon lamp. Fig (4.1 a) depicts the mercury xenon lamp spectrum recorded with our LIBS system and a Boltzmann plot for estimation of electron temperature. We used five (5) fingerprint wavelengths of Hg I transition lines at 296.7 {$5d^{10}$ 6s 6p $3P_0 \rightarrow 5d^{10}$ 6s 6d $^3D_1$}, 365.5 { $5d^{10}$ 6s 6p $^3P_2 \rightarrow 5d^{10}$ 6s 6p $^3D_2$}, 404.6 nm{$5d^{10}$ 6s 6p $^3P_0 \rightarrow 5d^{10}$ 6s 7s $^3S_1$}, 435.8 {$5d^{10}$ 6s 6p $^3P_1 \rightarrow 5d^{10}$ 6s 7p $^3S_1$}, and 576.9 {$5d^{10}$ 6s 6p $^1P_1 \rightarrow 5d^{10}$ 6s 6d $^3D_2$} nm for which their transition probabilities are well known. These spectral lines were selected in the range of 290 - 610 nm from the mercury xenon lamp LIBS spectrum. The estimated plasma temperature (T_e) was $T_e = 6{,}591 \pm 450\ ^0$ K using the Boltzmann plot as depicted in Fig (4.1 b).

Once we have calibrated our LIBS system, tested and estimated the electron temperature and electron density of mercury lines, we applied the same method for evaluation of electron temperature and electron density of plasma generated by tea samples. Fig (4.2 a) depicts the Boltzmann plot obtained using five (5) fingerprint wavelengths of Cr I transition lines at 403.9 $\{3d^5(^2I)4s \rightarrow 3d^5(^2I)4p\}$, 425.4 $\{3d^5(^6S)4s \rightarrow 3d^5(^6S)4p\}$, 520.5 $\{3d^5(^6S)4s \rightarrow 3d^5(^6S)4p\}$, 520.8 $\{3d^5(^6S)4s \rightarrow 3d^5(^6S)4p\}$, and 529.8 $\{3d^5(^6S)4p \rightarrow 3d^5(^6S)4d\}$ nm for which their transition probabilities are also well known. These spectral lines were selected in the wavelength range of (350-450 nm) and (450-550 nm) from (tea sample #1). The estimated plasma temperature (T_e) was T_e= 6864 ± 514 K using the Boltzmann plot as depicted in Fig (4.2 a). The linearity in the Boltzmann plot depicted in Fig. (4.2 a) is a good evidence that an LTE condition is prevailed. Table (4.1) and Table (4.2) shows the tabulated spectroscopic parameters obtained from National Institute of Standard and Technology (NIST) data base for atomic lines of Mercury (Hg) and Chromium (Cr) used for plasma temperature estimation in our study for tea samples. The emission line spectrum is mostly accompanied by certain level of broadening, which can be used to estimate the electron density. The major line broadening mechanism in the LIBS spectra are Stark broadening, pressure broadening and Doppler broadening. The Stark broadening is due to columbic interaction of charged species and is the primary mechanism causing the emission line broadening. The pressure broadening is as a result of the interaction of radiating atoms with the surrounding particles, which result in frequency disturbance [144,145]. Doppler broadening is due to Doppler shift experienced by various species in plasma plume exhibiting different velocity component V_z in the direction of observation. The influence due to Doppler broadening [~0.12 Å at full width at half maximum (FWHM)] can be neglected as compared to Stark broadening resulting from collisions from charged particles that dominate the plasma density

above $10^{14}cm^{-3}$ [74,146]. The FWHM of the Stark broadening profile of a well isolated line from neutral atom is related to electron density N_e (in cm^{-3}) as defined in Eq. (17). Where W is an electron impact parameter which is a function of the temperature and only changes by a factor of two over the temperature range of 10,000- 80,000K. The Stark broadened profile of an isolated atomic or singly charged ionic line is one of the most powerful spectroscopic techniques used in the calculation of electron density to a very reasonable accuracy. To estimate the electron density, we used the Stark broadened profile of Hg (I) 435.8 $\{5d^{10}\ 6s\ 6p\ ^3P_1 \rightarrow 5d^{10}\ 6s\ 7p\ ^3S_1\}$ at 435.8 nm and Stark broadened profile of Cr (I) transition $\{3d^5(^6S)\ 4p \rightarrow 3d^5\ (^6S)\ 4d\}$ at 529.8 nm, which are depicted in Fig (4.1 c) and Fig (4.2 b) respectively. The evaluated electron densities (n_e) using the Full Width at Half Maximum (FWHM) of 0.96767 and 0.23133 for Hg I and Cr I respectively are 1.2×10^{17} cm^{-3} and 1.03×10^{17} cm^{-3}. It is worth mentioning that the estimated electron density meet the EEDF criterion for LTE with the estimated electron density $n_e > 10^{16}$ cm^{-3} and KT = 0.59 eV, also the estimated n_e greater than the critical electron density (1.9×10^{16} cm^{-3}), which implies that McWhirter criterion is also satisfied for LTE condition. Based on our estimated plasma parameters (temperature and density), we can assume that our plasma is in LTE regime.

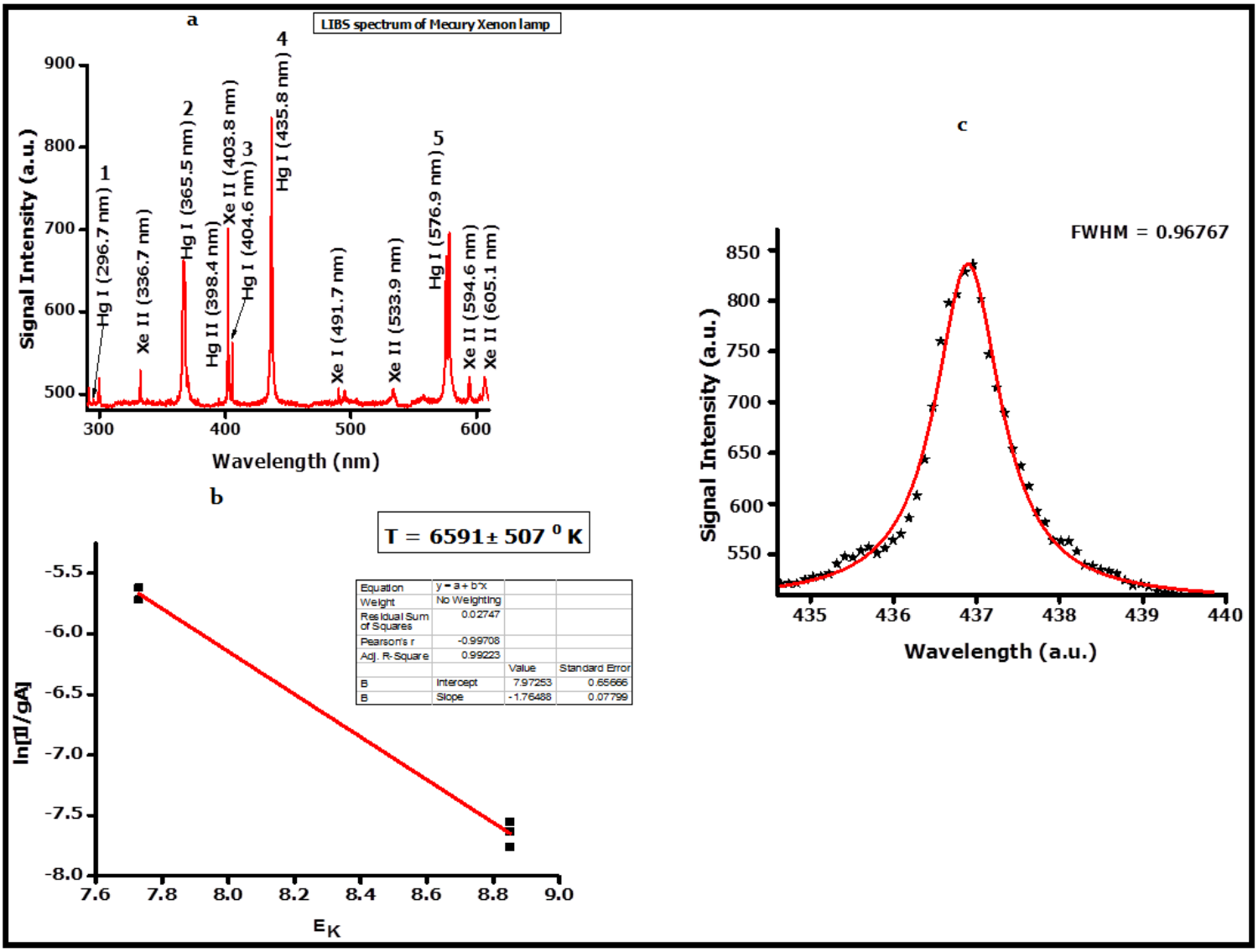

Figure 4.1. (a) Typical LIBS spectrum of mercury xenon lamp in the wavelength range 290-610 nm (b) Typical Boltzmann plot for plasma temperature estimation using LIBS spectrum from mercury xenon lamp (c) Typical Stark broadened profile of neutral atomic

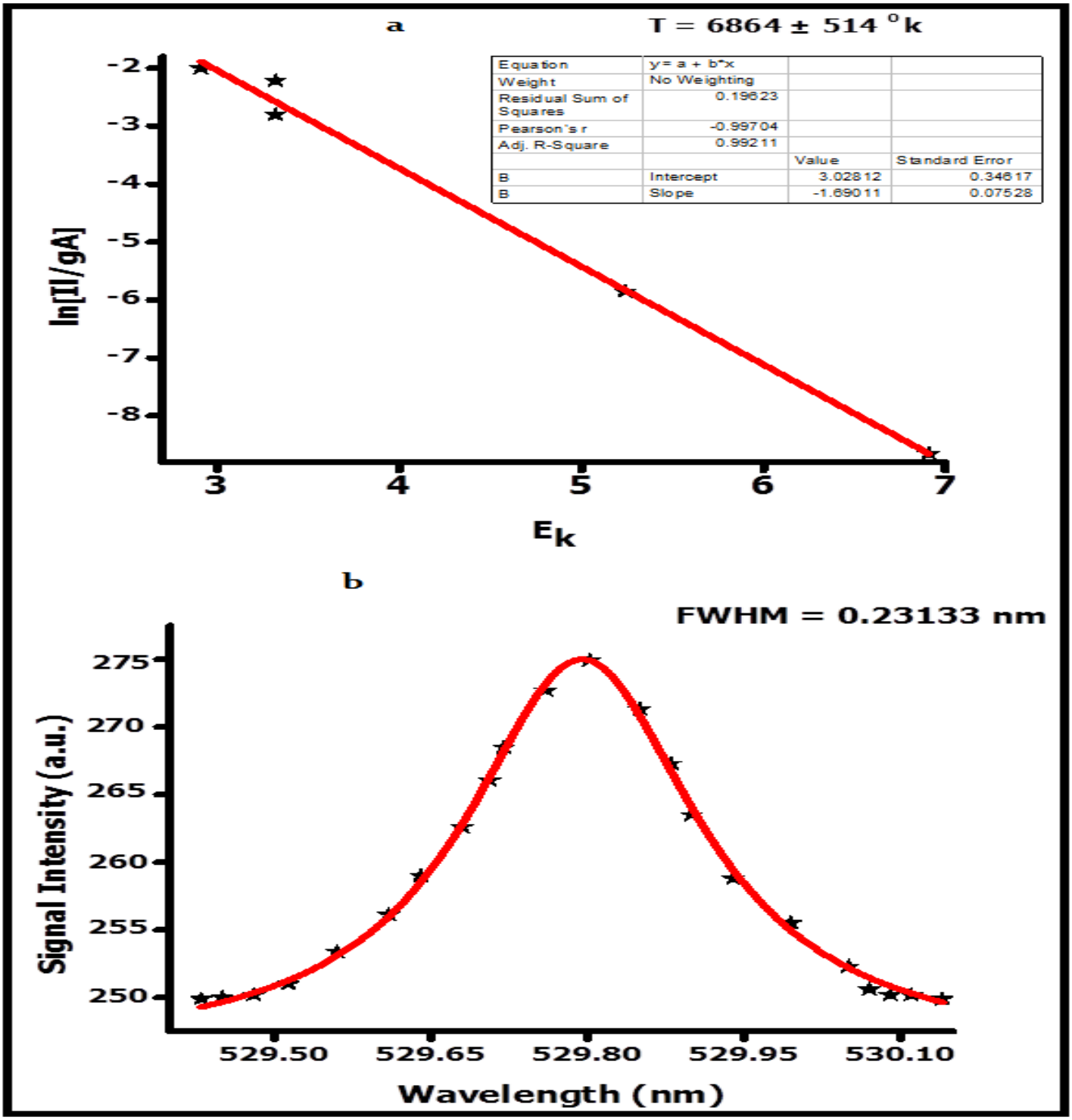

Fig 4.2. (a) Typical Boltzmann plot for plasma temperature estimation. Spectral lines of neutral chromium (Cr I) were used to plot the Boltzmann plot with plasma temperature of T = 6864 ± 514 0K (b) Typical Stark broadened profile of neutral atomic Cr (I)

4.2.3 Delay time and Incident laser energy optimization for detection of chromium, bromine, potassium and iron

Before conducting the LIBS experiment for the analysis of tea samples, it is important to optimize different LIBS parameters such as delay time, laser energy and others parameters. To attain best LIBS sensitivity in our case, we used sample #1 throughout the optimization process. The optimization of LIBS signal intensity versus delay time for detection of Fe II (275.6 nm) line and Cr II (286.5 nm) line within wavelength range 250-350 nm was achieved by plotting the ratio of LIBS signal intensity of Cr II (286.5 nm)/ LIBS signal intensity of Fe II (276.6 nm) against the delay time. The optimum delay time within the wavelength range 250-350 nm for the simultaneous detection of both Cr II (286.5 nm) and Fe II (276.6 nm) was found to be 357 ns corresponding to Cr II (286.5 nm) / Fe II (276.6 nm) signal intensity ratio of 1.24 is depicted in the Fig. 4.3a. Similarly, the optimization of LIBS signal intensity versus delay time for simultaneous detection of K I (766.48 nm) and Br (793.9 nm) within the wavelength range 750-850 nm was achieved by plotting the ratio of LIBS signal intensity of K I (766.48 nm)/ LIBS signal intensity of Br I (793.9 nm) against delay time is depicted in Fig. 4.3 b. The optimum delay time obtained from the plot was 317 ns corresponding to K I (766.48 nm)/ Br I (793.9 nm) LIBS signal intensity ratio of 2.07 as depicted in Fig. 4.3 b. Additionally, the optimization of laser energy was carried out within the wavelength range 750-850 nm. The various laser energies applied on the sample are 15 mJ, 15.4 mJ, 15.8mJ, 17.0 mJ and 17.52 mJ per pulse, and the various emission signal intensity was recorded for K I (766.48 nm) and Br I (793.9 nm) simultaneously to obtained the optimum laser energy. By plotting the ratio of LIBS signal

intensity of K I (766.48 nm)/ LIBS signal intensity of Br I (793.9 nm) against laser energies, the optimum laser energy was found to be 17.52 mJ is depicted in Fig. 4.4.

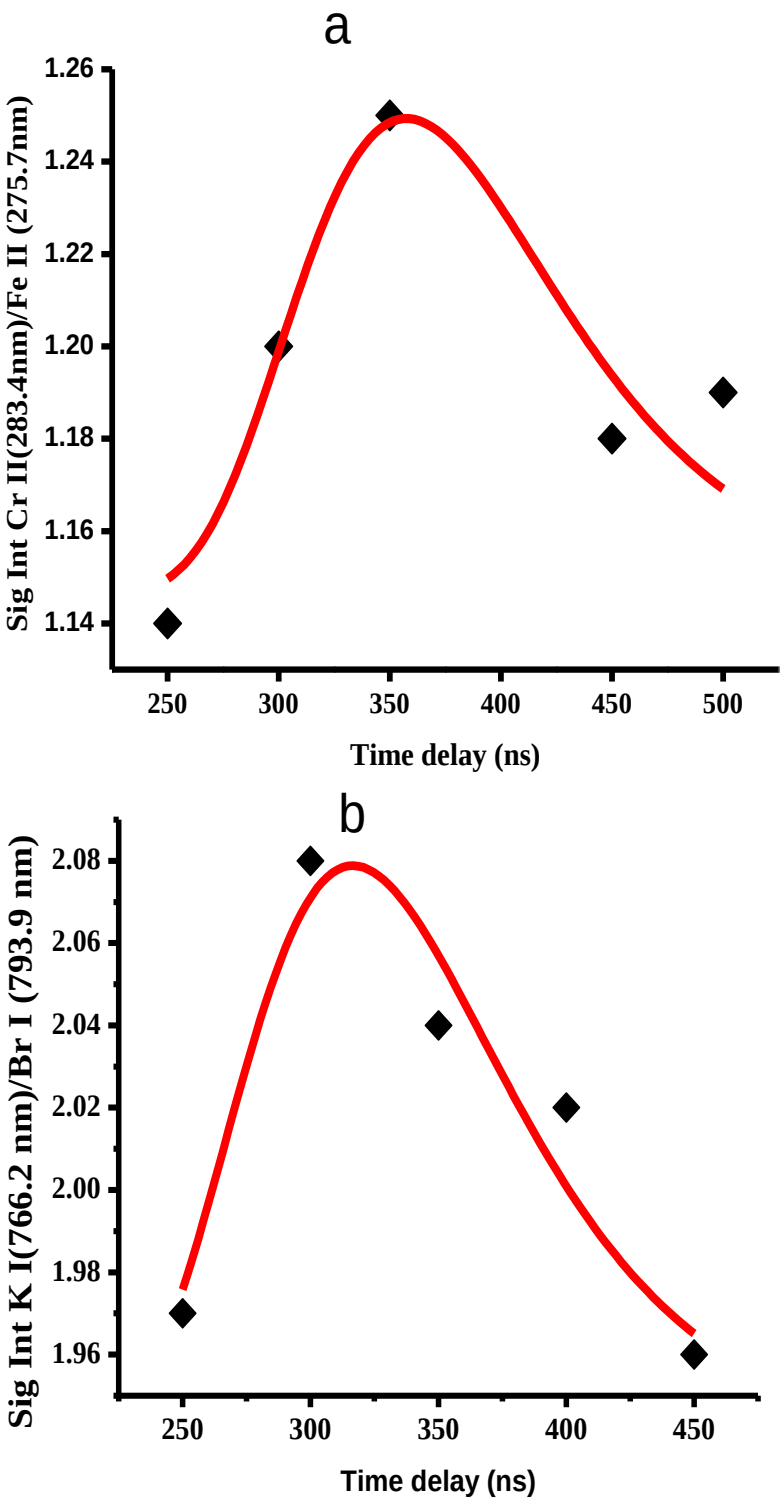

Figure. 4.3. The dependence of LIBS signal intensity ratio of emission lines K I (766.48 nm)/Br I (793.9 nm) and Fe II (275.6 nm)/Cr II (286.5 nm) Vs delay time for our tea sample

.

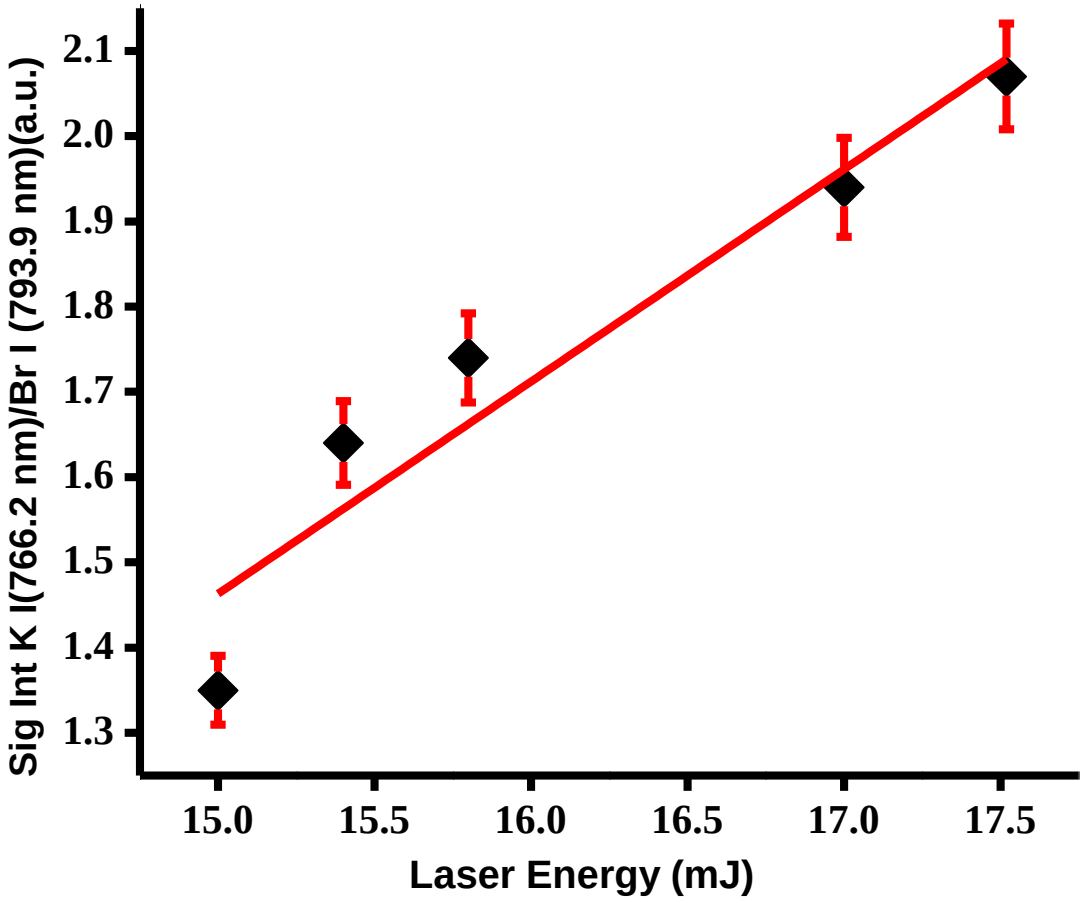

Fig. 4.4. The dependence of LIBS signal intensity ratio of emission line K I (766.29 nm)/Br I (793.9nm) on laser energy for the tea sample.

4.2.4 LIBS Qualitative analysis of tea samples

The optimized experimental laser parameters such as laser energy, time delay between the opening of ICCD shutter and laser pulse incident, number of accumulation and geometrical arrangement were all optimized and kept same for all the data acquisition process as described in the previous section. In order to identify the composition of tea samples, it is required to carry

out the compositional analysis first, and then afterwards to determine the elements of interest. Fig. 4.5 -4.10 shows a typical LIBS spectra for six brands (sample 1-6) of tea samples in the wavelength range of 380-730 nm, where the spectrally identified element are Iron (Fe), Titanium (Ti), Chromium (Cr), Aluminum (Al), Potassium (K), Magnesium (Mg), Bromine (Br), Silicon (Si) Carbon (C), Vanadium (V) and Calcium (Ca) using the spectra data published by National Institute of standard and technology (NIST). Fig. 5.11 shows a typical LIBS spectra for six brands (sample 1-6) of tea samples in the wavelength range of 250-350 nm, with strong ionic emission lines of Fe II at 275.6 nm and Cr II at 286.5 nm. The finger print wavelength or signature lines of Fe II (275.6 nm) and Cr II (286.5 nm) was identified in all brands of the tea samples as depicted in Fig. 5.11. Other atomic and ionic emission lines identified within the wavelength range 250-350 nm are Fe I (277. 2 nm), Fe I (283.8 nm), Fe I (297.3 nm), K I (310.5nm), Ca II (317.9 nm) and Si II (320.0 nm), with notable differences in their emission lines intensities, which indicates differences in their concentration from one tea sample to the other. Fig. 5.12 shows a typical LIBS spectra for the six brands of tea samples in the wavelength range of 760-800 nm, with strong atomic emission lines of K I at 766.5 nm and Br I at 793.9 nm, with varied emission line intensities from one tea sample to the other, which indicate different elemental content. The signature lines of K I (766.5 nm) and Br I (793.9 nm) are well identified in all brands of the tea sample as depicted within a box in Fig. 5.12. Other atomic and ionic emission lines identified within the wavelength range 760-800 nm are Cu II (777. 9 nm), Cu II (774.4 nm) and Si II (784.9 nm) with notable differences in their emission lines intensities, which indicates the difference in their concentration from one tea sample to the other sample.

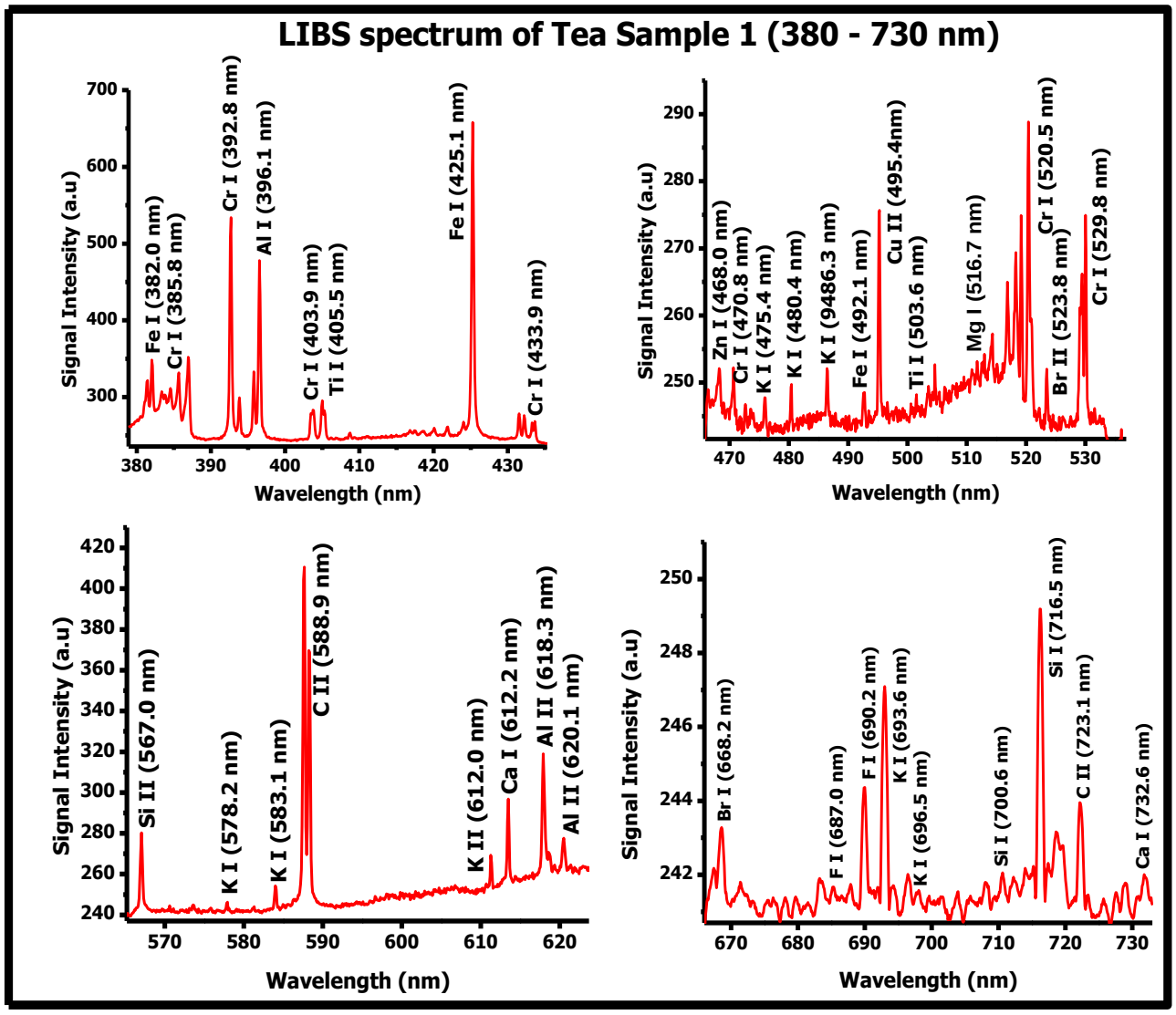

Figure 4.5: Typical LIBS spectra of tea sample #1 from wavelength range 380 -730 nm.

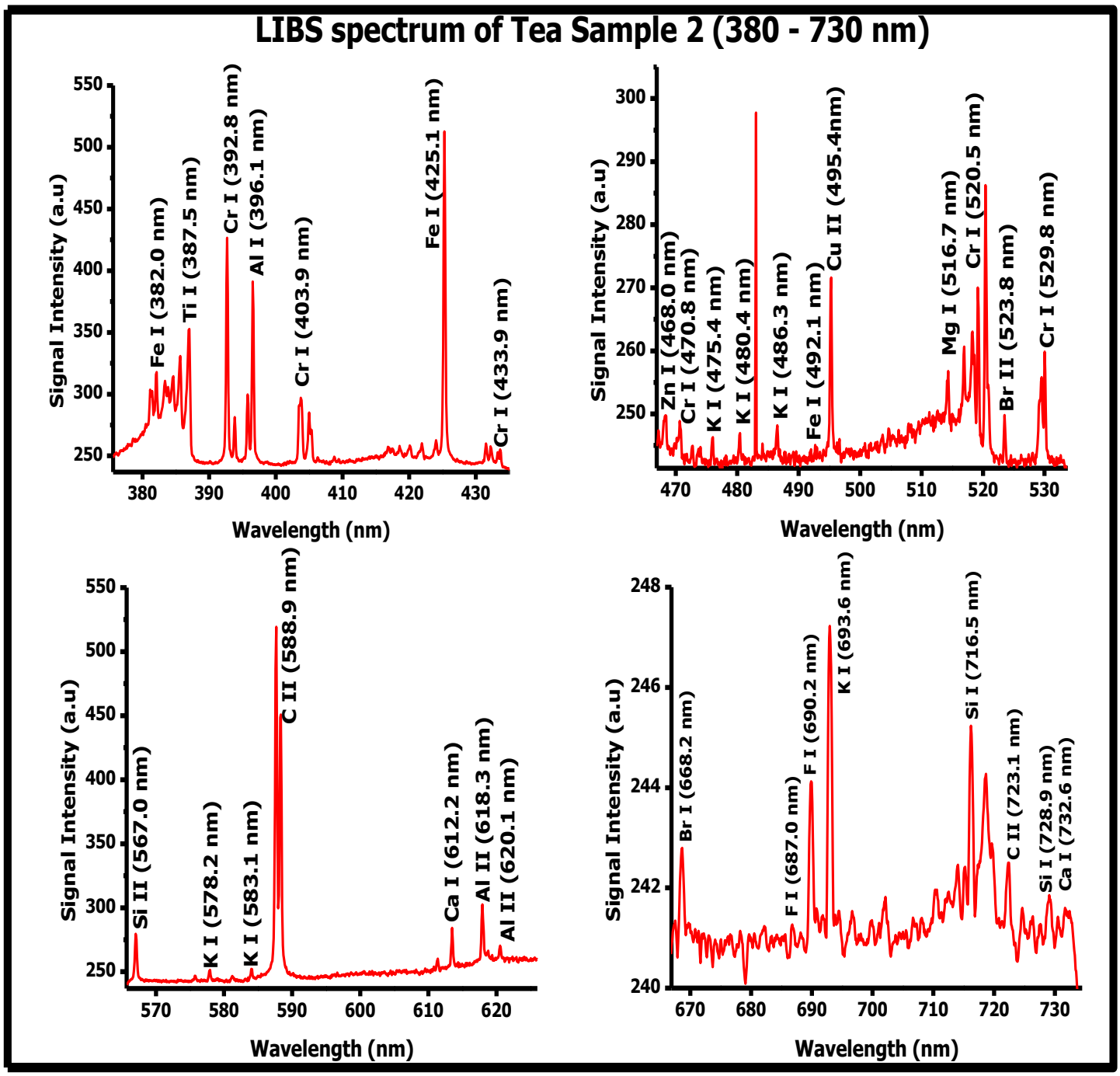

Figure 4.6: Typical LIBS spectra of tea sample #2 from wavelength range 380 -730 nm.

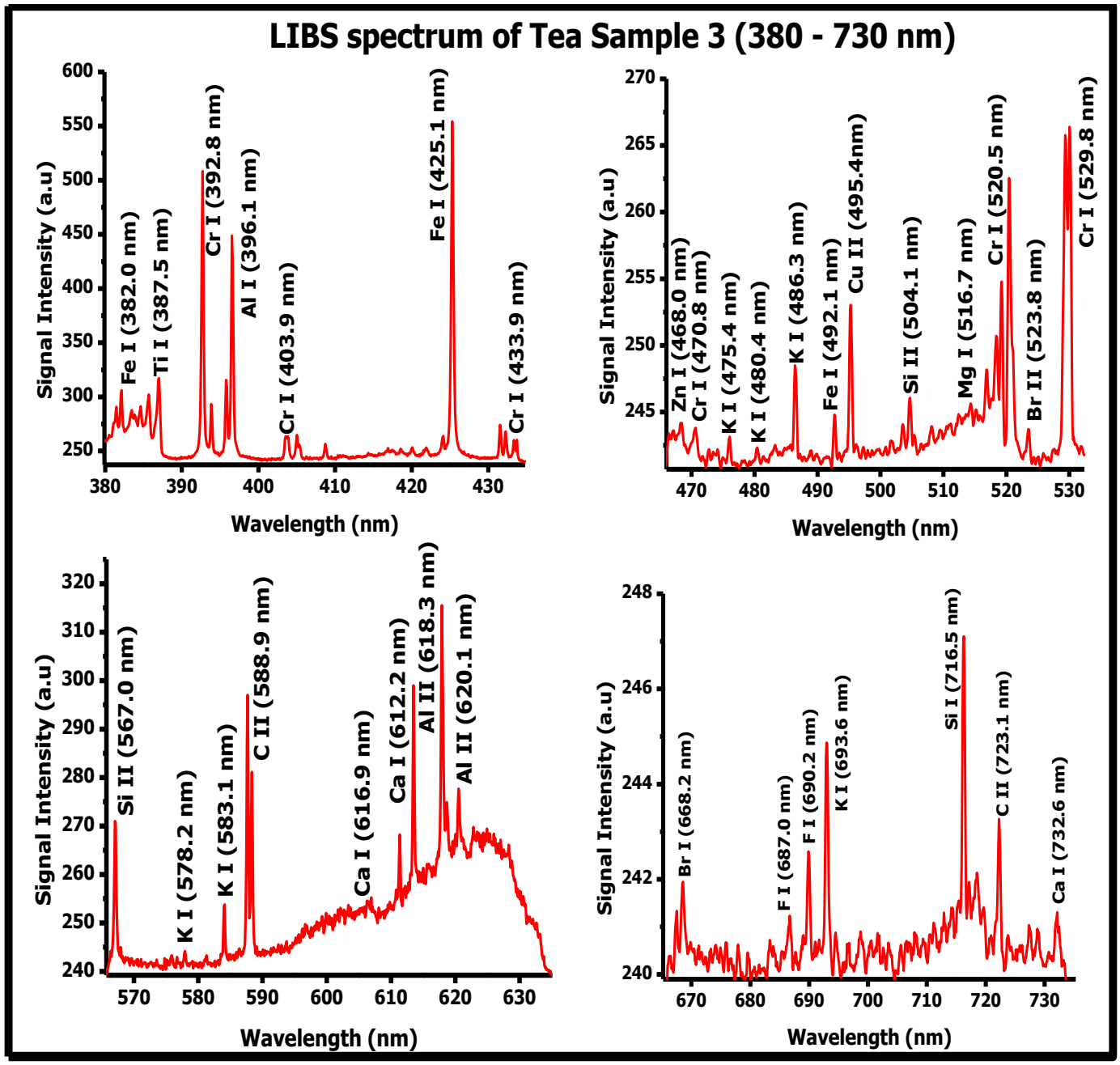

Figure 4.7: Typical LIBS spectra of tea sample #3 from wavelength range 380 -730 nm.

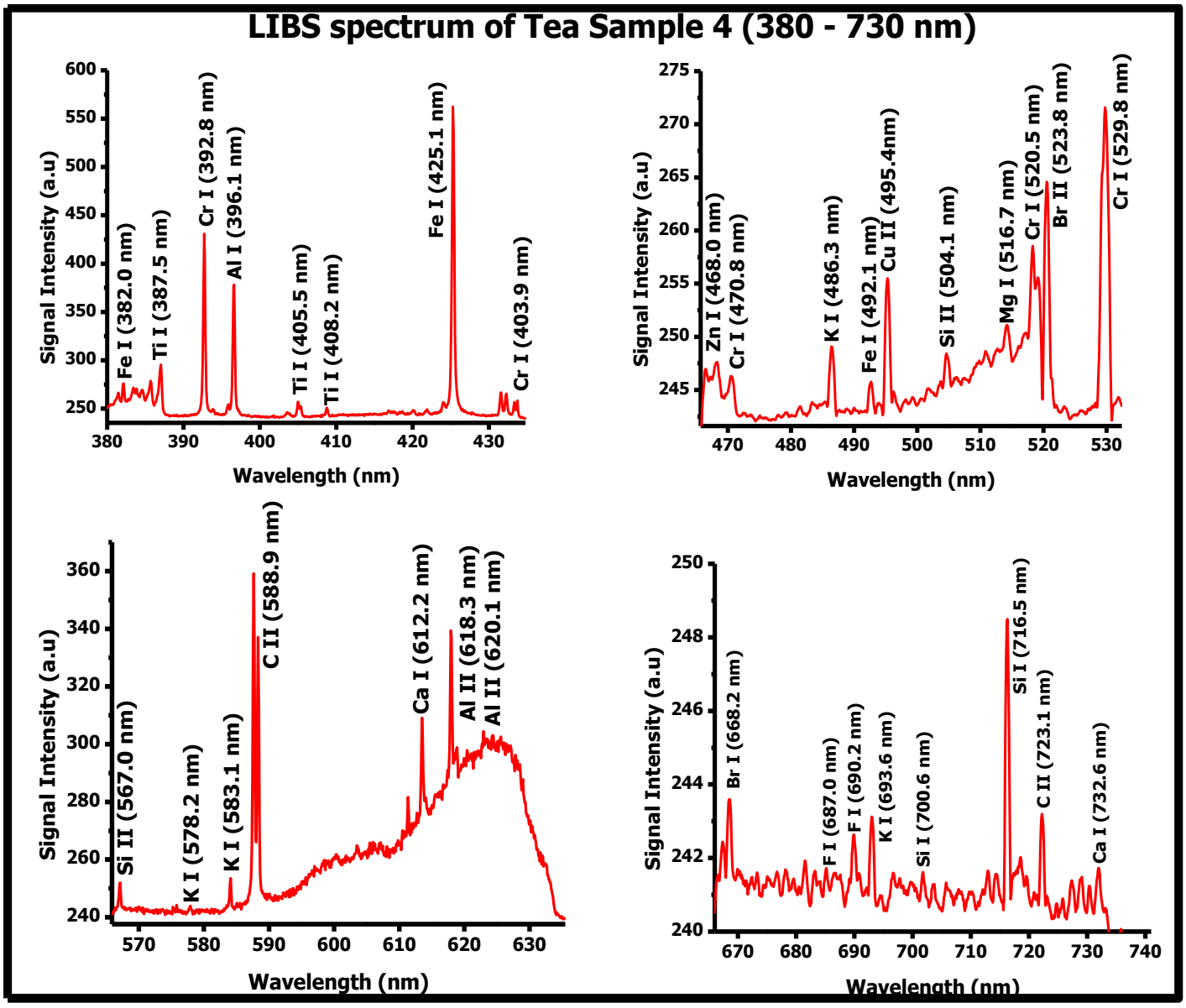

Figure 4.8: Typical LIBS spectra of tea sample #4 from wavelength range 380 -730 nm.

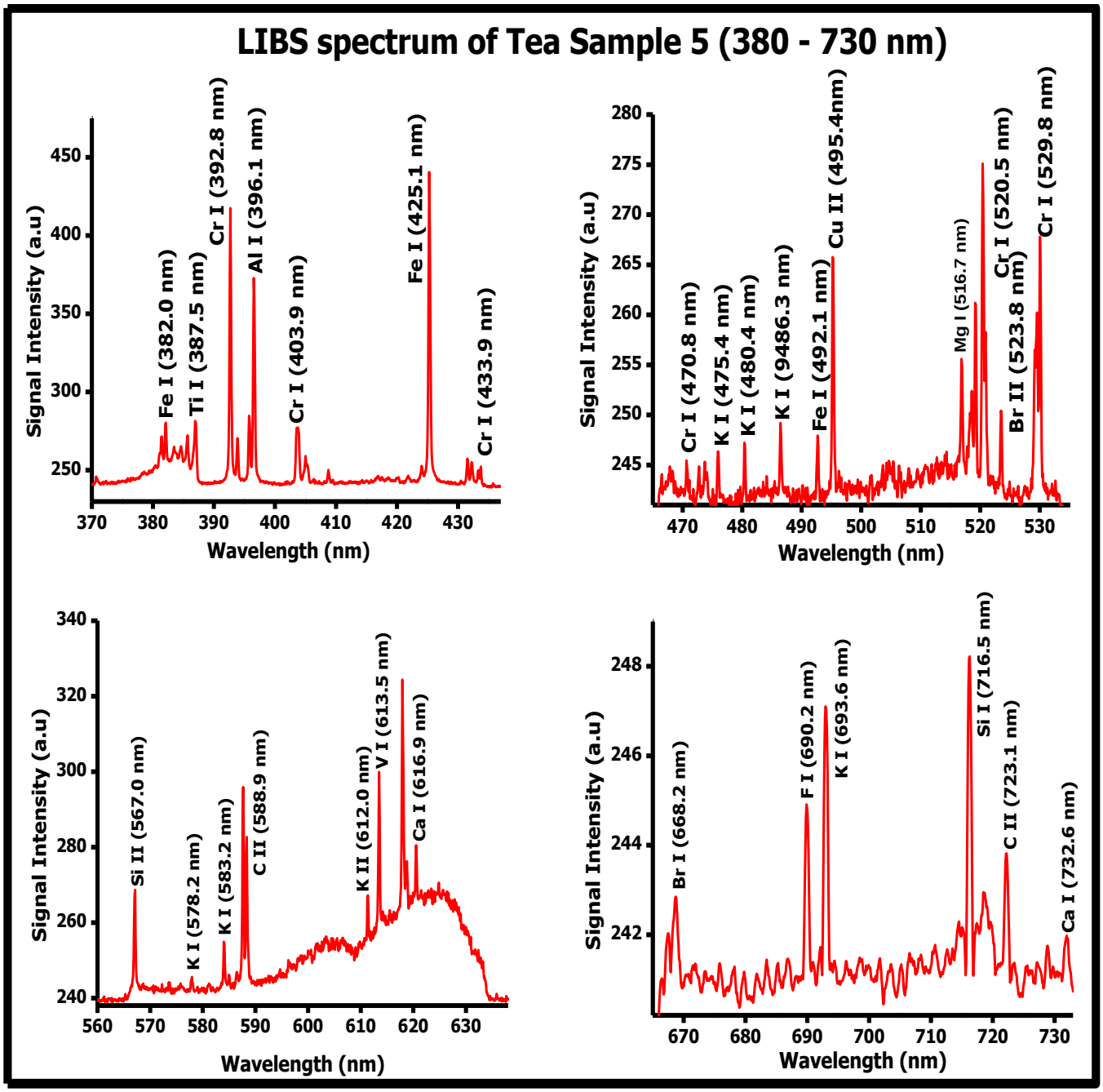

Figure 4.9: Typical LIBS spectra of tea sample #5 from wavelength range 380 -730 nm.

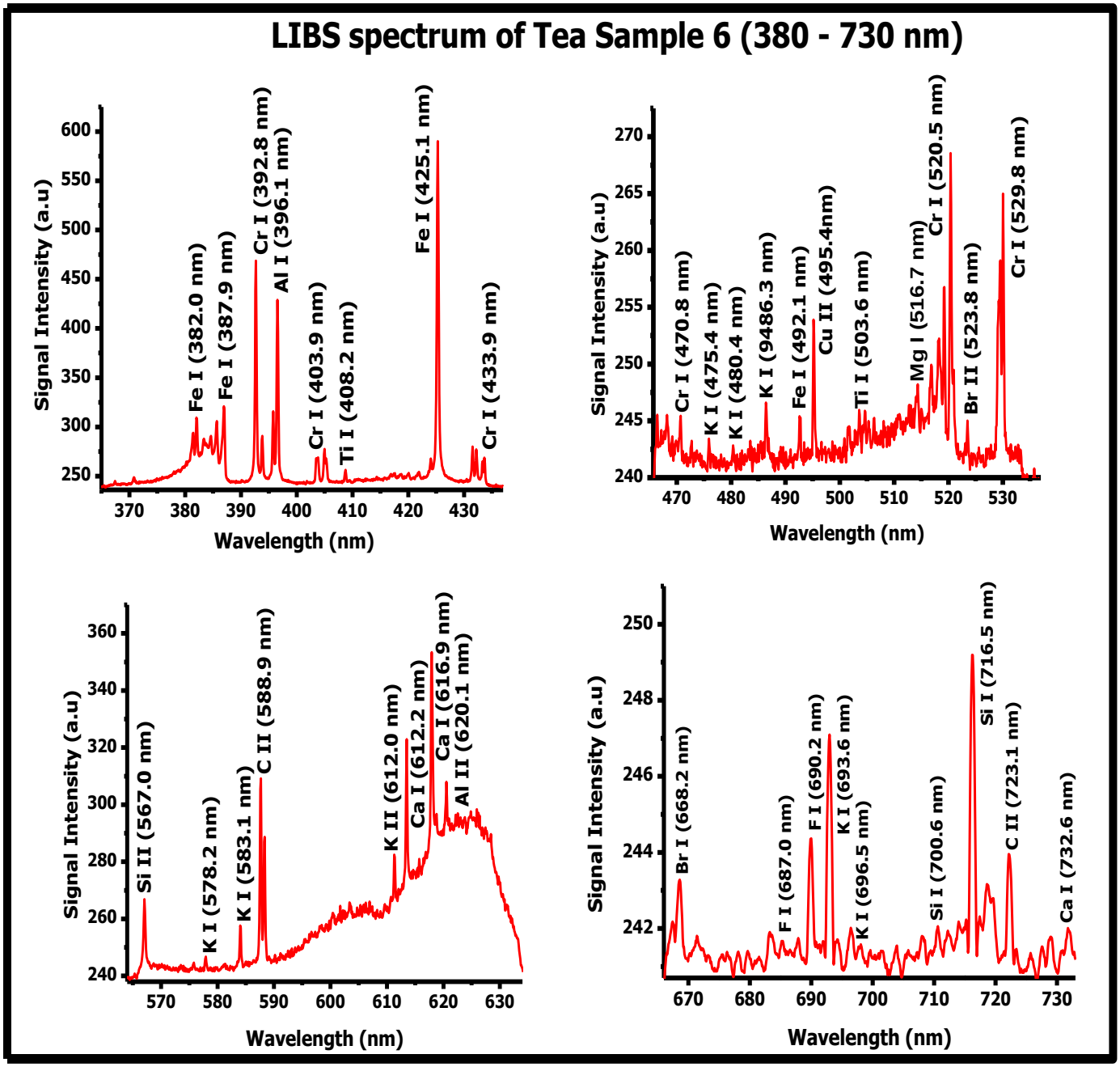

Figure 4.10: Typical LIBS spectra of tea sample #6 from wavelength range 380 -730 nm.

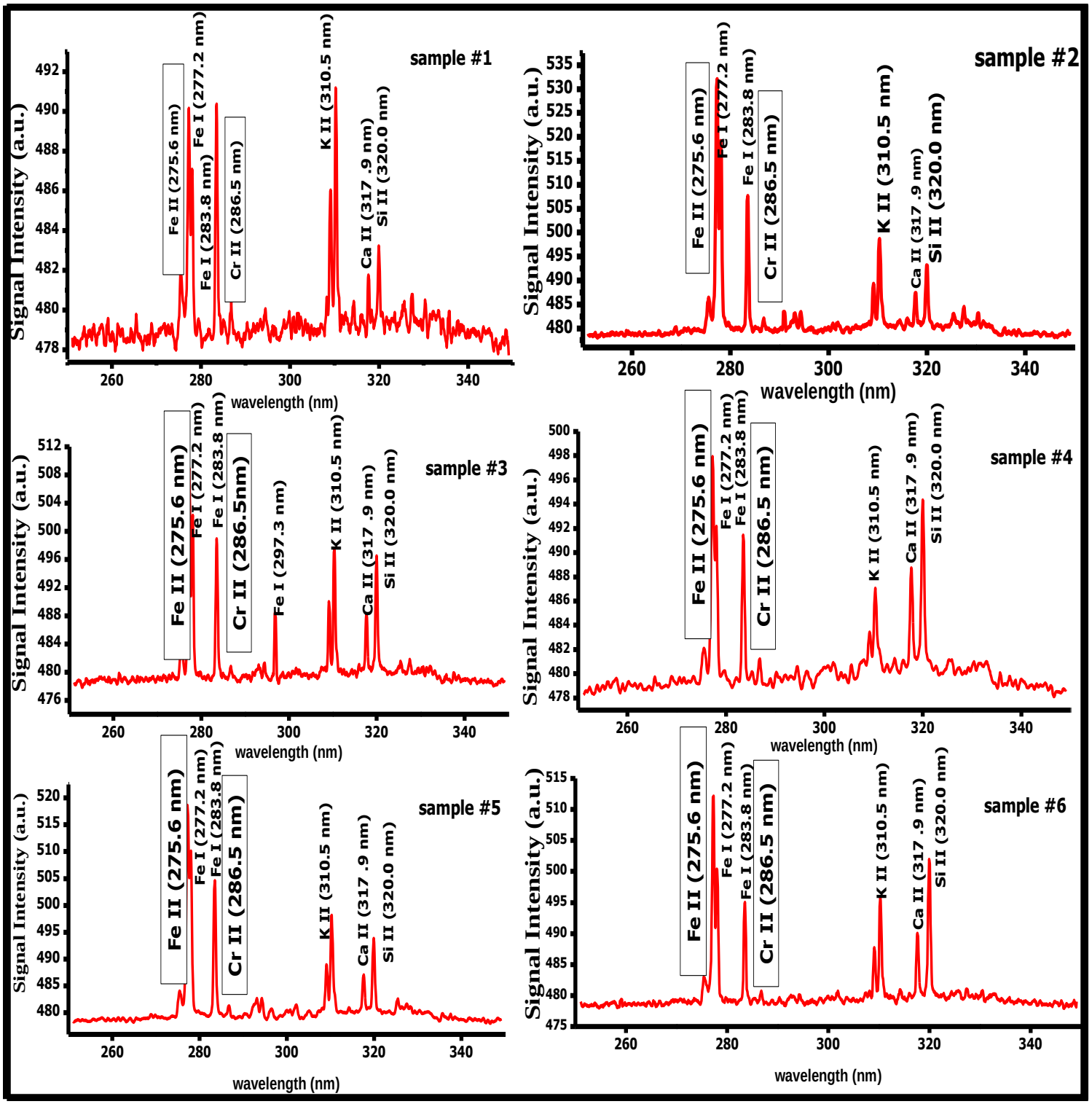

Fig 4.11 Emission line spectra of Iron and chromium in the wavelength range 250-350 nm for tea (sample 1-6). The signature line for Fe II (275.6 nm) and Cr II (286.5 nm) are enclosed in a box.

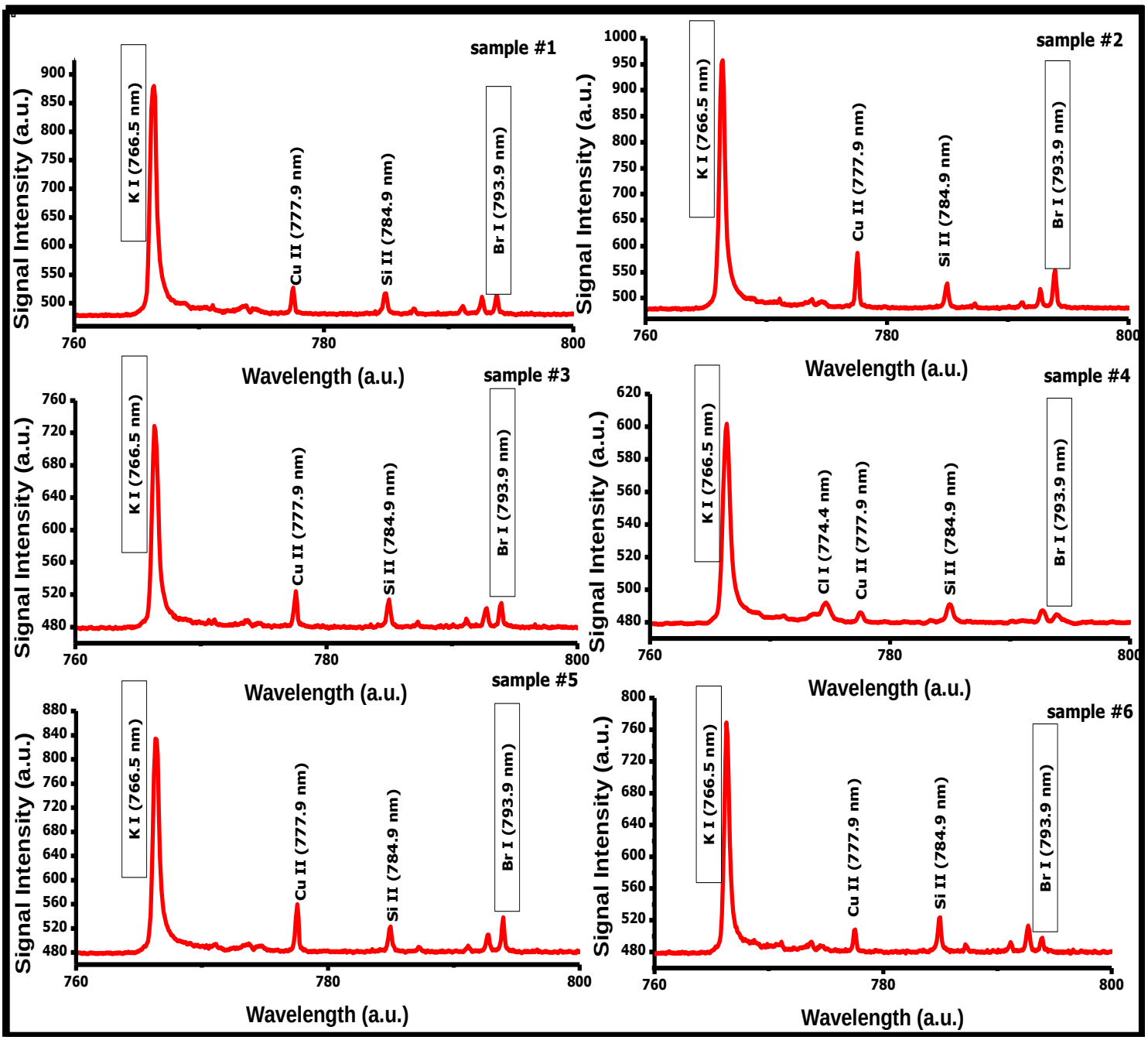

Fig 4.12. Emission line spectra of potassium and bromine in the wavelength range 750-850 nm for tea (sample 1-6). The signature lines for K I (766.5 nm) and Br I (793.9 nm) are enclosed in a box.

4.2.5 LIBS Quantitative analysis of Tea sample

In quantitative LIBS analysis, ionic and atomic emission line intensities can be used for quantification of different species in the sample (e.g. in parts-pert-million)[73]. The quantification usually is conducted by constructing a calibration curve based on some set of samples (usually above three) with different known concentration of a specific analyte. The calibration curve provides a means to estimate the concentration of a specific species in an unknown sample. A plot of emission line intensities of a particular specie versus its concentration gives the calibration curve. Fig. 4.13 depicts typical calibration curves for the quantification of different nutritional and toxic elements (Fe, Cr, K, Br, Cu, Si, and Ca) present in the six brands of the tea sample. Each value of R^2 on Fig. 4.13 are coefficient indicating accuracy of our linear fit (i.e. R^2 is very close to 1). From the calibration curves, the concentration of each element was determined and tabulated in Table 4.3.

To further confirm our LIBS quantification results, we determined the concentration of the same element in all the tea samples using standard analytical technique like ICP-MS, the results obtained are also tabulated in Table 4.3, which are in excellent agreement with ours LIBS results as depicted in Fig 4.14. The concentration of iron, chromium, potassium and bromine estimated in all the tea samples are between 378-656 ppm, 96-124 ppm, 1421-6785 ppm, 99-1476 ppm, 17-36 ppm, 2-11ppm and 92-130 ppm respectively. The estimated concentration of iron in all tea samples are in good agreement with previously reported results[147]. The estimated concentration of iron (Fe), calcium (Ca) and potassium (K) in various tea samples shows that the tea samples are highly rich in iron (Fe), Calcium (Ca) and potassium (K), which are highly needed in our human body system for good health, with sample #1 having the highest concentration of K. On the other hand, there are also some toxic element (Chromium and

Bromine) with concentration above the permissible limit set by Saudi Food and Drug Authority (SFDA), with sample #2 having the highest concentration of Cr and Br.

The limit of detection (LOD) of the nutritional and toxic element in the tea samples were also determined according to equation (19) defined as $3\sigma/S$, where σ is the standard deviation of the least concentrated sample and S is the slope of the calibration curve[45]. The LOD estimated for Fe, Cr, K, Br, Cu, Si, and Ca in tea sample were 22, 12, 16, 11, 6, 1 and 12 ppm respectively as tabulated also in Table 4.3.

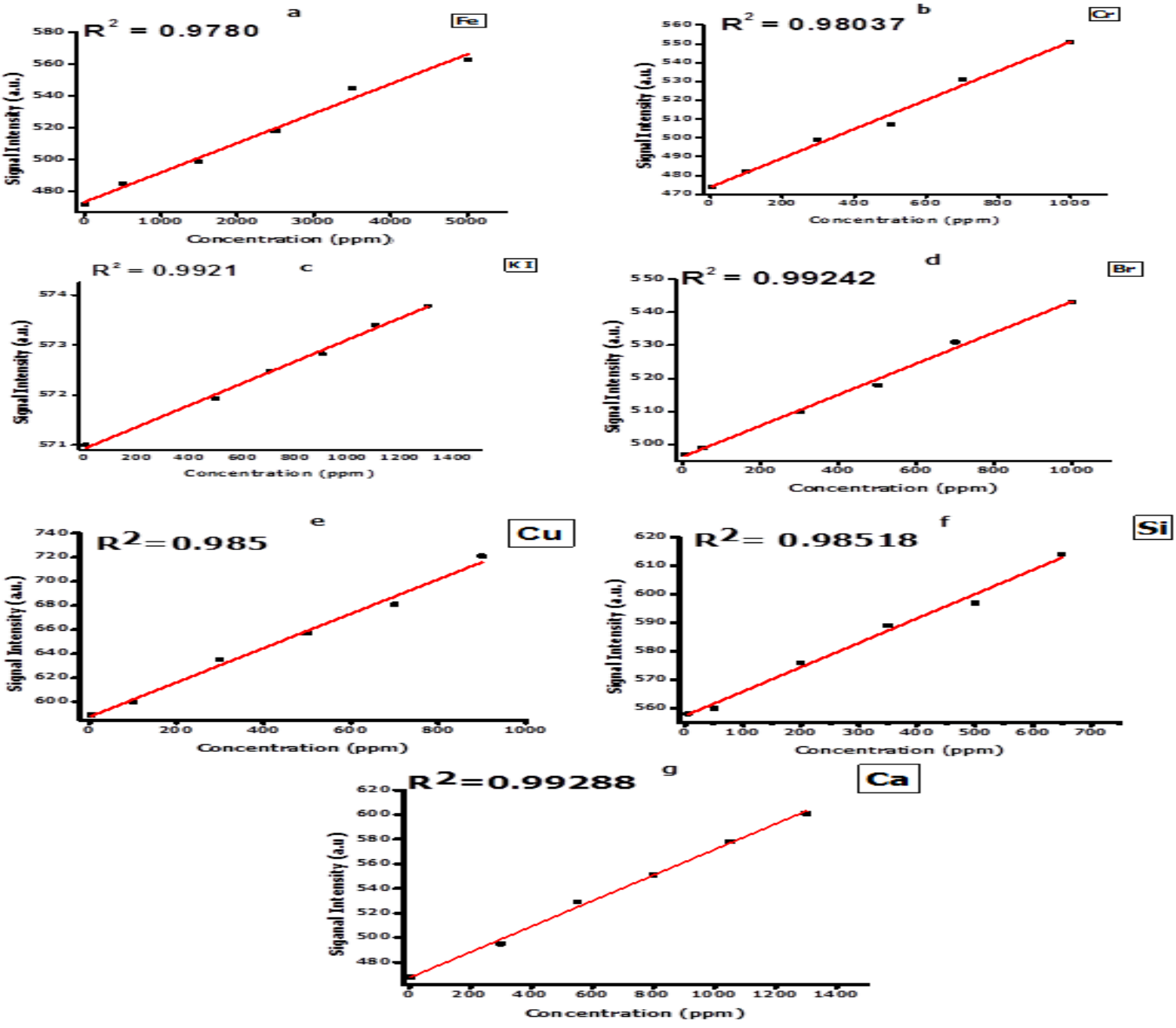

Figure 4.13: A calibration curve for (a) Iron Fe II (b) Chromium Cr II (c) Potassium K I (d) Bromine Br I (e) Copper Cu II (f) Silicon Si II (g) Calcium Ca II

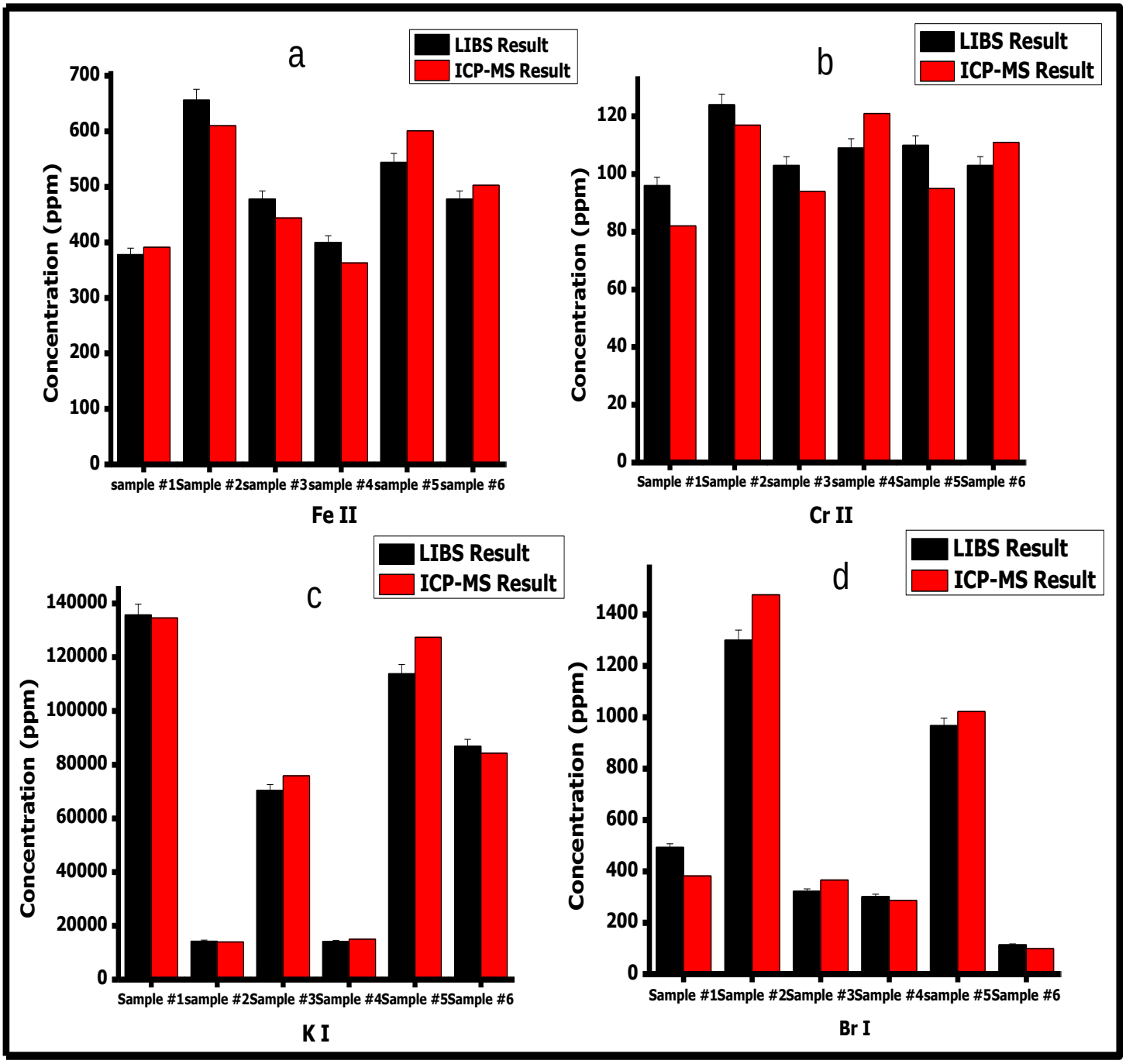

Figure 4.14. Comparison between Concentrations of different element obtained from LIBS and ICP-MS technique for (a) Fe II (b) Cr II (c) K I (d) Br I.

Table 4.1. Spectroscopic parameters of neutral mercury (Hg I) line taken from NIST data base used for plasma temperature estimation.

Wavelength (nm)	Signal Intensity	Statistical weight		$T_{ransition}$ probability	Energy of the upper level	
		g_i	g_k	A_{ik} (S^{-1})	Ei (eV)	Ek (eV)
296.7	494	1	3	4.5e+07	4.67	8.85
365.5	664	5	5	1.8e+07	5.46	8.85
404.6	564	1	3	2.1e+07	4.67	7.73
435.8	836	3	3	5.57e+07	4.89	7.73
576.9	698	3	5	2.36e+07	6.71	8.85

Table 4.2. Spectroscopic parameters of neutral chromium (Cr I) line taken from NIST data base used for plasma temperature estimation.

Wavelength (nm)	Signal Intensity	Statistical weight		$T_{ransition}$ probability	Energy of the upper level	
		g_i	g_k	A_{ik} (S^{-1})	Ei (eV)	Ek (eV)
403.9	279	15	15	6.70E+07	3.85	6.91
425.4	658	7	9	3.15E+07	0	2.91
520.5	289	5	3	5.09E+07	0.94	3.32
520.8	259	5	7	5.06E+07	0.94	3.32
529.8	266	7	7	3.00E+07	2.9	5.24

Table 4.3. Comparison of LIBS and ICPMS estimated concentration, Resolution of different emission lines and Limit of Detection (LOD) for different Nutritional and toxic element detected in Tea samples.

Quantified Element detected in Tea	Wavelength (nm)	Sample Names	Comparison Between LIBS and ICM-MS results.		Limit of Detection (LOD)
			LIBS Concentration (ppm)	ICP Concentration (ppm)	
Fe	275.6	Sample#1:	1378	391	22
		Sample#2:	656	610	
		Sample#3:	478	444	
		Sample#4:	400	363	
		Sample#5:	544	601	
		Sample#6:	478	503	
Cr	286.5	Sample#1:	96	82	12
		Sample#2:	124	117	
		Sample#3:	103	94	
		Sample#4:	109	121	
		Sample#5:	110	95	
		Sample#6:	103	111	
K	766.5	Sample#1:	6785	6732	14
		Sample#2:	1761	1897	
		Sample#3:	3523	3793	
		Sample#4:	1421	1500	
		Sample#5:	5690	6369	
		Sample#6:	4341	4213	

Br	793.9	Sample#1:	493	382	11
		Sample#2:	1300	1476	
		Sample#3:	322	366	
		Sample#4:	302	287	
		Sample#5:	967	1022	
		Sample#6:	114	99	
Cu	777.9	Sample#1:	34	33	6
		Sample#2:	36	35	
		Sample#3:	22	17	
		Sample#4:	17	20	
		Sample#5:	33	36	
		Sample#6:	29	32	
Si	784.9	Sample#1:	5	7	1
		Sample#2:	13	11	
		Sample#3:	4	3	
		Sample#4:	7	9	
		Sample#5:	2	2	
		Sample#6:	6	5	
Ca	317.9	Sample#1:	105	109	12
		Sample#2:	115	104	
		Sample#3:	92	86	
		Sample#4:	121	117	
		Sample#5:	123	119	
		Sample#6:	130	121	

4.3 Spectro-chemical analysis and nutritional composition of date palm fruits using laser Induced breakdown spectroscopy and cross validation of results with inductively coupled plasma mass spectrometry.

4. 3. 1 Introduction

Palm dates (*phoenix dactylifera L*) is primitively grown tree. Its fruit has been in use, particularly in Arab countries, for nearly 6,000 years. It is one of the staple foods for Arabs [148]. Carbohydrates, amounting to more than 70 % (including sucrose, glucose and fructose) are the major ingredients in dates [149-151]. Besides carbohydrates and food fibers, dates also serve as a central source of vitamins and food minerals. Date pulps contain high amount of several elements like Fe, Ca, Co, Cu, F, Mg, Mn, K, P, Na, S, B, Se and Zn. Primary fluorine in dates helps fight tooth decay[152,153]. Dietary fiber ratio in dates ranges from 6 to 25 % in flesh and almost 80 % in seeds. Dates also have high amounts of proteins, lipids, vitamins, carotenoids and phenolic compounds[149]. Besides, dates are rich reserves of easily soluble compounds (70% to be exact) like fructose, sucrose, glucose, dietary fibers and less fats and proteins. Dates contribute healthy components like vitamins riboflavin, thiamine, biotin, folic acid etc. Phytochemicals like plant sterols, carotenoids, phenolics, anthocyanins, procyanidins and flavonoids are found in abundance in date pulp. Plant sterols, bearing numerous health advantages, are usually termed phytosterols. On a laboratory analysis of date fruit sterols, it was observed that they have cholesterol, isofucosterol, , β-sitosterol and stigmasterol. Carotenoids, a class of naturally found fat-soluble pigments; not only provide a bright colour to the plants, they are also a rich source of vitamin A and act as anti-oxidants and help fight against the harmful effects of free radicals[154]. Vegetable flavonoids have a lot of advantages for health. They act as anti-oxidants and help to protect against radical scavenging. They fight various chronic

diseases of cardiovascular origin and reduce the speed of certain processes in body that help to grow cancer[155]. On account of the above mentioned properties, date fruits are treasure house of energy and it is estimated that 314 Kcal of energy can be obtained by consuming about 100 grams of dates. The Arabs use date pits (generally thought of as waste product) to prepare caffeine-free drinks. Date pit powder is also used to prepare non-caffeinated coffee. An approximate of 5.1 g/100 g protein, 9.0 g / 100 g fat, 73.1 g/100 g dietary fiber, 3942 mg/100 g phenolics and 80400 µ mol/ 100 g anti-oxidants are found in date pits; a sure symbol of nutrition. Date consumption is a natural way of strengthening body against premature graying of hair, formation of wrinkles. The result of date consumption is a healthy glowing skin and youthfulness restoration. Date kernels also show similar characteristics, particularly beneficial for women whose skin ages and wrinkles fast.

Date pulp boiled in milk and then softened down, serves as a healthy tonic for pregnant women and breastfeeding mothers. Similarly, dried dates, pounded and crushed and mixed with an assortment of almonds, pistachio nuts, quince seeds, sugar and spices are very beneficial for the health of pregnant women and new mother[155]. Dates are usually given to the patients of respiratory ailments, asthma, chest infections, fevers of various sorts, high blood pressure and fatigue; as a complete compulsory medication. Different infectious diseases and ailments such as atherosclerosis, diabetes, hypertension and cancer have also been successfully treated with dates. Folk medicine has been employing dates as main ingredient ever since the beginning of recorded history. Pathogenesis of chronic diseases takes oxidative stress as one of its most common factors. Dietary anti-oxidants play a crucial proactive and positive role in combating and

controlling degenerative disorder such as cardiovascular, neurological diseases, cancer and gastric ulcer.

In this study, we focused on the detection of nutritional and toxic elements present in dates with emphases on calcium (Ca) and magnesium (Mg) as a nutritional element and chromium (Cr) as a toxic element; using laser induced breakdown spectroscopy (LIBS). Calcium is a crucial element for decent human functioning, especially with respect to maintaining and building calcified tissues like teeth and bones[156]. It is highly needed for a number of vital regulatory functions such as, coagulation of blood, transmission of impulses, activation of enzyme reactions, contraction and relaxation of muscles including heartbeat, and simulation of hormone secretion[156]. Magnesium has got huge biological importance in more than 300 metabolic reactions including nucleic acid synthesis (DNA, RNA), cellular energy production and protein synthesis. Magnesium is indispensable for ample brain energy and smooth transmission of communication through central nervous system [157]. It is also essential in the prevention of atherogenesis and cardiovascular diseases. However, chromium doses above the adequate level can be toxic and carcinogenic, resulting in a number of diseases in human beings. Chromium is naturally found in plants and gets into food chain through media such as air, water and soil and then invades body. Chromium can cause pathogenesis of some cancers in kidneys, liver, lungs and gastrointestinal tract. Therefore, knowledge of the amount of chromium in dates is of upmost importance[158].

There are a number of previous published works, where laser induced breakdown spectroscopy (LIBS) was used to study some plant products. M . Galiova et al [159] uses Single Pulsed Laser induced breakdown spectroscopy to map elements like Copper (Cu) and Silver (Ag) in sun flower (Helianthus Annuus). The focus of this was to study the distribution of Cu and Ag in sun

flower. The spectral line of Cu and Mg used for mapping was 324.75 nm and 328.07 nm respectively. Preeti Dhar et al[160] also employ LIBS to examine the relationship between trace element and antilipemic & antidiabetic potential in medicinal plant called Babchi (Psoralea corylifolia). The LIBS analysis of Babchi (Psoralea corylifolia) shows the presence of trace element such as Mg, Si, Na, K, Ca, Zn and Cl. The intensity ratio of these elements was analyzed to determine the concentration of the detected elements. And lastly, Mingyin Yao et al [161] uses LIBS to extract heavy metal element of pericarp and flesh of Citrus Nanfeng tangerines. The heavy element detected in pericarp and flesh of Citrus Nanfeng tangerines are Pb, Cd, Hg, Cr, and As. From relative intensity of the emission line these elements, the relative profile concentration were determined.

4.3.2 Validation of Local Thermodynamic Equilibrium condition for date samples

In order to characterize laser induced plasma, it is of paramount to determine the plasma parameters such as electron temperature and electron number density of the plasma for spectroscopic application. It also help us to ascertain if our plasma is in optically thin condition, which is a prerequisite to eliminate severe effect of intensity saturation and self-absorption effect. When laser pulse interact with test date sample surface, the electron in the outer most part of atoms get excited such that when the vibrational energy is greater than the binding energy of target, the bonding is subdued and evaporation of the target starts. The electron temperature can be determined without need of total number density and partition function. Magnesium (Mg) spectral lines used for the Boltzmann plot (i. e employing equation 2) were 277.9 nm, 382.9 nm, 383.2 nm and 383.8 nm, which were identified as 3s 3p $^3P_2 \rightarrow$ 3p2 $^3P_2$, 3s 3p $^3P_1 \rightarrow$ 3s 5d $^3D_2$, 3s

$4s\ ^3S_1 \rightarrow 3s\ 5p\ ^3P_1$, $3s\ 3d\ ^1D_2 \rightarrow 3s\ 6f\ ^1F_3$ respectively as depicted in Figure 4.15 and Boltzmann plot is depicted in Figure 4.16. The estimated electron temperature from the Boltzmann plot was $T_e = 5660\ ^0k$. The spectroscopic data from NIST data base used for the Boltzmann plot is as shown on Table 4.4. The electron number density was estimated from its relationship with Full Width at Half Maximum (FWHM) of the Stark broadening profile as shown in the equation 3. The FWHM of magnesium line Mg I (277.9 nm) was calculated from the Lorentzian fitting of experimentally obtained line profile as depicted in Fig. 4.17. The calculated FWHM was 0.2879 nm and the resulting electron number density was $3.47 \times 10^{16}\ cm^{-3}$. The spectral line Mg I (277.9 nm) was selected because it well isolated from other spectral lines. In order to validate if our plasma is in local thermodynamic equilibrium, we employ McWhirter criterion which is given by equation 1. The estimated critical electron number density was $4.45\ X\ 10^{16}\ cm^{-3}$, which is much lower than the estimated electron density and consequently satisfying the necessary condition for LTE.

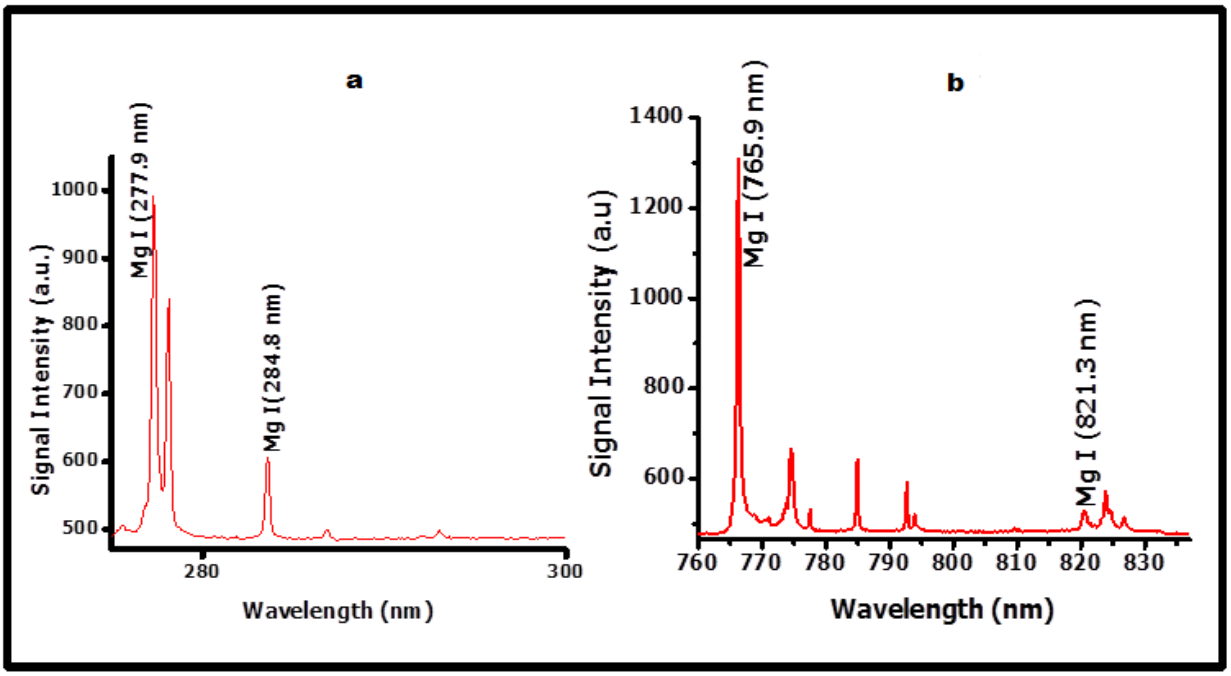

Figure 4.15: LIBS spectrum showing spectral lines used for Boltzmann plot. This spectrum was obtained from sample two of the dates sample.

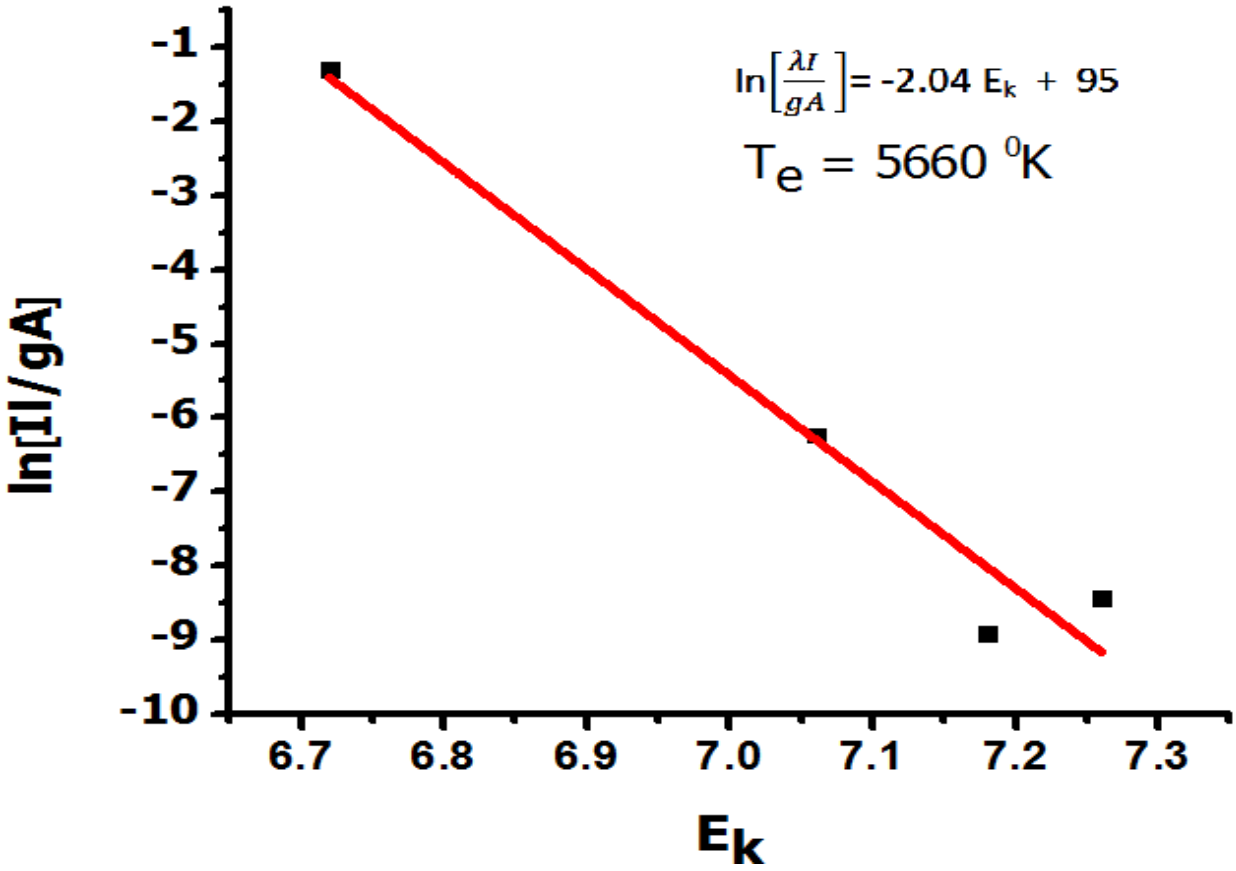

Figure 4.16: Boltzmann plot from Mg (I) LIBS spectral lines from dates sample.

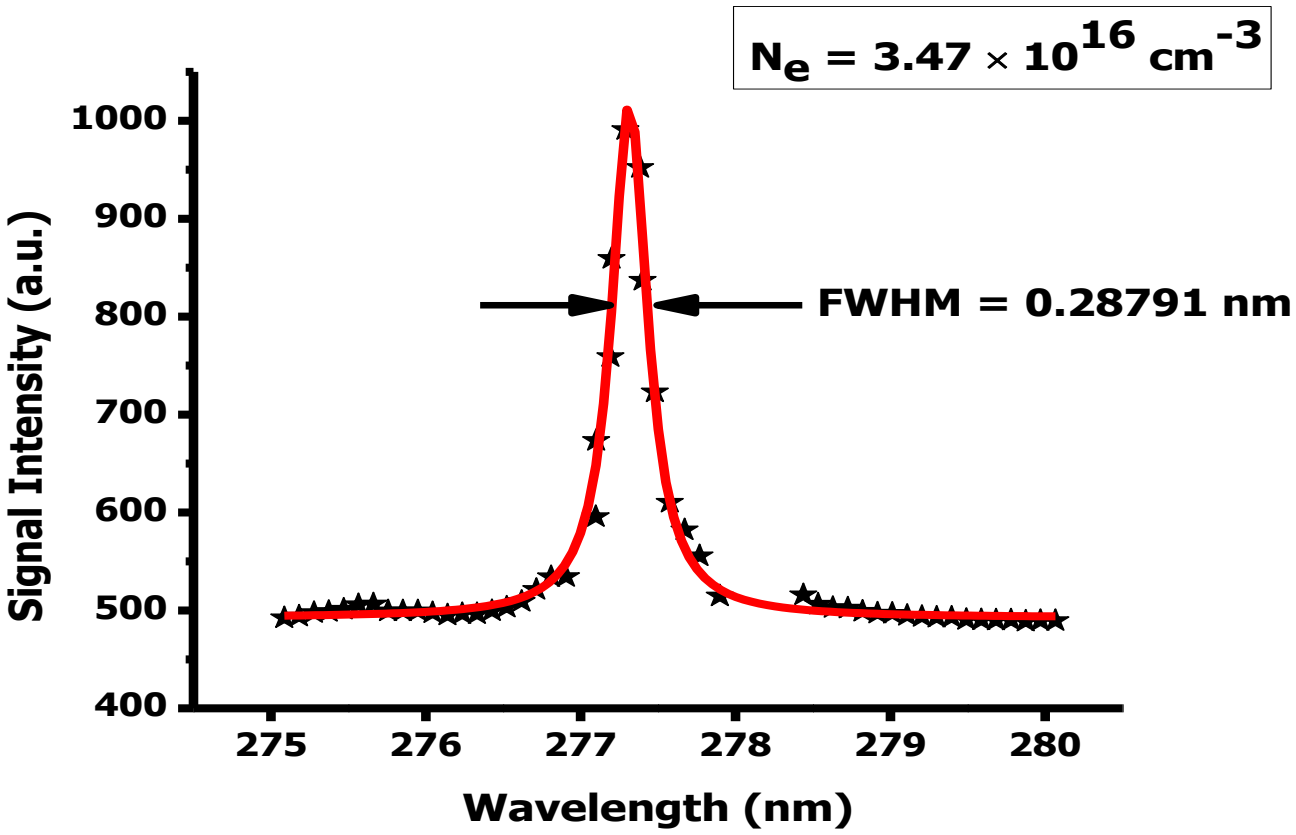

Figure 4.17: Stark broadening profile of Mg (I) at 277.9 nm for electron number density estimation.

Table 4.4: Spectroscopic data from NIST data base, indicating Mg (I) spectral lines used for Boltzmann plot.

Wavelength (nm)	Transition Assignment	Statistical weight		$T_{ransition}$ probability	Energy of the upper level	
		g_i	g_k	A_{ik} (S^{-1})	Ei (eV)	Ek (eV)
277.9	3s 3p $^3P_2$ → 3p^2 $^3P_2$	5	5	4.09e+08	2.72	7.18
284.8	3s 3p $^3P_1$ → 3s 5d $^3D_2$	3	5	1.77e+07	2.71	7.06
765.9	3s 4s $^3S_1$ → 3s 5p $^3P_1$	3	3	1.23e-06	5.10	6.72
821.3	3s 3d $^1D_2$ → 3s 6f $^1F_3$	5	7	4.38e-06	5.75	7.26

4. 3. 3 Optimization of time delay for detection of chromium in Dates sample

In order to identify the optimum time delay between the incident laser pulse and the acquisition of LIBS spectrum for Cr I 520.4 nm in test date sample, the LIBS signal intensity of signature line of Cr I 520.4 nm was studied for various time delays ranging from 250 – 850 ns in steps of 100 ns. The delay time was controlled by Q-switch trigger pulse and the Intensified charged coupled device (ICCD) camera. A typical plot of LIBS emission line intensities versus time delay for Cr I at 520.4 nm wavelength is depicted on Fig. 4.18. From Fig. 4.18, it can be clearly seen that the optimum delay time for detection of Cr I at 520.4 nm wavelength was at 550 ns.

The optimum delay time for other element like Mg and Ca was found to be between 400 – 600 ns. For each data point Fig. 4.18, an average spectrum for 15 laser pulses shot was recorded. The recording of the averaged spectra reduces the background noise to a great extent as compared to the single shot spectrum of the sample. But throughout this study we used the 550 ns delay time for our LIBS spectrum acquisition, which is the optimum delay time for Cr I (520.4 nm) detection and also because of its closeness to average delay time of the three elements.

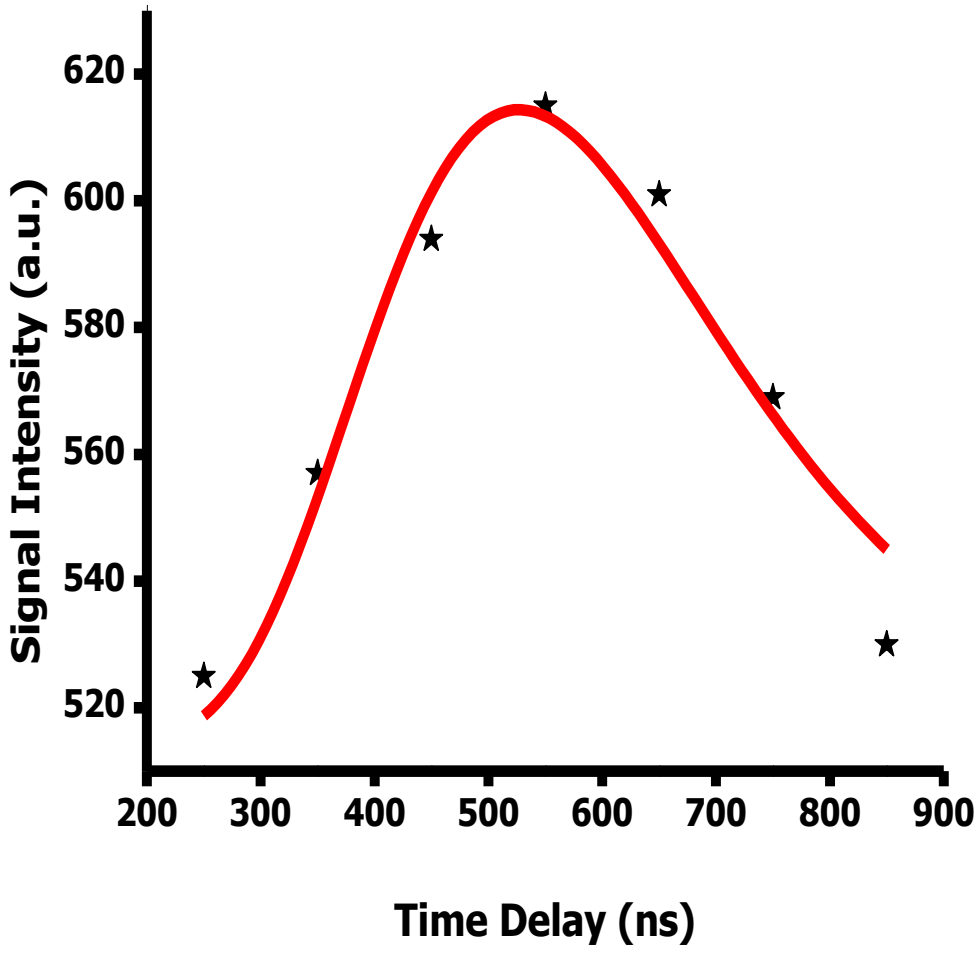

Figure 4.18: LIBS signal Intensity dependence on Time Delay for Cr I in Test Date Sample.

4. 3. 4 Optimization of Laser Fluence for detection of chromium in Dates samples

In order to investigate the dependence of LIBS signal Intensity on laser fluence, we recorded the emission line intensity for Cr I 520. 0 nm at different laser energies using sakary test sample. Laser energy was measured using energy meter (Ophir model 300) and was varied between 15 - 17.54 mJ with laser spot size of 150 μm in diameter. The corresponding laser fluence was between the range of 85 and 99 J/cm^2. The time delay t_d of 500 ns was used where the optimum LIBS signal intensity of Cr I 520.4 nm was achieved. Figure 4.19 depicts the LIBS signal intensity dependence of Cr I 520.4 nm on laser fluence. It was observed that LIBS signal intensity dependence of Cr I 520.4 nm on laser fluence shows linear dependence between laser fluence 85 -91 J/cm^2 and later stated to flatten between laser fluence 91 – 99 J/cm^2, which may be as a result of self-absorption, with optimum laser fluence at 99 J/cm^2. Self-absorption often occurs due to atoms in the plasma having higher energies with respect to atoms on its surface. Thus, when the atoms in the plasma de-excite to produce resonance lines, the outer atoms absorb the energy leading to less intense spectral lines.

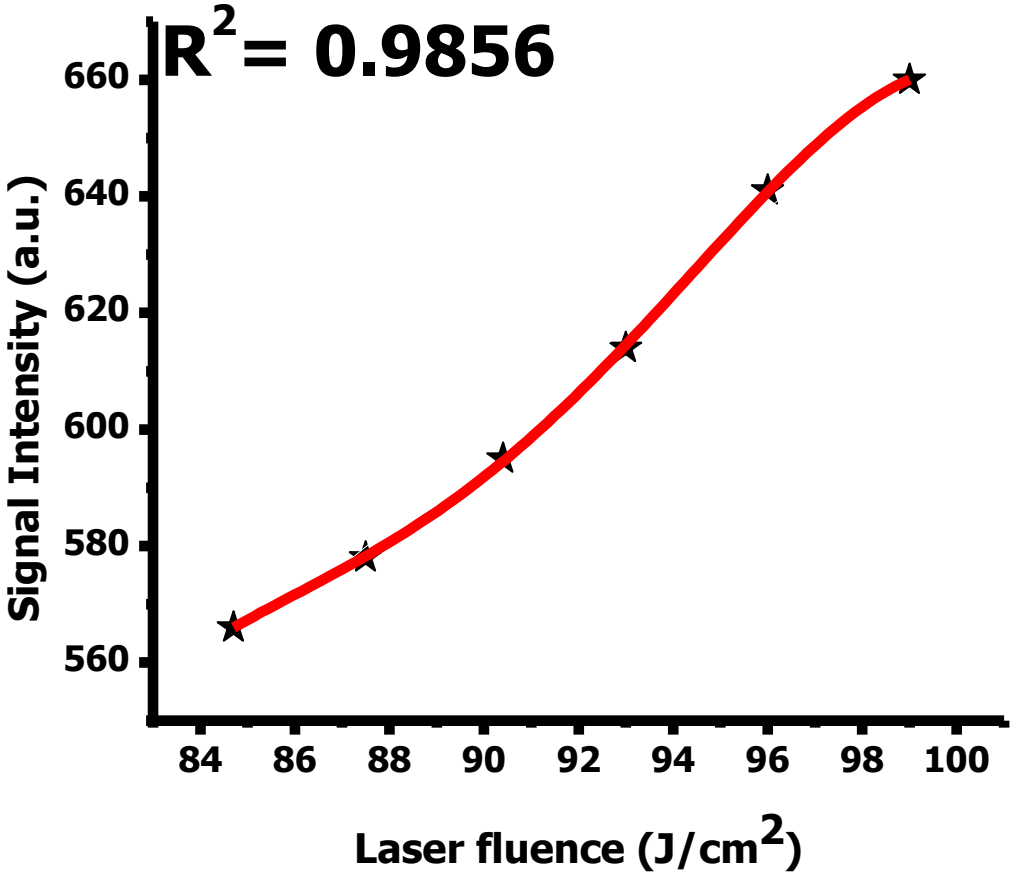

Figure 4.19: Plot of dependence of LIBS signal Intensity of Cr I (520.4 nm) emission line on laser fluence imparted on date sample surface

4.3.5 Qualitative and Quantitative Analysis of Dates samples.

For the qualitative and quantitative analysis of elements present in the date samples, LIBS spectra were recorded over a 250–850 nm wavelength range for different brands of dates samples. Prior to recording of spectra a best compromise was reached between the high line intensity and low background signal after plasma breakdown at an approximate time delay t_d of order of 550 ns. Figures 4.20 -4.23 depicted the emission

spectra of date samples recorded at a 550 ns time delay t_d. The laser pulse energy was fixed at 17.54 mJ, which is the optimum laser energy. The distance between the optical fiber and the plasma was 10 mm. The LIBS spectra of the date samples were recorded to identify each element present in the date samples within the wavelength range of 250- 850 nm. The most sensitive lines (finger print wavelength) for identification of elements were found between 250-550 nm regions using NIST database (see fig 4.24). The finger print wavelength corresponding to different element present in date test samples are clearly distinguishable from low background signal intensity. Spectra recorded for all date samples were very rich, comprising of singly charged ions (II) and neutral species. The spectra of all brands reveal the presence of Magnesium, Iron, Calcium, Titanium, Aluminum, Chromium, Nitrogen, fluorine, copper and Potassium. It was observed that there was no qualitative but quantitative differences between the different date brands samples (see Fig 4.24). The close resemblance of the spectra should be noticed, with Mg I (at 277.9 nm), Fe I (at 282.2 and 382.0 nm), Ca II (at 317.9 nm), Ti I (at 381.8, 387.5, 392.9 and 405.5), Al I (at 396.1 nm), Cr I (at 425.4 and 520.4 nm), and K I (at 495.6 nm) as depicted in figure 4.24. The presence of magnesium, calcium and chromium in date samples is confirmed by single persistent line (277.9, 317.9 and 520.4 nm respectively) as depicted in figure 4.24. Furthermore, the presence of chromium is further verified by the non-persistent line at finger print wavelength 405.5 nm. The finger print wavelength (as specified in Table 4.5) for each element of interest was selected for quantitative and qualitative analysis. One of the way to achieve quantitative analysis is to calibrate the system using known concentration of an element in the same sample matrix.

The preparation of these standard samples allows the correlation between the spectral line intensity and the corresponding concentration of element in question. Fig 4.25 depicts the comparison of LIBS signal intensity for Mg, Ca and Cr in the different date samples. The spectral lines intensity of Mg, Ca and Cr used for the comparison in the figure 8 are Mg I (277.9 nm), Ca I (317.9 nm) and Cr I (520.4 nm) respectively. The emission line intensity of plasma is given by equation 18. From Eq. 18, one can determine the population density N of an atom or ions excited from ground state i to upper state j, which depends on the mass of ablated material and the incident laser energy as depicted in Fig. 4.19.

A calibration curve for the three elements was constructed. From the self-constructed calibration curve, we able to determine the concentration of Mg, Ca and Cr. The analysis of calibration data was used for the estimation of limit of detection of our LIBS system for each element (see Table 4.5). The limit of detection is estimated by equation 19. In order to determine the concentration of nutritional element such as magnesium and toxic element such as calcium and chromium in the test date sample, 10,000 ppm (parts per million) solution of Mg, Ca and Cr were used to prepared standard sample of known concentration in deionized (DI) water. . The very high purity laboratory salts (99 %) used for preparation Mg, Ca and Cr solutions are Magnesium fluoride, Calcium sulphate, and Potassium dichromate respectively. These solutions with known concentration of Mg, Ca, and Cr were mixed thoroughly with paste date samples; while ensuring that the same set of date samples used for the LIBS spectrum acquisition were also used for calibration to minimize the matrix effect. The wet paste was then dried in the Oven at 60 ^{0}C temperature during one day for

preparation of standard samples to draw the calibration curves. The standard concentration for Mg, Ca and Cr ranges 200 to 2000 ppm, 400 to 2400 ppm, and 100 to 1200 ppm respectively. The persistent signature line of Mg, Ca and Cr used in the construction of calibration curve are 277.9, 317.9 and 520.4 nm respectively. From the calibration curve in Figure 4.26, we were able to predict the concentration of important nutritional elements such as Mg & Ca, and also toxic element like Cr. It is clear from Table (4.5) that the concentration of Mg and Ca are higher as compared to Cr concentration in our date samples. For example the concentration of nutritional elements like Mg and Ca ranges from 34.76 – 196.43 ppm and 187.21 – 515.32 ppm respectively, while the concentration of toxic element Cr was found to be lower ranging from 1.72 – 7.76 ppm (see Table 4.5). The concentration of Mg and Ca shows how highly nutritional are the date samples. It is worth mentioning that the maximum permissible limit set by food and drug agency and other regulatory bodies for Cr is 1 ppm, which implies that the concentration of Cr in each date samples were little higher than the permissible limit in some date samples and way higher in others as tabulated in Table 4.5. In order to further cross confirm our results, the conventional ICP-MS technique was used to cross check our LIBS results, and it was found that both are in good agreement with each other (see Table 4.5). The estimated limits of detection (LODs) of our LIBS system for Mg, Ca and Cr using Eq 19. were 2, 17, 1 ppm, respectively. In addition, since the level of nutritional element is high, and the fact that only one toxic element was detected, then date consumption could be recommended for individual who are interested in increasing the level nutritional elements such as magnesium (Mg) and calcium (Ca) to take more of these dates fruits, however for the individual who are have dietary restriction on the consumption of chromium (Cr), are

advised to minimize the intake of these dates fruits. This study confirms that date is a significant source of trace elements.

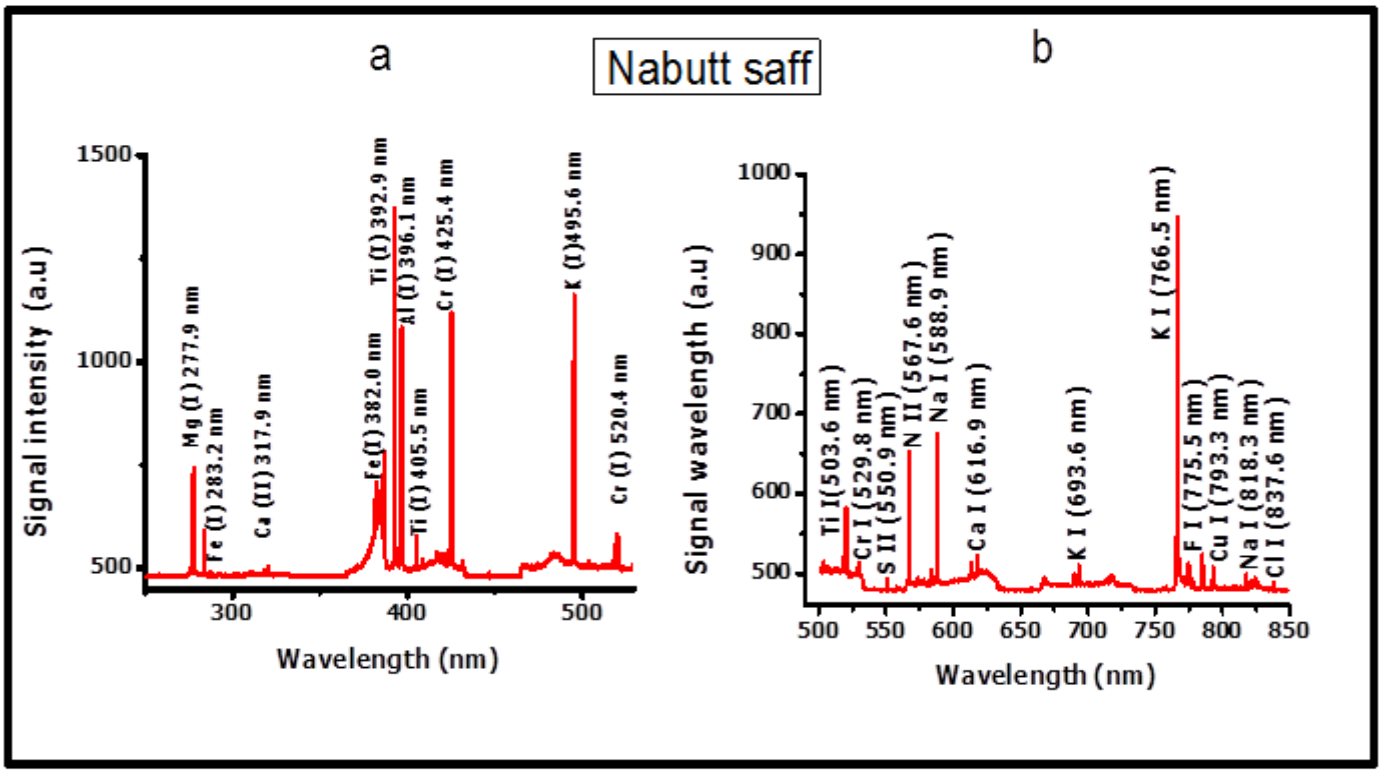

Figure 4.20: Typical LIBS spectra of date sample (Nabutt saff) from wavelength range 350 -850 nm.

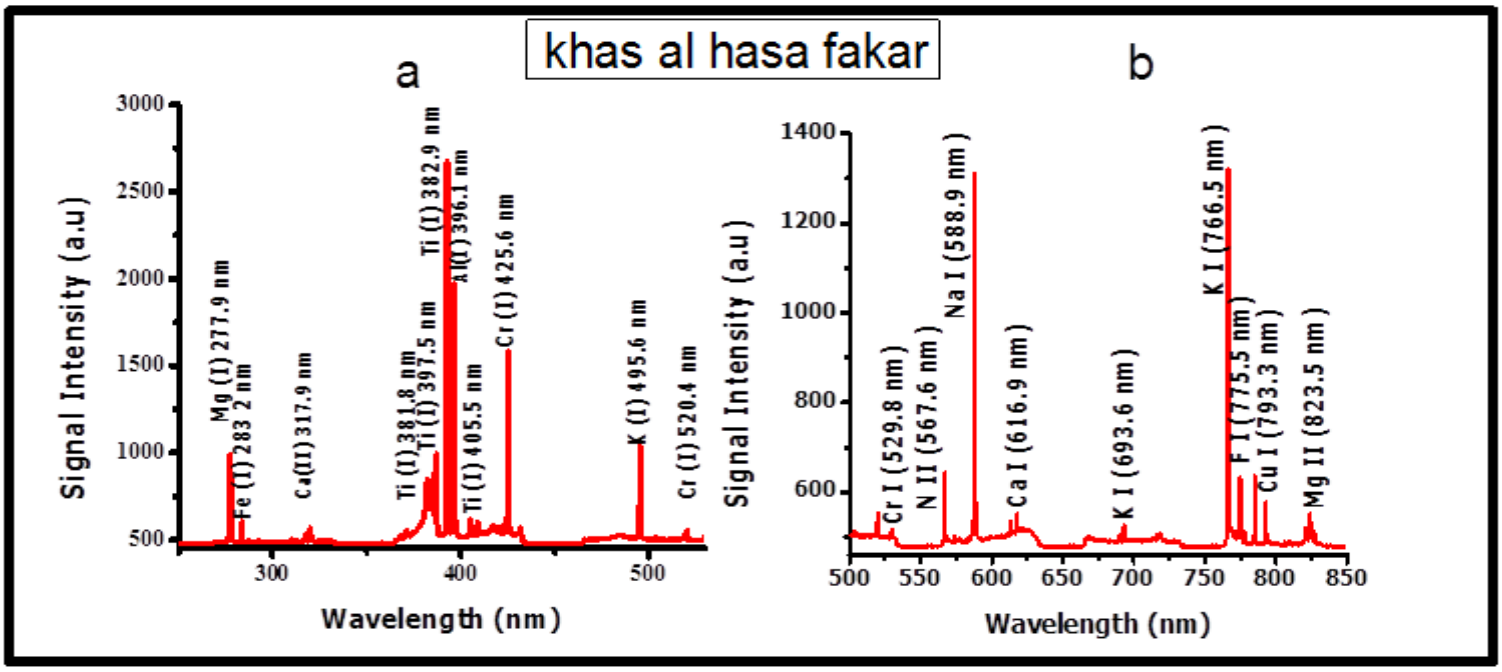

Figure 4.21: Typical LIBS spectra of date sample (Khas al hasa fakar) from wavelength range 350 -850 nm.

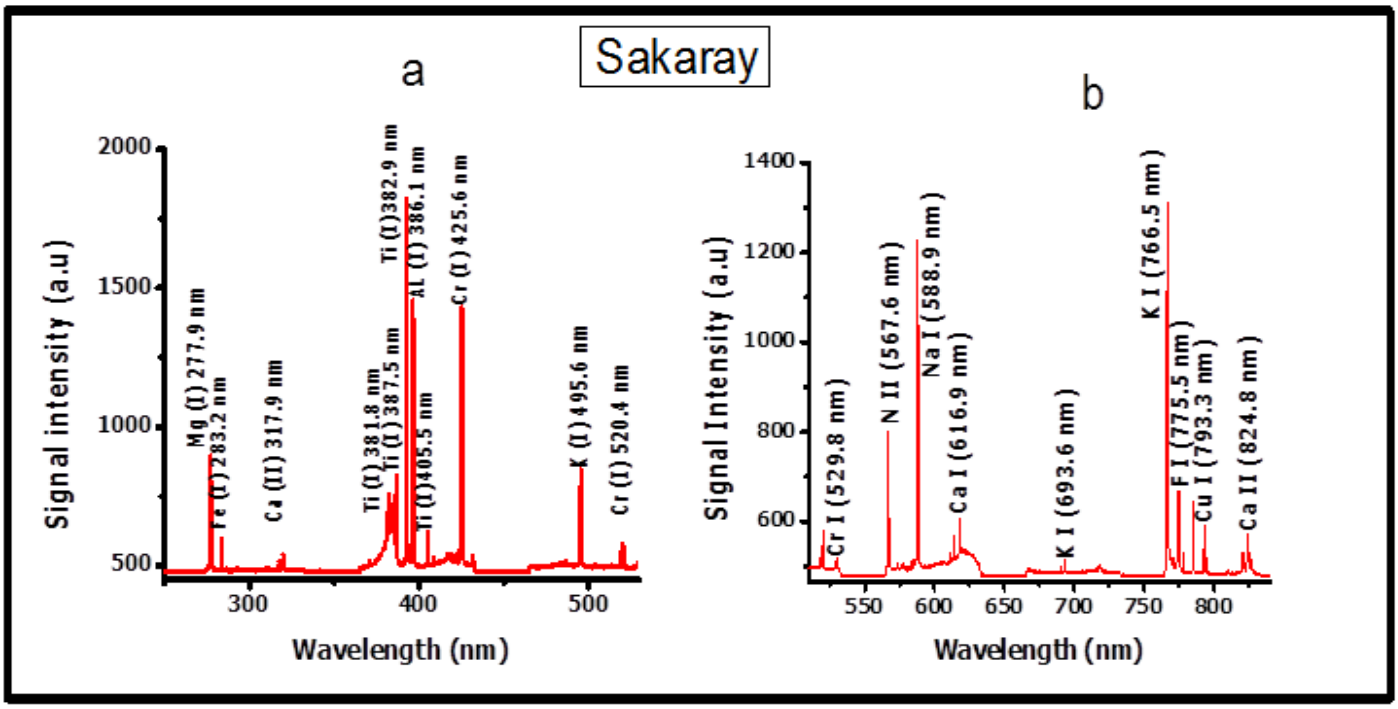

Figure 4.22: Typical LIBS spectra of date sample (Sakaray) from wavelength range 350 - 850 nm.

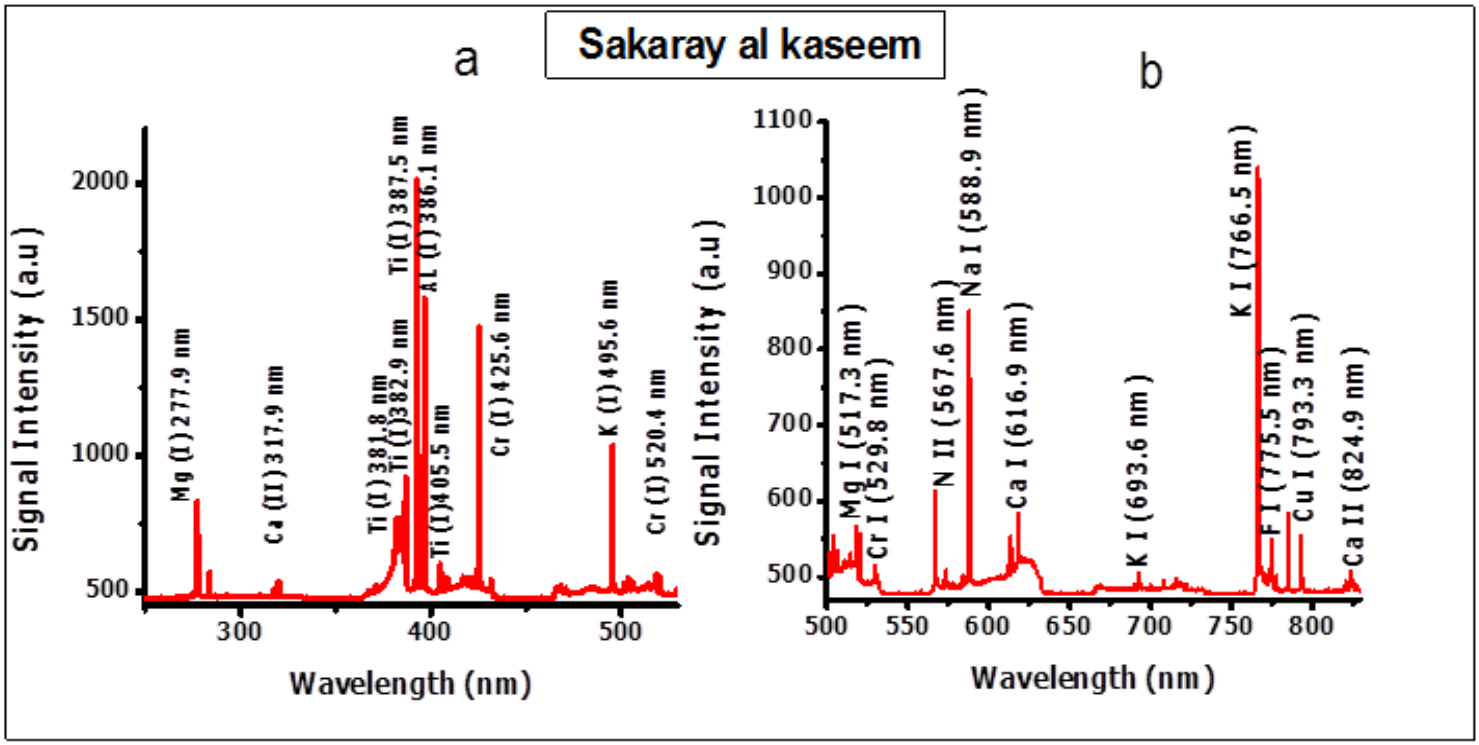

Figure 4.23: Typical LIBS spectra of date sample (Sakaray) from wavelength range 350 - 850 nm.

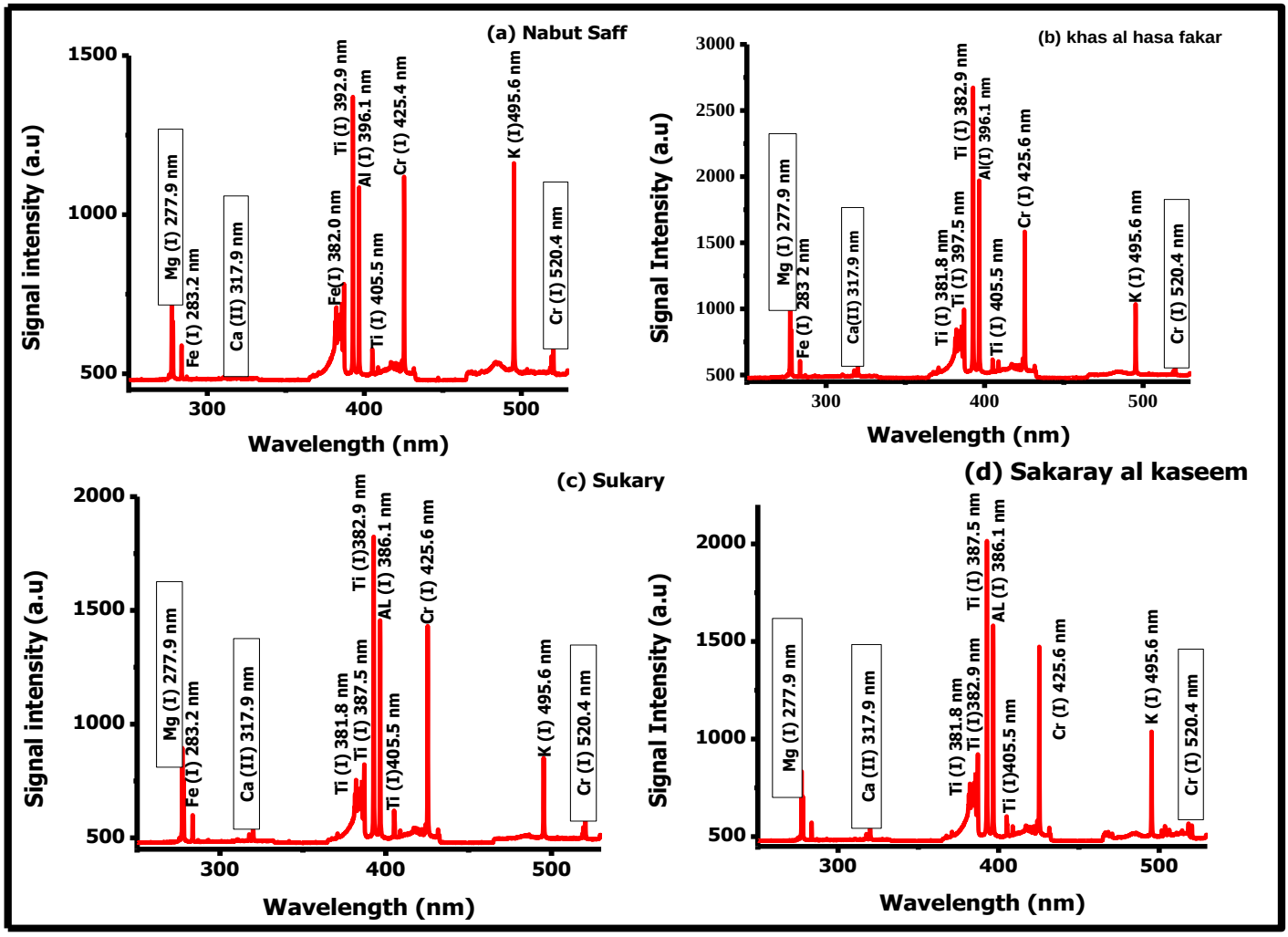

Figure 4.24: Typical LIBS spectrum showing different element detected in four different date samples at time delay td of 550 ns and laser energy of 17.54 mJ.

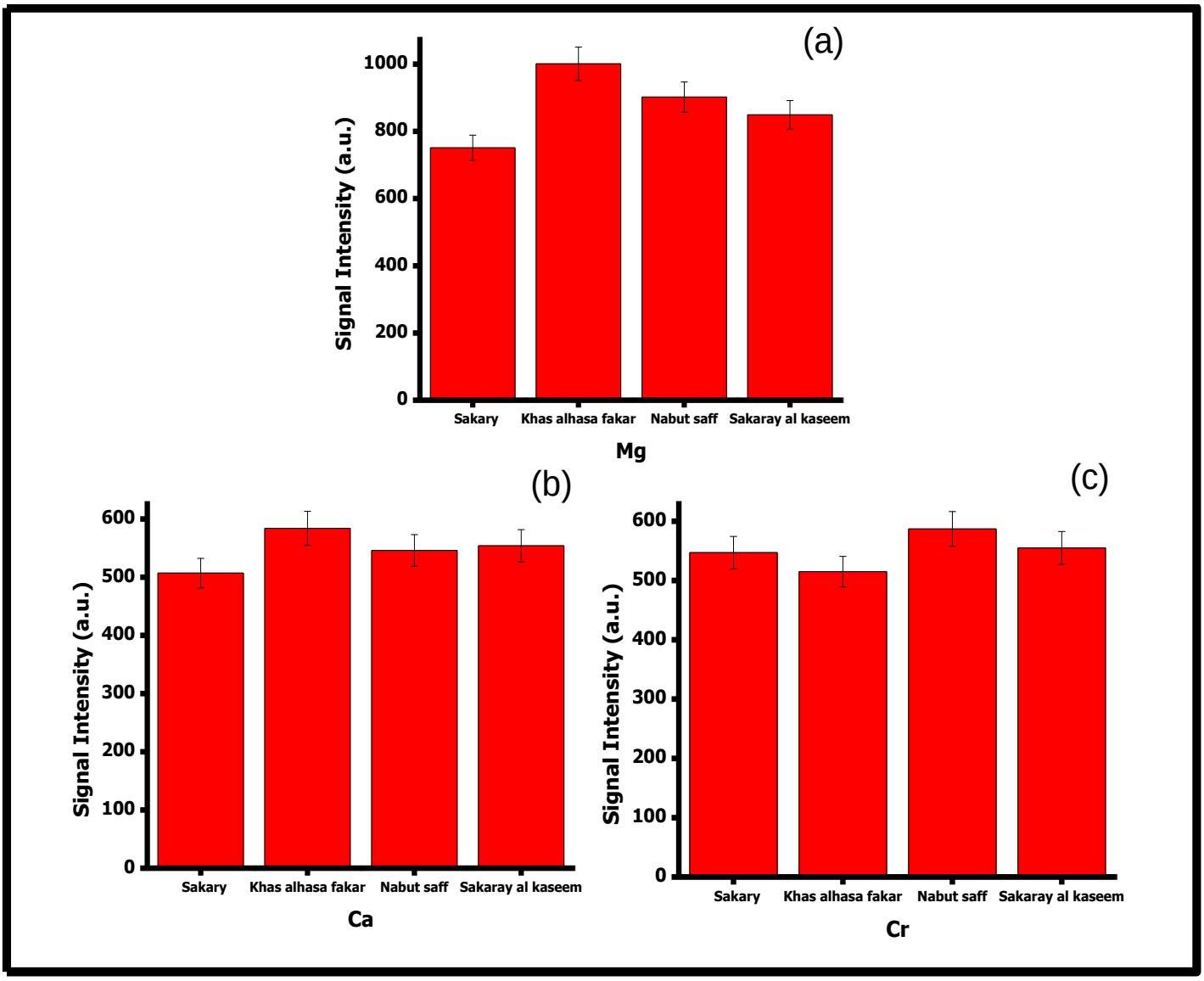

Figure 4.25: Chart plot showing comparison of LIBS signal Intensity of (a) Mg (b) Ca (c) Cr in different date samples

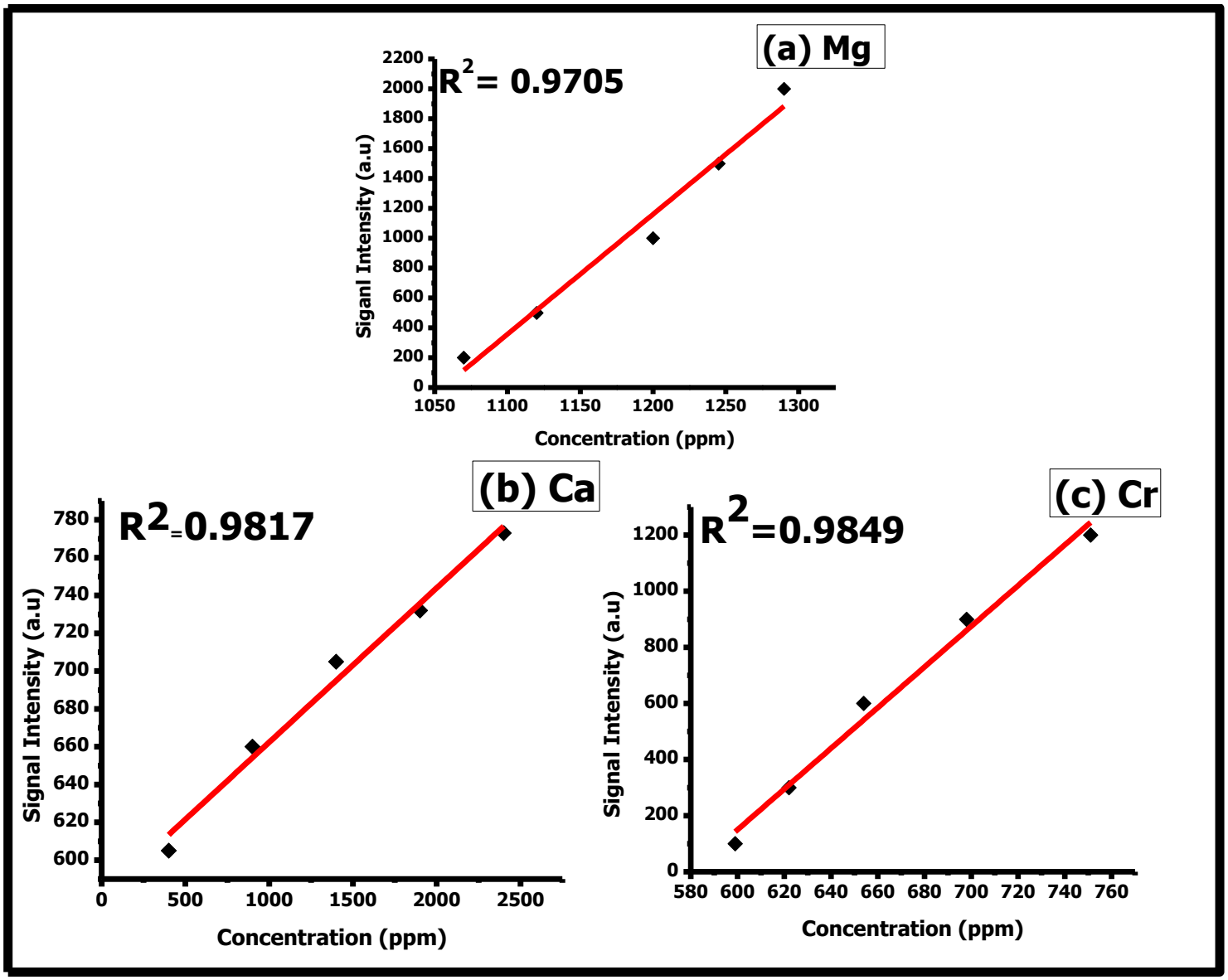

Figure 4.26: Calibration curve for LIBS measurement of (a) Mg (b) Ca (c) Cr

Table 4.5: List of Nutritional and Toxic elements detected by LIBS and ICP-MS techniques and their Concentrations in various Dates samples

Element Detected in Date Sample	Wavelengths (nm)	Optical Transition Assignment	Sample Type	Comparison of LIBS and ICPMS Mean Concentration Value		Limit of Detection (ppm)
				LIBS (ppm)	ICPMS (ppm)	
Mg	277.9	$3s\,(3p)\,^3P_2 \rightarrow 3p^2\,^3P_2$	Sakary	68.76	76.54	2
			Khas alhasa fakar	206.56	196.43	
			Nabut saff	37.21	34.76	
			Sakaray al kaseem	37.10	40.87	
Ca	317.9	$3p^6\,(4p)\,^2P_{3/2} \rightarrow 3p^6\,(4p)\,^2P_{3/2}$	Sakary	507.89	515.32	17
			Khas alhasa fakar	301.65	320.45	
			Nabut saff	220.01	208.24	
			Sakaray al kaseem	169.87	187.21	
Cr	520.4	$3d^5\,(^6S)\,4s \rightarrow 3d^5\,(^6S)\,4p$	Sakary	4.88	5.21	1
			Khas alhasa fakar	1.72	1.57	
			Nabut saff	7.76	6.02	
			Sakaray al kaseem	4.98	5.52	

4.3 Determination of carcinogenic Fluorine in cigarettes using pulsed UV laser induced breakdown spectroscopy

4. 3. 1 Introduction

Tobacco leaves is main raw material used in manufacturing cigarettes. It is a well-established fact that tobacco consist of various toxic elements that can cause health problems during the consumption of the cigarettes. Over 4000 chemicals have been identified as ingredients of cigarette[162]. Tobacco is known to consist of various compounds among which are hydrocarbon, oxygen containing compounds, nitrogen containing compounds, heavy metals, non-metals, ions, and halogen-containing compounds are prominent. It is reported that the approximate composition of halogen-containing compounds is 1.5 % in tobacco[162]. Halogens (especially, fluorine (F), chlorine (Cl), and bromine (Br)) can produce very dangerous compound during burning of cigarette. In the process of burning, 2.4% of these halogens is transferred to smoke and eventually inhale as organo-halogens which are as well harmful to the body[163].

Fluorine is among the top 15 most abundant elements on the earth's crust. The main source of fluorine exposure to human beings are through food, water and other daily used products. Too much intake of fluoride result into dental and skeletal fluorosis. It is reported that over 25% of the population of Saudi Arabia suffer from dental fluorosis even though study revealed that the level of fluoride in drinking water in Saudi Arabia (SA) is negligible[164]. Even the lungs cancer cases are rising rapidly specially in the smoker population of SA. Due to these facts, we were

motivated to investigate the fact that, there must be other sources of fluoride ingestion among the population in Saudi Arabia. It has been proven that the proportion of fluorosis as a result of water fluoridation is now less compared to other sources like cigarettes and diet. Fluoride get into the body through gastrointestinal track and stored right there as a hydrofluoric acid[165]. It causes muscle fiber[166], severely distorts spermatogenesis[167] and disrupt calcium current in neurological systems[168]. Due to limited awareness on the fluoride level in tobacco, it is usually ignored when calculating the total dietary intake of fluoride. The minimal recommended level for daily oral fluoride ingestion was determined to be 0.05 ppm per day[169], as recommended by non-observable adverse effect level (NOAEL). Estimation of the lethal fluoride doses are 16 to 64 ppm in adult and 3 to 16 ppm in children[169]. Due to these facts, this study is highly desirable to determine the level of fluoride in tobacco cigarettes.

To determine fluorine concentration in various tobacco cigarette brand, the widely used methods are ion selective electrode and ion chromatography [170-172]. These two methods are not straightforward and involve the conversion of solid sample to solution, which is in ionic form within the solution. This process of conversion of solid sample into solution is very tedious and requires chemicals. Molecular absorption spectrometry is another method of fluorine determination but always requires high homogeneity of the sample to be tested. The principle of this method is based on the molecular absorption of gallium mono-flouride (GaF) [69,70,173-175] and requires high-resolution continuum sources absorption spectrometry (HR-CS MAS) and limit of detection is not very good.

A simple and rapid method to the afore-mentioned methods tested in this study is Laser induced breakdown spectroscopy (LIBS). This method uses the solid sample directly in ambient air at atmospheric pressure, with minimal sample preparation of just making the solid sample

into pallet. LIBS is a very fast developing technique for quantitative and qualitative analysis of all element present in the solid sample. This technique involves a short laser pulse evaporating a small amount of material (usually in micrograms), thereby creating a plasma plume. This plasma plume consists of free atoms and ions in different excitation states. As the plasma cools down, the excited elements de-excite and emit radiations; these emitted radiations are then recorded with high resolution spectrometer to investigate elemental composition with the help spectroscopy technique. Such spectral lines are basically utilized [66,67,71]. Plasma is generally characterized by different parameters namely: electron density, plasma temperature and degree of ionization. Generally speaking, there are two types of ionized plasma, the weakly and the highly ionized plasma. The weakly ionized plasma is the one in which the ratio of the electron to other species is less than 10 %, while in highly ionized plasma the atoms are usually tripped of many of their electron resulting in very high electron to atoms/ions ratios. LIBS plasma is characterized under the weakly ionized plasma region[102]. To the best of our knowledge LIBS has never been used to determine the fluoride level in tobacco cigarettes and therefore the goal of this study is to optimize the experimental parameters with the aim of improving the limit of detection, the signal to noise ratio and linearity of the calibration curve for detection of fluoride in tobacco cigarettes. Laser fluence and the various experimental parameters of LIBS set up were optimized using the fluorine finger print line 690.2 nm in order produce optically thin plasma in local thermodynamic equilibrium (LTE). These parametric optimizations were essential to achieve the best limit of detection to detect the trace amount of fluorine in tobacco cigarettes samples.

4.3.2 Investigation of Local thermodynamic equilibrium condition of LIBS Plasma Using Tobacco sample.

Spectral line intensities in the recorded LIBS spectra can be used to detect and quantify the elements present in the test sample with the conditions that the laser induced plasma are optically thin and in local thermodynamic equilibrium (LTE). The elemental compositions of the optically thin plasma are the same as that of the sample. In an optical system like the plasma generated by pulsed laser ablation, LTE condition holds if the electron-ion and electron- atoms collision processes are very fast and prevail the radiative process. The plasma generated as a result of laser ablation is complicated and can be understood by the following physical laws: The plasma particle obeys maxwellian velocity distributions, population in the energy level follows the Boltzmann's statistics, ionization process and can be described by Saha's equation and radiation density obeys Plank's law. Along the boundary of the plasma where electron density is low and movement of the boundary region is rapid, LTE is not a good assumption [64,100]. All that is needed is for equilibration to occur in small regions of space, although it varies from region to region[100]. However moving slightly deeper into the plasma volume, the conditions could change more slowly and collision occurs more rapidly, and in this case LTE is valid. In order to ascertain if LTE is reached, the electron density must sufficiently be high enough for collision to dominate the population of levels. This criterion was originally formulated by McWhirter and is now called McWhirter criterion [66,67] and given by eqn. 8. In order to ascertain if the plasma is in LTE condition, its plasma temperature and electron density were calculated using Boltzmann's plot method and stark broadening respectively. Some of the crucial factors in obtaining a good Boltzmann plot are the accurate line intensities, accurate transition probabilities, and well-spaced upper levels. In order to have a Boltzmann plot, spectrally

isolated characteristics atomic transition lines of neutral barium (Ba I) in wavelength range of 300 nm – 400 nm and 580 nm – 680 nm were recorded for sample #1, using optimized conditions. The different wavelengths identified and selected of (Ba I) were 307.158 nm, 350.110 nm, 649.9 nm and 652.731 nm as depicted in Fig. 4.27. All these characteristic transition lines of barium were then used to estimate the plasma temperature, where plasma temperature T = 6555 ^{0} K was estimated from slope of Fig. 4.28. Table (4.6) shows the statistical weight, transitional probabilities and upper energy level that were used for plasma temperature estimation, which were all obtained from National Institute of Standard and Technology (NIST) data base[176].

Spectral line in an optical spectrum is characterized with a non-zero line width and its central line usually shift from its nominal central wavelength. This broadening and shift could be as a result of Doppler, instrumental, natural and stark broadening [25,72]. Since our experiment was carried out under atmospheric pressure, stark broadening is the only dominant mechanism, other afore mentioned mechanism are negligible under these conditions[177]. Stark broadening in spectral lines are basically from collisions between ions and electrons. Stark broadening can also introduce shift of energy levels, which results in shift of wavelength positions of spectral lines [102].

The line profile for Stark broadening is described by a Lorentzian function with full width at half maximum $\Delta\lambda_{1/2}$ and electron density is related by the equation (16). In order to calculate the electron density of our plasma, stark broadening profile of a singly ionized atomic transition line of barium (Ba I) at 307.158 nm was used because it is isolated and free from interference from other spectral lines. Fig. 4.29 shows a fitted Lorentzian curve for an isolated line of barium (Ba I) at 307.158nm used for the electron density estimation. The full width at half maximum

(FWHM) of 0.47376 was estimated from the fitted Lorentzian curve and electron impact parameter w from the reference data base[178]. The electron density was estimated to be 3.44 X 1018 cm-3. Since the critical value of plasma electron density is 4.79 X 1016 cm-3, then our electron density is much greater than the critical value, which implies that our plasma in this study is in local thermodynamic equilibrium (LTE). Therefore we can conclude that there was no much self-absorption and our emission are fully radiated from the plasma and also the plasma is transparent to the laser beam. Consequently our spectra are optimized and our plasma can be described using thermodynamic parameters.

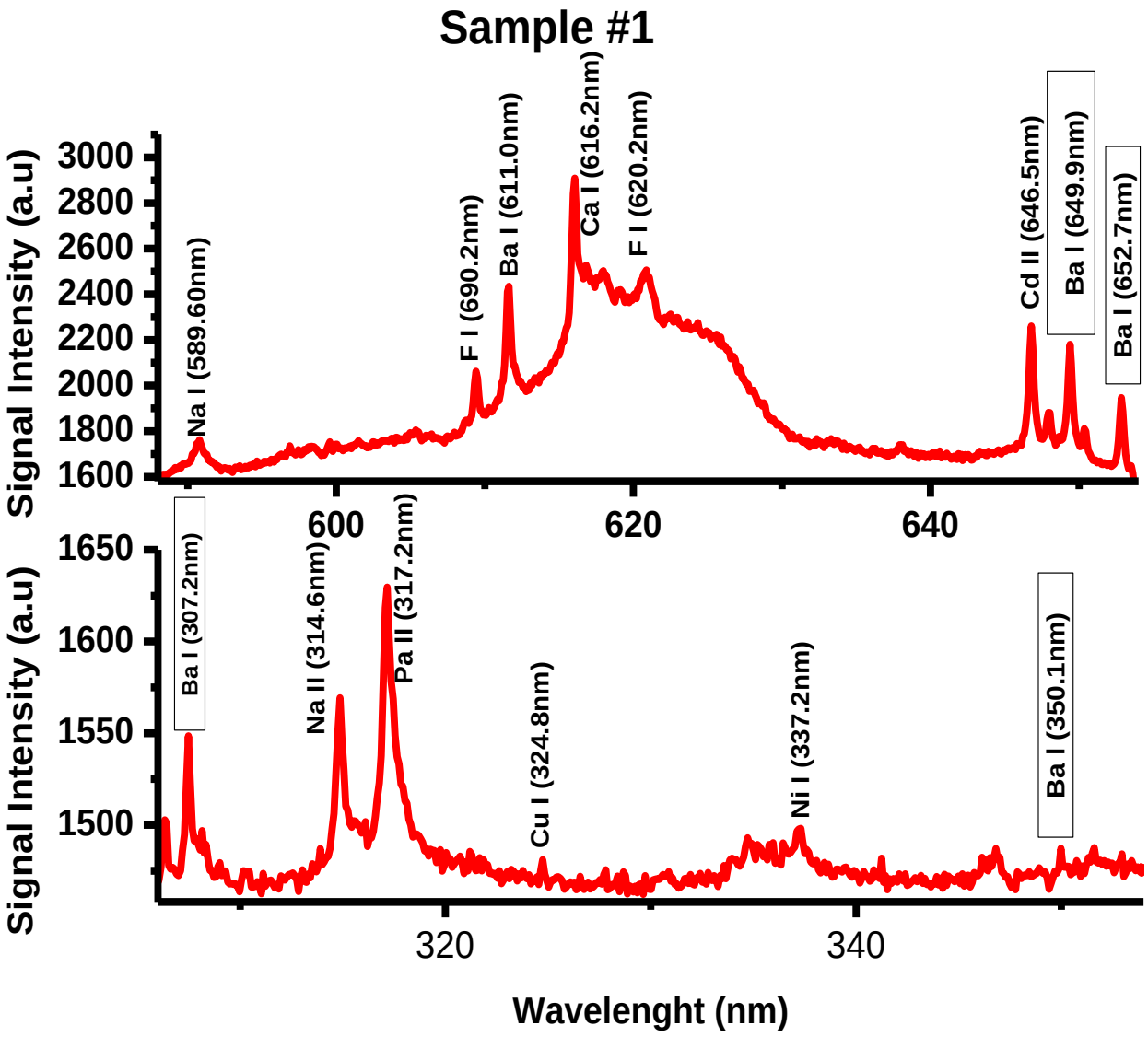

Fig. 4.27. Selected isolated atomic transition line of barium (Ba I) for plasma

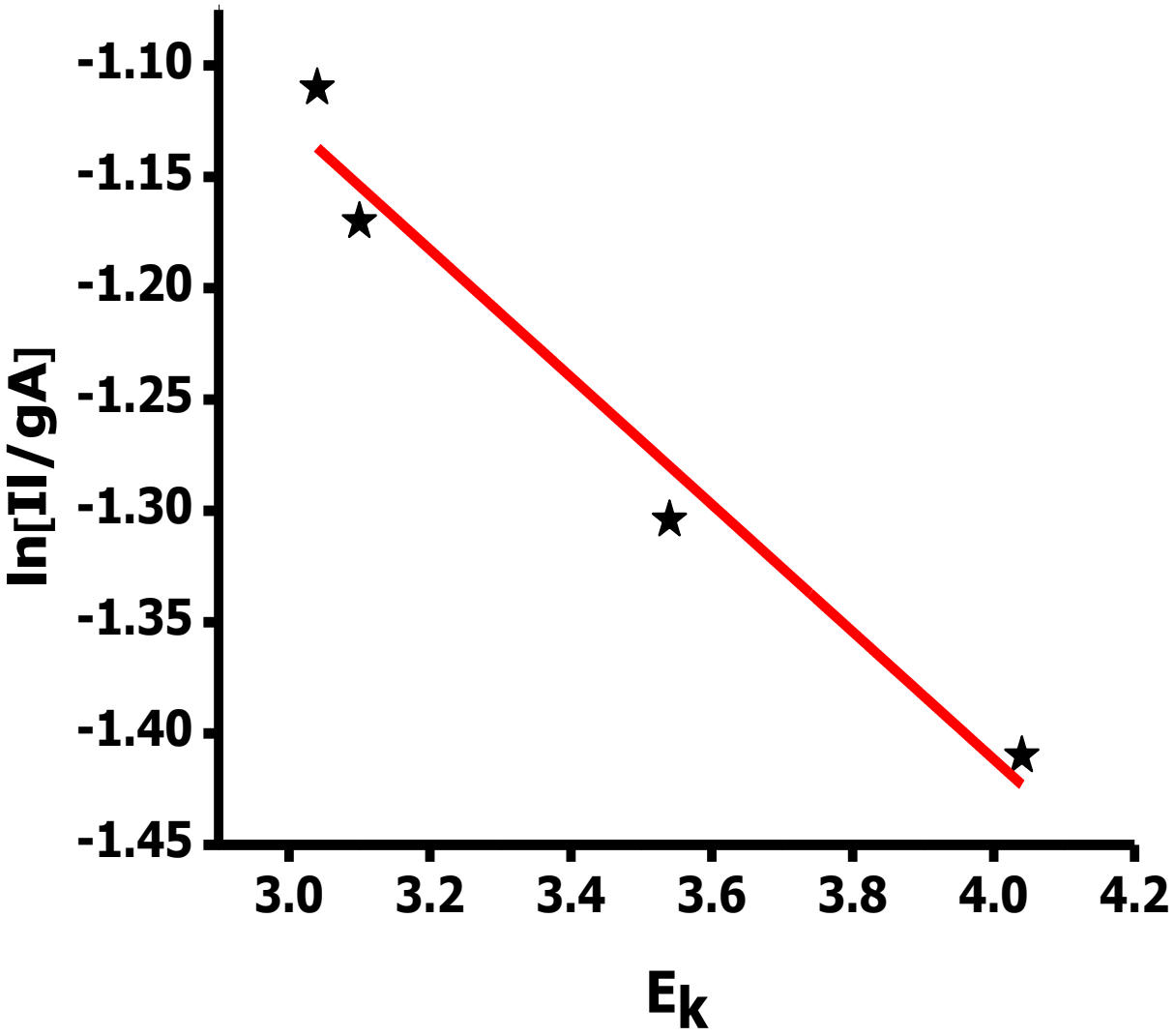

Fig. 4.28. Boltzmann plot to calculate plasma temperature of the tobacco cigarette.

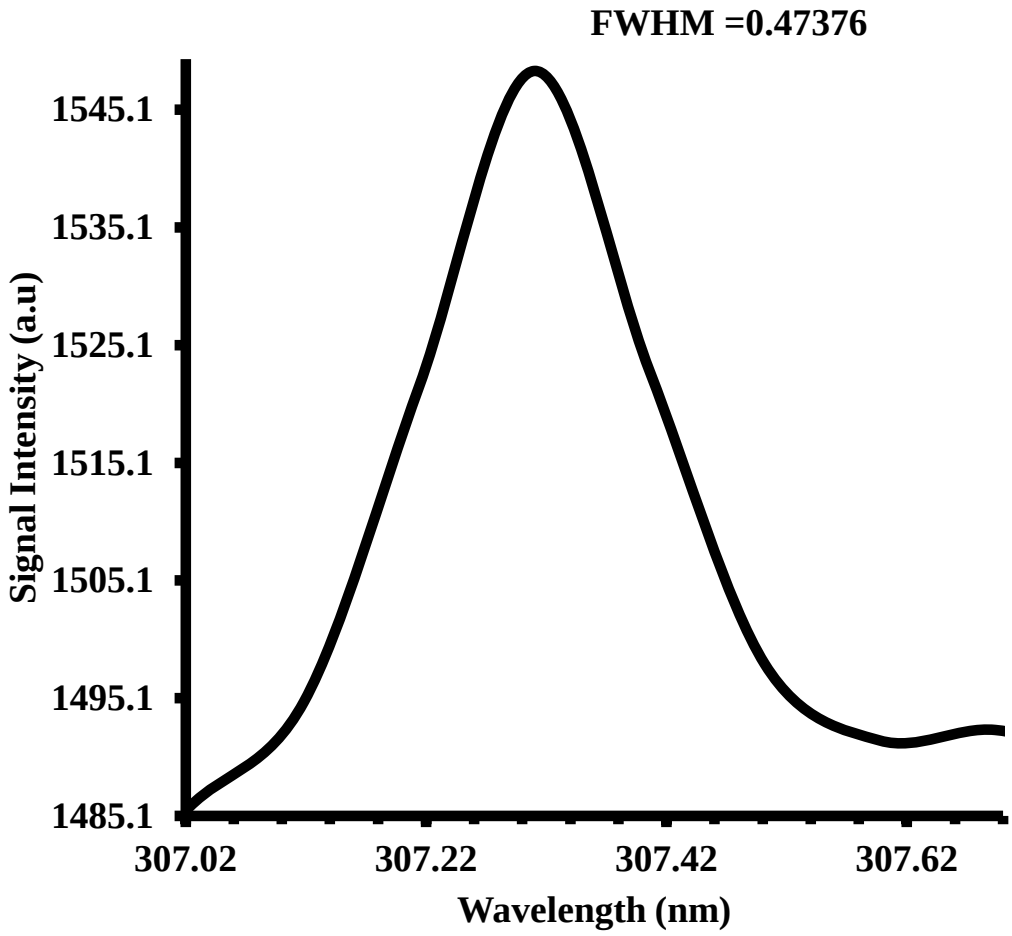

Fig.4.29. Stark broadening profile for characteristics atomic transition lines of neutral barium (Ba I) to estimate electron density.

Table. 4.6. Selected wavelength for characteristics atomic transition lines of neutral barium (Ba I) and other parameters used for Boltzmann's plot

Wavelength (nm)	g_k	A_{ki} X 10^8	E_k (eV)	Transition Array
307.2	3	0.41	4.04	$6s^2$ (^{0}S) → 6s (^{0}S) 7p
350.1	3	0.35	3.54	$6s^2$ (^{0}S) → 5d(^{0}S) 6p
649.9	7	0.54	3.10	6s 5d (^{2}D) → 5d (^{2}D) 6p
652.7	5	0.33	3.04	6s 5d (^{2}D) → 5d (^{2}D) 6p

4.3.3 Optimization of LIBS signals intensity for detection of fluoride in tobacco.

In a typical LIBS study, it is highly recommended to detect the optimum time delay between the incident laser beam and the opening of the shutter of camera for detection of any element of interest[54,136,179], like in our case for the fluoride (F I) in cigarette using the characteristic finger print wavelength of 690.2 nm for F I. The time delay between the laser excitation and spectrum acquisition determines the LIBS signal intensity level of the atomic specie to be detected. Usually due to high plasma temperature after laser excitation, there are many kinds of excited ionic, atomic and molecular species present in the plasma plume, giving rise to an unstructured broad continuum in the LIBS spectrum. In an attempt to check this broadening, the spectrum acquisition time was delayed to a certain value ranging from few hundreds of nanoseconds to few thousands of nanoseconds as depicted in Fig. 4.30. In LIBS analysis, both neutral and singly ionized atomic species are of interest and when the time delay is below 200 ns, most of the atomic transition are from the singly ionized atoms, and for time delay above 200 ns, the transition from neutral atoms are recorded. A typical plot of LIBS signal intensity (at a finger print wavelength of 690.2nm) dependence on time delay for persistent line of F I is depicted in

Fig. 4.30. As clear from Fig. 4.30, 720 ns is the optimum delay time for maximum LIBS signal intensity.

Moreover, in order to determine the optimum laser energy for the LIBS signal intensity of F I (at same finger print wavelength of 690.2nm) in tobacco, with all other parameters such as the LTE, time delay and laser beam diameter wre kept constant in accordance with the previous findings. The laser energy was varied from 15 mJ to 18.46 mJ at different interval as depicted in Fig. 4.31, with the corresponding LIBS signal for F I (690.2nm) been recorded and is depicted in the Fig. 4.31. It can be noticed from Fig. 4.31, that the LIBS signal intensity shows a linear dependence on the laser energy with the intensity increasing with increase in laser energy from 15 mJ to 18.46 mJ per pulse. At higher laser energies (> 15.5 mJ) the increment factor of the LIBS signal intensity reduces steadily as saturation set in, with the optimum laser energy was found at 18.46 mJ per pulse. However at 17.54 mJ per pulse of incident laser energy was found to generate appreciable LIBS signal intensity and precision for detection of F I (690.2nm) in our cigarette samples.

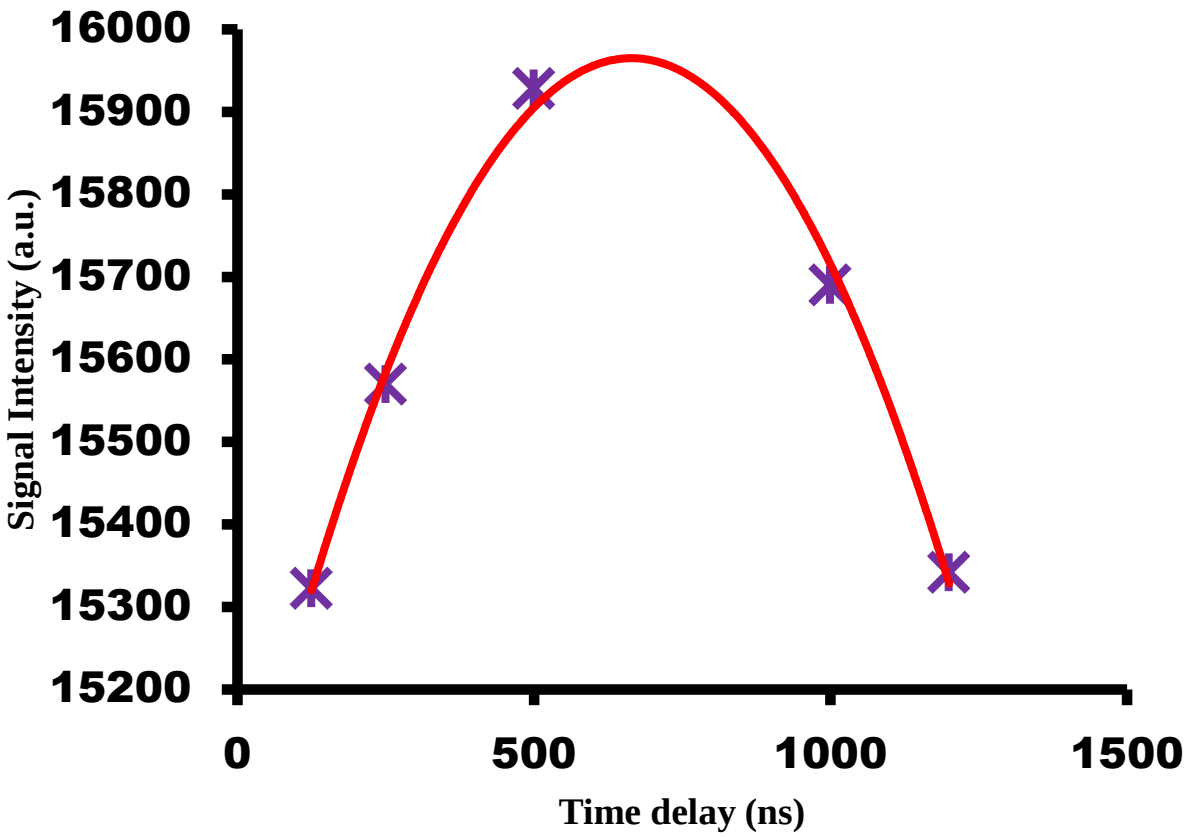

Fig. 4.30: LIBS signal intensity dependence on time delay for fluorine line (F I 690.2 nm) in tobacco cigarette.

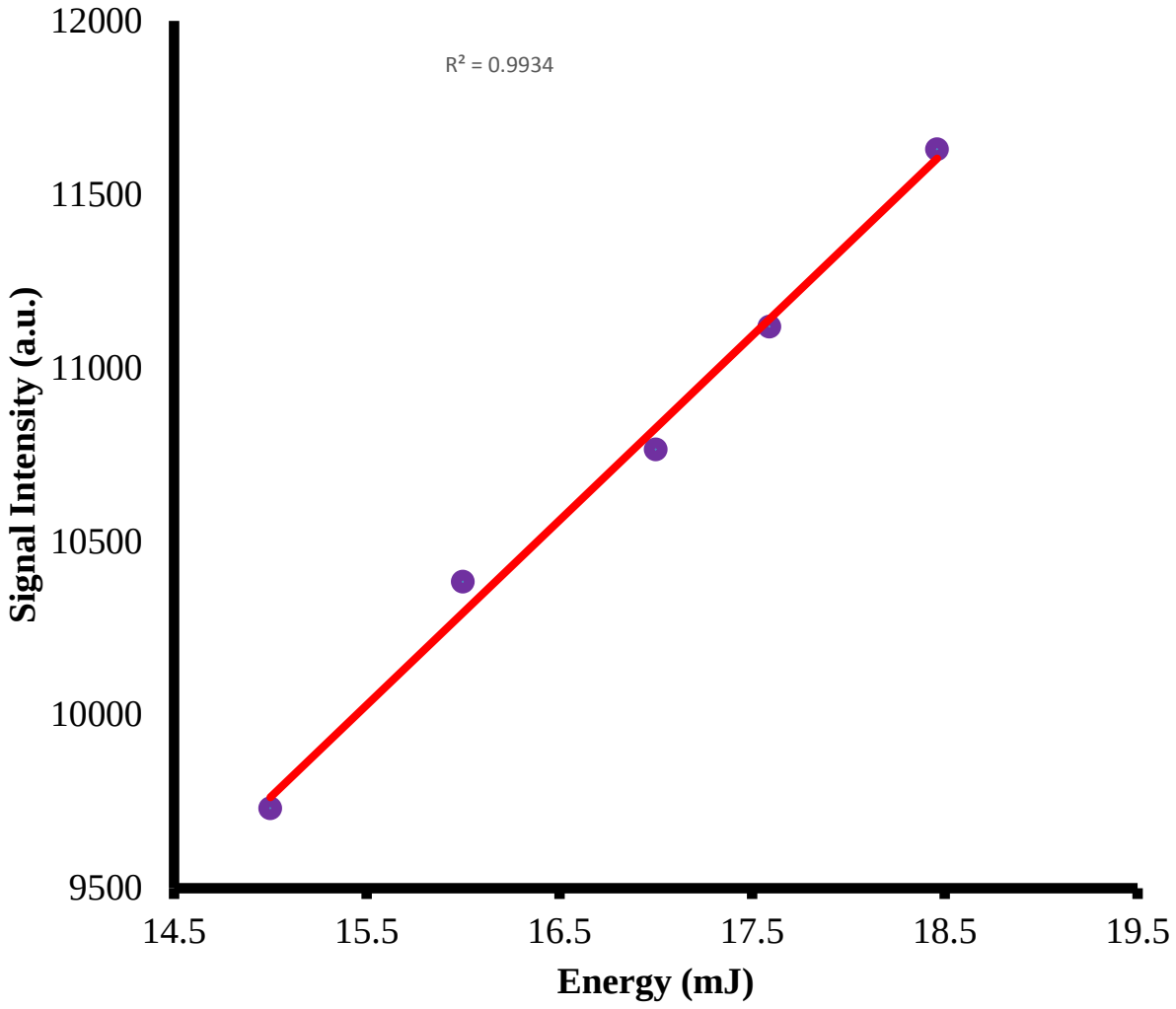

Fig. 4.31: LIBS signal intensity dependence on laser energy for fluorine line (F I 690.2 nm) in tobacco cigarette.

4.3.4 Detection of fluoride in Tobacco sample

After optimizing the all the main experimental parameters, our LIBS system was set for fluoride detection in the various brands of cigarettes. Time delay between the laser excitation and spectrum acquisition was kept at 720 ns, the laser energy was maintained at 17.54 mJ per pulse, the distance between the focal volume of the plasma plume and the optical fiber was set as 10 mm and the angle between test sample and the optical fiber was fixed at 45 ^{0}. Under these

experimental conditions, a typical spectrum of the tobacco samples were recorded in wavelength range 660-760 nm and is depicted in Fig. 4.32. A persistent spectral line of fluorine (at finger print wavelength of 690.2nm) was identified in all our samples within the specified wavelength range of the spectrum. The identification of recorded spectral lines was database conducted, using standard data published by National Institute of Standard and Technology[176]. Fig. 4.32 here indicates all the identified spectral lines in all different brands of tobacco samples, the identified F I lines are enclosed in the box, Table (4.7) shows other elements identified within this wavelength range, which are bromine, barium, sodium, copper, carbon, nickel and calcium. The maker line at 690.2 nm is due to atomic transition from, $2s^2\ 2p^4\ (3p)\ 3s \rightarrow 2s^2\ 2p^4\ (3p)\ 3s$ electronic state and the line is usually of moderate intensity. There are other transition line of neutral F I within our wavelength range which are very weak peak due to self-absorption.

4.3.5 Calibration Curve for the quantitative and qualitative estimation of fluorine concentration in different brands of tobacco cigarette.

As discussed in previous sections, we ensured the presence of optically thin plasma under our experimental conditions thus the system can be well calibrated to high degree of precision. The calibrated samples were prepared by adding known concentrations of fluoride to the sample matrix (samples #1) and subsequently we used fluorine line 690.20 nm as the marker line for drawing the calibration curve. The added concentrations of sodium fluoride were (NaF) are 15, 30, 60, 122, 231, 348, 420 and 537 ppm. The respective LIBS signal intensity spectra for each respective fluoride concentration added to the sample #1 matrix is depicted in Fig. 4.33 which shows a linearity in the growth of the LIBS signal intensity versus the F I concentration. The results displayed in the Fig.4.34 were used to plot the linear calibration curve, as depicted in Fig. 4.34 for the detection of fluoride in various cigarette samples. The calibration curve was used to

quantify the fluoride concentration present in the test samples #1, #2, #3 and #4 which were found to be 233.9, 340.9, 316.6 and 360.1 ppm respectively. The concentrations of fluoride detected in this study are considered to be more than the minimum permissible level set by food and drug regulatory agencies[180]. In order to ascertain the degree of sensitivity of our LIBS system, one has to estimate the limit of detection (LOD) using the calibration data[181]. LOD is the minimum amount of concentration of an analyte on a sample which can be reliably detected by a system[182] and can be estimated by using Eq. (19).

Using Eq. (19) the calculated LOD of our LIBS system is 14.4 ppm as shown in Table 4.8.

In this study, we were able ascertain the level of exposure and ingestion of fluoride concentration in different brands of tobacco cigarette, which was between 224 – 360 μg for each gram of tobacco cigarette intake. The level of intake depends on the habit of different persons, and generally since tobacco is not swallowed, only some fractions of the afore-mention amount are ingested during their consumption, which ultimately becomes available in the body through absorption. The experience gained from this work can be used for the elemental analysis of leaves, plants and vegetables.

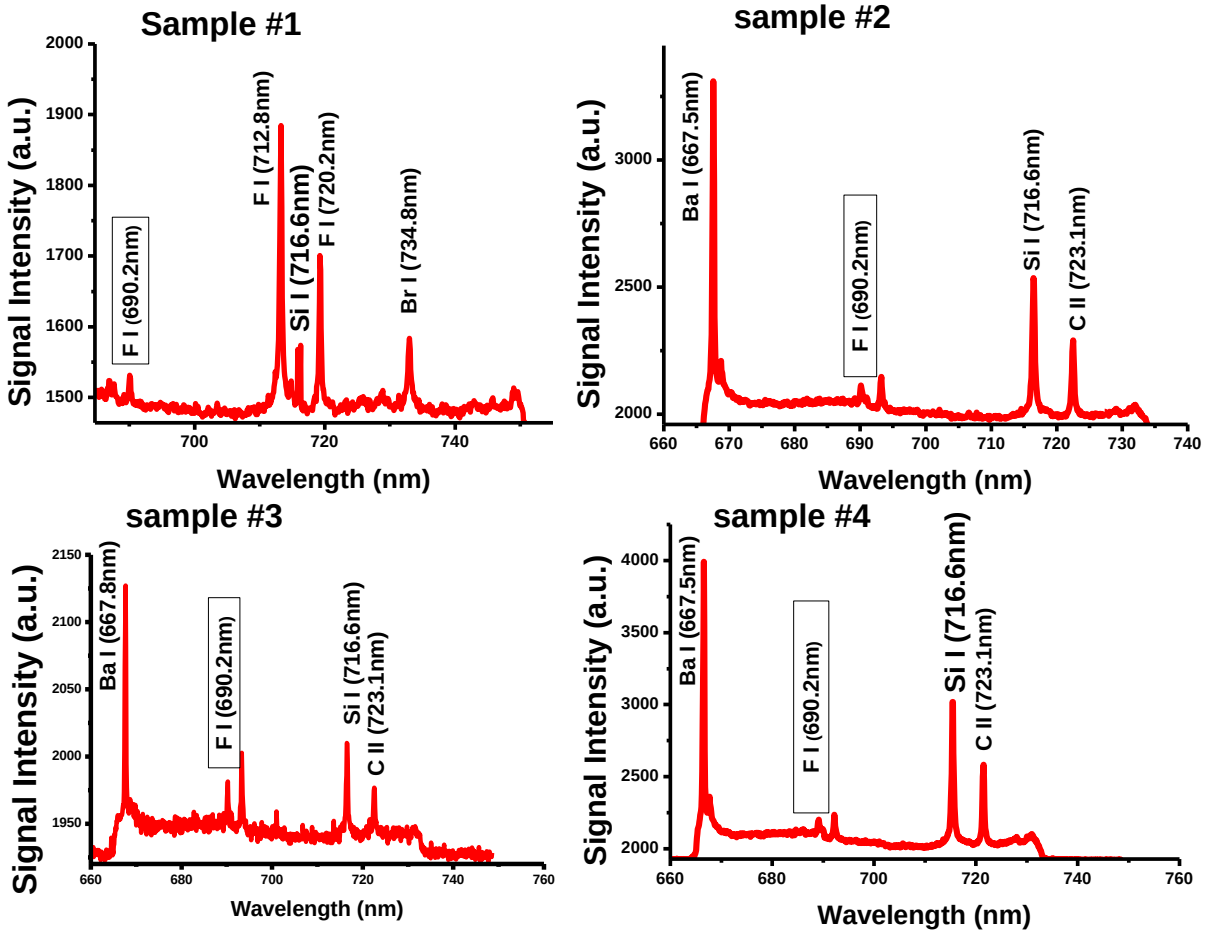

Fig.4. 32 Typical LIBS spectra for F I line in tobacco cigarette (sample 1-4) within the 660–760 nm wavelength range. The identified F I line is indicated as enclosed in the box.

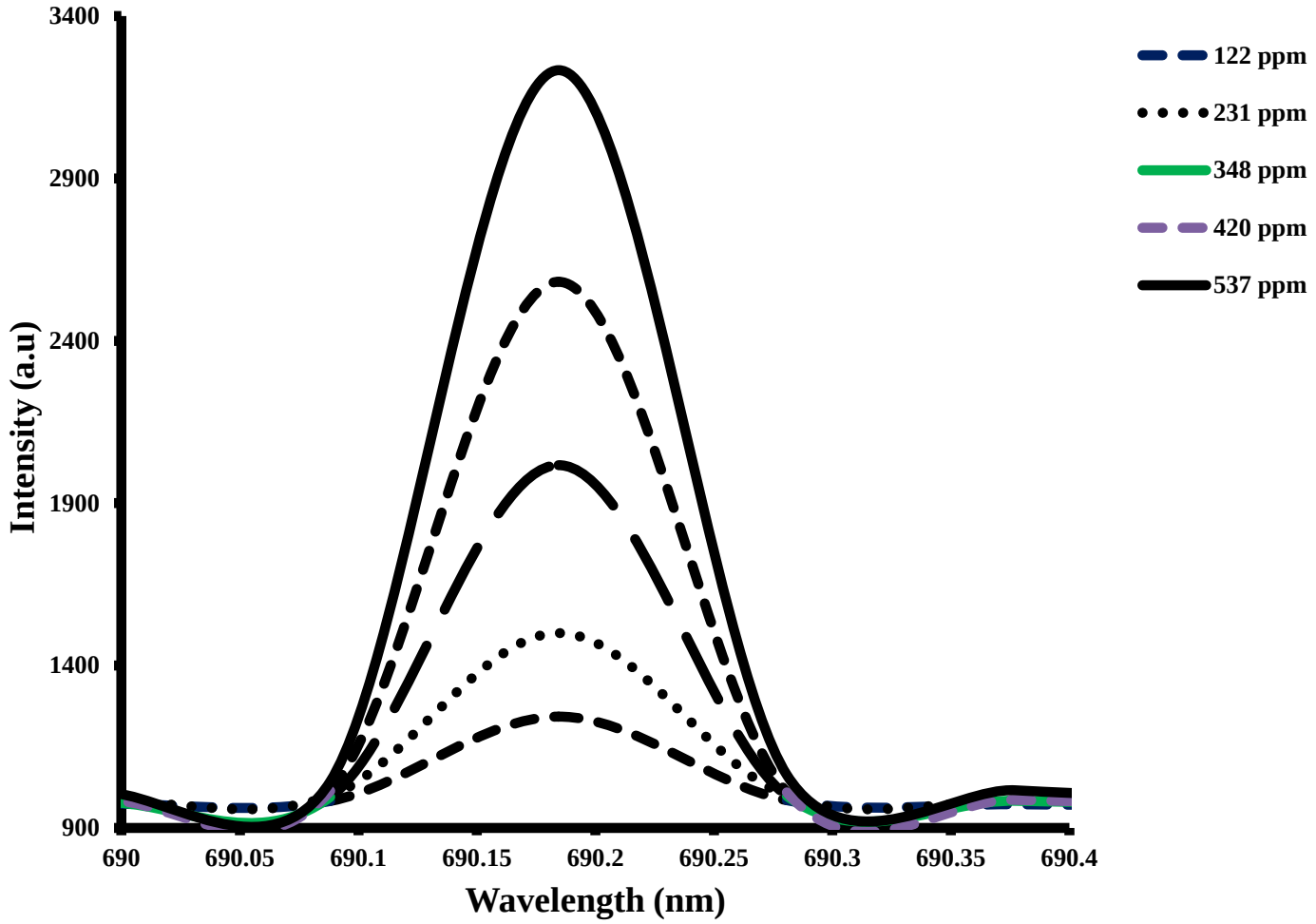

Fig. 4. 33. Superimposed LIBS Spectra of standard samples having 122, 231, 348,420 and 537 ppm fluoride concentrations for plotting the calibration curve.

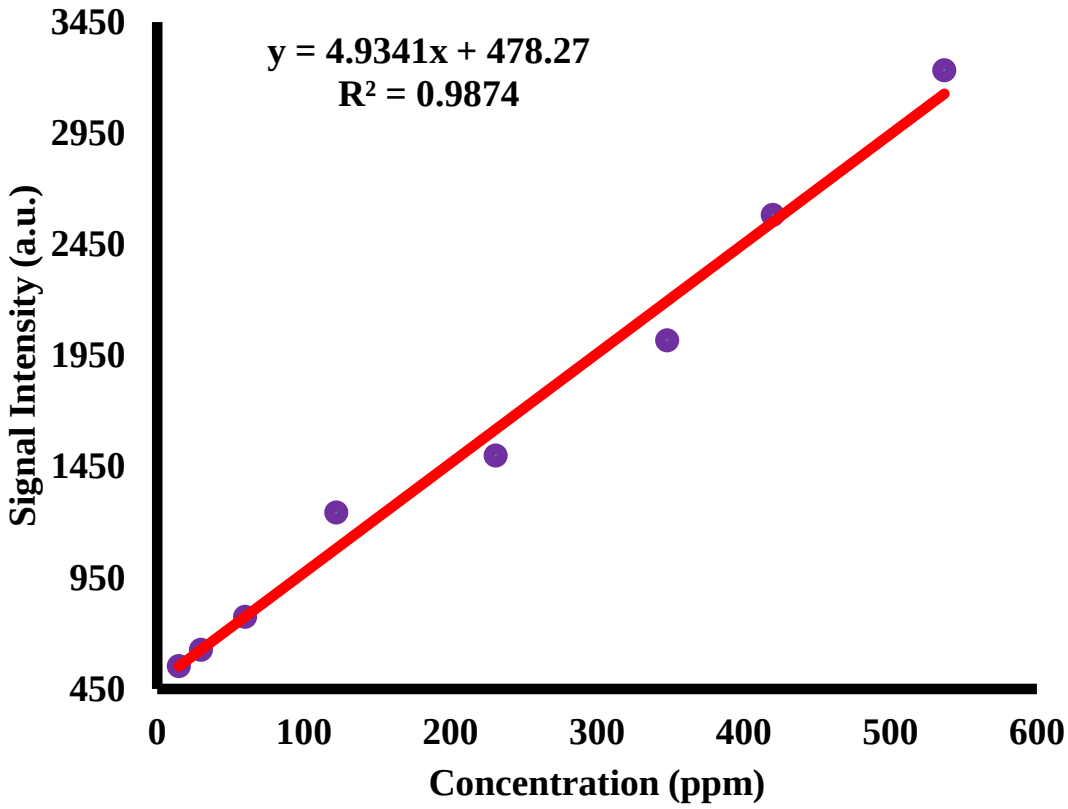

Fig. 4.34. LIBS calibration curve for fluorine in tobacco cigarette.

Table 4.7. Finger print wavelengths, assignment of atomic transitions and other parameters for various atomic lines of all the elements detected in tobacco cigarettes including neutral barium (Ba I) used for the Boltzmann's plot.

Element	Finger print Wavelength (nm)	g_k	$A_{ik}X\ 10^8$	E_k (eV)	Optical Transition Assignment Lower State→Upper State	LIBS signal Intensity (arb. units)	
Na I	589.6	5	0.62	2.10	$2p^6\ 3s\ ^2S_{1/2}\rightarrow 2p^6\ 3p\ ^2P_{1/2}$	1774	
Na II	314.6	4	0.45	41.12	$2p^5\ 3p \rightarrow 2p^5\ 3d\ ^{2P}{}_{3/2}$	1571	
Ba I	307.2	3	0.41	4.04	$6s^2\ ^1S_0\rightarrow 6s\ 7p\ ^1P_1$	1550	
	350.1	3	0.35	3.54	$6s^2\ ^1S_0\rightarrow 5d\ 6p\ ^1P_1$	1489	
	611.08	5	0.15	3.22	$6s\ 5d\ ^3D_3\rightarrow 5d\ 6p\ ^3P_2$	2453	
	652.7	5	0.33	3.04	$6s\ 5d\ ^3D_2\rightarrow 5d\ 6p\ ^3D_2$	1955	
	667.5	4	0.19	2.99	$6s\ 5d\ ^3D_2\rightarrow 5d\ 6p\ ^3D_1$	Sample #2	1579
						Sample #2	2543
						Sample #2	3034
Ca I	616.2	3	0.48	3.91	$4s\ 4p\ ^{3P}{}_2\rightarrow 4s\ 5s\ ^3S_1$	2928	
Cu I	324.8	4	0.14	3.81	$3d^{10}\ 4s\ ^{2S}{}_{1/2}\rightarrow 3d^{10}\ 4s\ ^2P_{3/2}$	2200	
Ni II	337.2	3	0.41	3.67	$3d^8\ 4s^2\ ^3F_3\rightarrow 3d^8\ 4s4p\ ^3G_4$	1499	
Br I	734.8	6	0.12	9.73	$4p^4\ 5s\ ^3P_{3/2}\rightarrow 4p^4\ 5p\ ^3P_{5/2}$	1587	
C II	723.1	4	0.35	18.05	$2s^2\ 3p\ ^2P_{1/2}\rightarrow 2s^2\ 3d\ ^2D_{3/2}$	Sample #2	2302
						Sample #3	1978
						Sample #4	2607

Table.4.8 Concentration of fluorine detected in various tobacco cigarette samples using our LIBS setup.

		Sample #1	233.9	
690.2	$2p^4\ 3s\ {}^4P_{3/2} \rightarrow$	Sample 2	340.9	14.4
	$2p^4\ 3p\ {}^4D_{5/2}$	Sample #3	316.7	
		Sample #4	360.2	

4.4 Detection of toxic elements using Laser Induced Breakdown Spectroscopy in smoker and nonsmoker's teeth and investigation of periodontal parameters

4.4.1 Introduction

The harmful effects of nicotine, carbon monoxide, and other noxious gases of tobacco smoke are well known. However, there is no systematic study reported regarding the tracing of heavy metals such as cadmium, lead, and arsenic present in the periodontium due to heavy tobacco smoking. Hence, there is a high demand to develop a reliable and fast technique for detection of these elements, which have serious effects on smokers' teeth in general and on overall health in particular. Over the past few years, oral health research has significantly contributed to the understanding of the mechanisms that lead to the deterioration of the hard and soft tissues supporting the teeth. Taking records of the number of cigarettes smoked per day and the amount of years tobacco was consumed into consideration, a dose-response relationship could be established. Various potential significant and pathogenic effects of tobacco related substances may affect the periodontal tissues and the immune system or the composition of the oral flora. Moreover, there is enough evidence that tobacco consumption may change the genetically determined susceptibility for periodontal diseases [183-188].

Analytical epidemiological studies have been quite successful in identifying a handful of risk factors for the onset of the disease and its progression. These include colonization at high levels by certain sub-gingival bacteria, environmental exposures such as cigarette smoking, and systemic conditions such as diabetes mellitus. Importantly, the molecular basis of host susceptibility has recently begun to be unraveled. Research findings are now focused on creating multifactorial models to assess the risk of the disease, prior to the development of irreversible damage. Importantly, the role of periodontal infections, as a modifier of systemic health, is being increasingly explored [191-196]. It was concluded that there was strong association between cigarette smoking and the risk of periodontitis [197-199]. The odds of having severe periodontitis increased considerably among smokers and showed a dose-dependent relationship with the amount of cigarette consumption. In this study, a chemical analysis of teeth surface was conducted using a laser induced breakdown spectroscopy (LIBS) technique, which was assembled recently at our laboratory. Toxic elements such as cadmium and arsenic were detected with the LIBS technique in smoker's teeth, which could cause the periodontal problems. These toxic elements were also detected in the teeth of nonsmokers (who are passive smokers) due to environmental contamination and poor dental hygienic conditions. However, the concentration of toxic elements in nonsmoker teeth was much less than in the smoking group.

4.4.2 Local thermodynamic Equilibrium for tooth samples

Optically thin plasma indicates the absence of self-absorption of the emission lines in the plasma. For optically thin plasma and Local Thermal Equilibrium condition, the spectral line intensity can is written by Eq. (18), where $I_{ik,z}$ is the relative intensity due to electron transition from a higher energy state k to a lower state i in an atom with ionization z, $E_{i,z}$ corresponds to the upper energy level and $g_{i,z}$ is the upper energy level statistical weight, $A_{ik,z}$ is the transitional

probability, $\lambda_{ik,z}$ is the spectral line wavelength, $U_z(T)$ is the atomic partition function at temperature T, L is the plasma characteristic length, N_z is the emitting atoms density, K is the Boltzmann constant and T is the plasma temperature. Local Thermal Equilibrium (LTE) condition is required to satisfy optically thin plasma and avoid self-absorption effect. Eq. 15 was applied on the strongest observed spectral lines of the calcium.

The chosen lines used for plasma temperature estimation are shown with an arrow in figure 4.35 which were emission lines of Ca at 422.67 nm, 445.48 nm, 585.75 nm, and 646.26 nm. By plotting the left hand side expression versus energy of the upper level $E_{i,z}$ for the spectral lines of a single atomic species in the ionization state z, the temperature can be calculated from the slope 1/KT. The spectroscopic parameters Aik,z, gi,z and Ei,z were taken from the NIST data base[200] and tabulated in table (4.9). The average of the calculated plasma temperature for excitation wavelength 266 nm, laser energy 40 mJ and 400 ns delay time was 11813 ± 513 K, which were calculated from the slope of Fig. 4.36a.

LTE condition was satisfied in the plasma when it has a sufficiently high electron density, and hence the minimum electron density for LTE condition was calculated using Mcwhirter criteria defined in Eq. (8), where n_e, ΔE and T are the electron density, the largest transition energy corresponding to the shortest wavelength used in plasma temperature calculation[80]. Broadening of plasma spectral lines originates from Stark effect (caused by energy levels splitting due to plasma induced electric field and has FWHM ~ 0.1-1 nm), the Doppler effect (caused by the thermal motion of the ions and has FWHM ~ 0.01-0.1 nm), Van Der Waals effect (caused by Van Der Waals' dipolar force, negligible in high ionized plasma and has FWHM ~ 0.01 nm) and instrumental reasons [201-204]. The Stark effect broadening dominants, and thus is used to estimate the electron density from the full width at half-maximum (FWHM) of the

neutral calcium line at 422.67 nm. Stark broadening is described by Lorentzian function, and the FWHM is directly proportional to the electron density as given in Eq. (17), where Δλ is the FWHM of stark broadening profile at an electron density of 10^{17} cm^{-1} obtained from Grime's book by interpolating at the calculated plasma temperature. Fig. 4.36b shows the data points and the Gaussian fitting of Ca I 422.67nm spectral line with a FWHM of 1.15895 nm. Therefore, the electron density at 400 ns delay time and plasma temperature (11813 K) was 3.0×10^{22} cm^{-3} which was higher than the estimated minimum electron density 3.83×10^{17} cm^{-3}; hence in our experiment the laser induced plasma was optically thin and is in LTE condition.

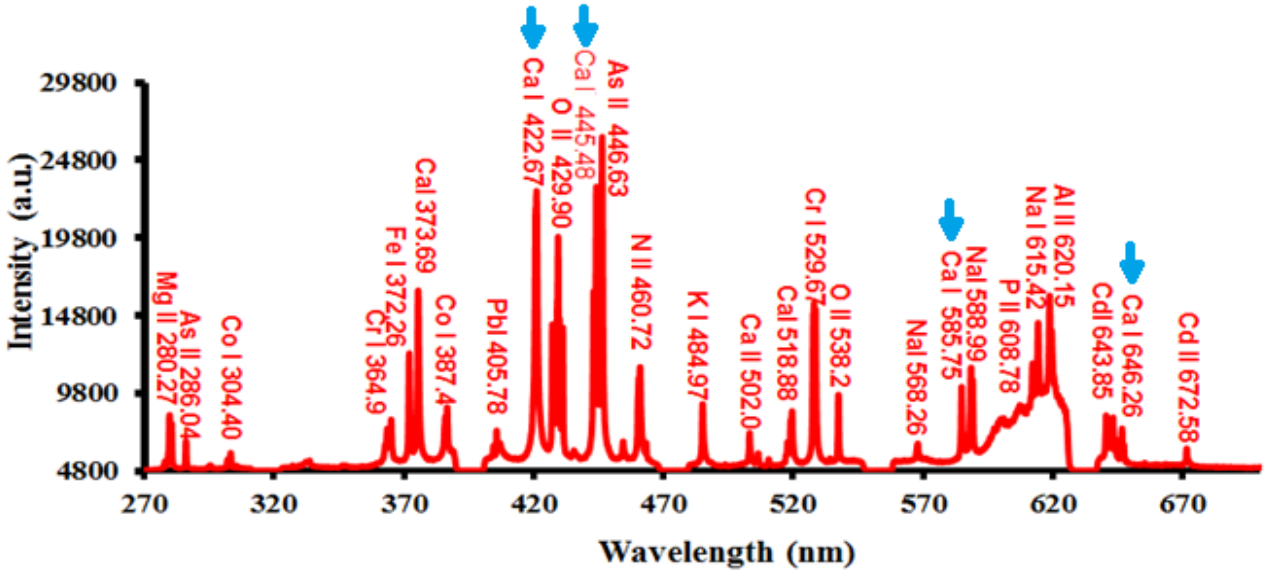

Fig. 4.35. Spectrum showing spectral lines use for plasma temperature estimation. Spectrum was from non-smoker's teeth.

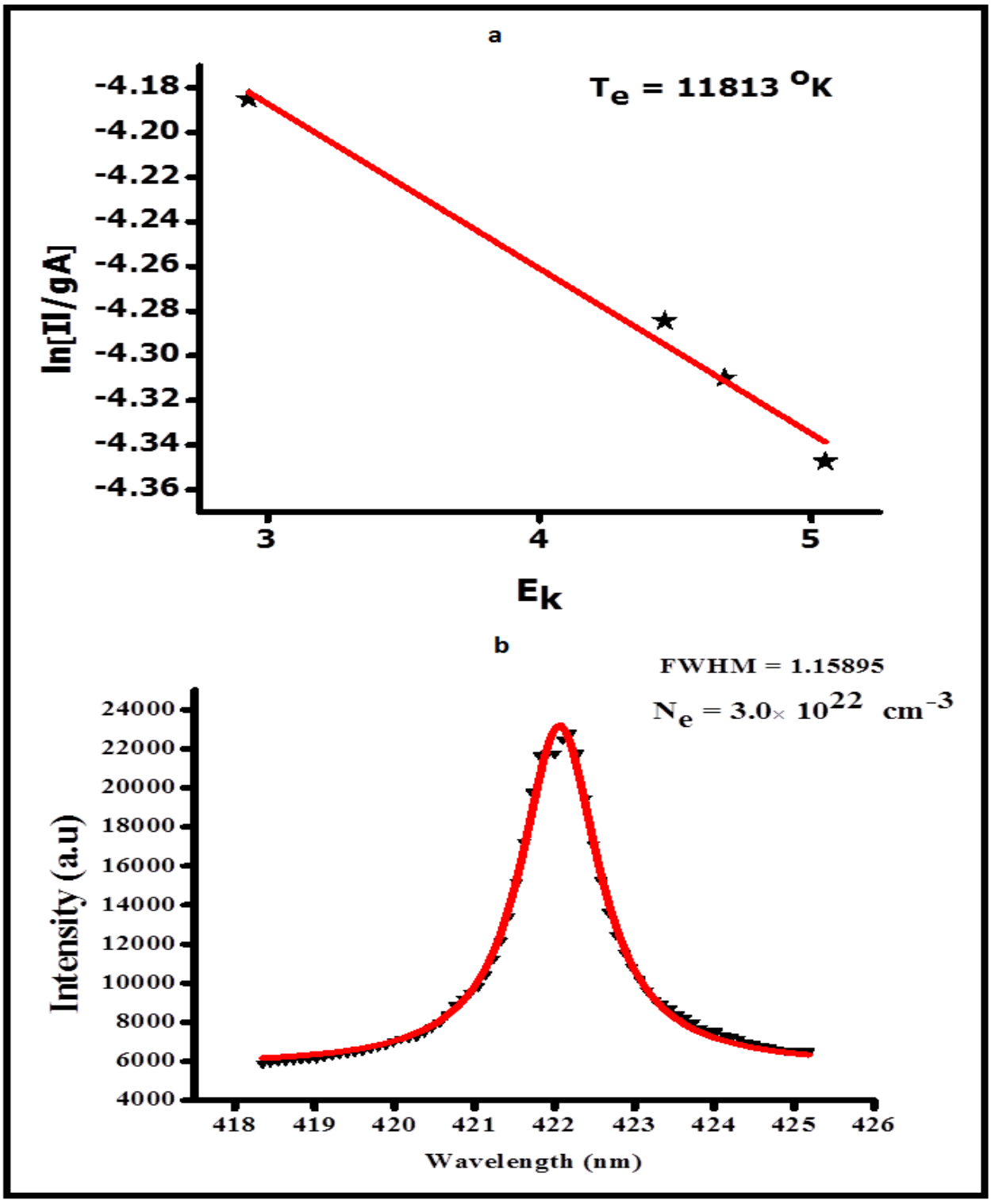

Fig.4.36. (a) Boltzmann plot to calculate the plasma temperature of plasma plumes. (b) Stark broadening profile for characteristics atomic transition lines of Ca I (422.67 nm) to estimate the electron density.

Table 4.9 Spectroscopic parameters of neutral Calcium (Ca I) lines used for estimation of plasma temperature.

Wavelength (nm)	Signal Intensity	Statistical weight	Transition probability	Energy of the upper level
		g_k	A_{ik} (S^{-1})	Ek (eV)
422.67	22487	3	2.180E+08	2.93
445.48	24780	7	8.7E+07	4.68
585.75	10207	5	6.6E+07	5.05
646.26	7525	7	4.7E+07	4.46

4.4.3 Quantitative LIBS spectroscopy of Teeth sample

The laser induced breakdown spectroscopy analysis is based on identifying emission of the neutral and singly ionized atoms by creating plasma and exciting atoms through highly focused laser radiations. These lines are identified by so called finger print wavelength for the elements presented in the teeth samples. The LIBS technique works by inducing plasma at high temperature at a spot on the sample using extreme powerful laser pulses. In this plasma, dissociation through bond breaking occurs in different stages which is followed by thermionic emission, heating, melting, excitation and ionization[203]. The laser energy and delay time were investigated in this experiment as well. The delay time (time after laser pulse) must be smaller than the life time of the excited electrons for LIBS analysis. The main parameters that could affect the sensitivity of the LIBS system for individual elements are the transitional strength of the elemental line (transition probability), incident laser energy, delay time (time between the firing

of the laser pulse and opening of the camera shutter), which were selected during the measurements. Experiments were performed to find optimal conditions for temporal delay, incident laser energy for the analysis of different teeth samples under investigation. LIBS spectra of different teeth samples were recorded over a 200–650 nm wavelength range for qualitative and quantitative analysis under the optimum experimental conditions. Optimization of the LIBS spectrometer prior to its application for teeth analysis was important so that the LIBS spectra and the intensities of lines collected were accurate.

In order to do the spectral analysis of teeth samples using LIBS, the spectral lines were measured under different laser fluences by scanning the spectrometer in the 200-700 nm region and after optimizing all the parameters like focusing of incident laser beam, optimum collection of plasma emission, gate width and delay-time. After achieving the optimal experimental conditions, the LIBS spectra of different teeth samples were recorded and depicted in Figs. 4.37-4.39. Figs 4.37-4.39 depicts the LIBS spectra and identifies the different elements presented in the teeth samples in the 270 -700 nm wavelength regions. The identification of the atomic transition lines was carried out using NIST spectral data base [20] and finger print wavelength of each element presented in the teeth samples was identified. As shown in Figs. 4.37-4.39, the carcinogenic metals such as lead (Pb), cadmium (Cd) and arsenic (As) were detected along with trace metals like calcium (Ca), phosphorus (P), sodium (Na) and magnesium (Mg). Fig. (4.40) is a chart plot of mean LIBS signal intensity recorded for carcinogenic elements like Pb, Cd and As in smoker, non-smoker and controlled groups.The spectral marker lines (finger print wavelengths) of these elements were used for the calibration and quantifications of these elements. The identified LIBS spectrum is due to either the emission of the neutral or singly ionized transitions of Ca,

phosphorus (P), lead (Pb), cadmium (Cd), Oxygen (O), Nitrogen (N), Iron (Fe), Potassium (K) and arsenic (As).

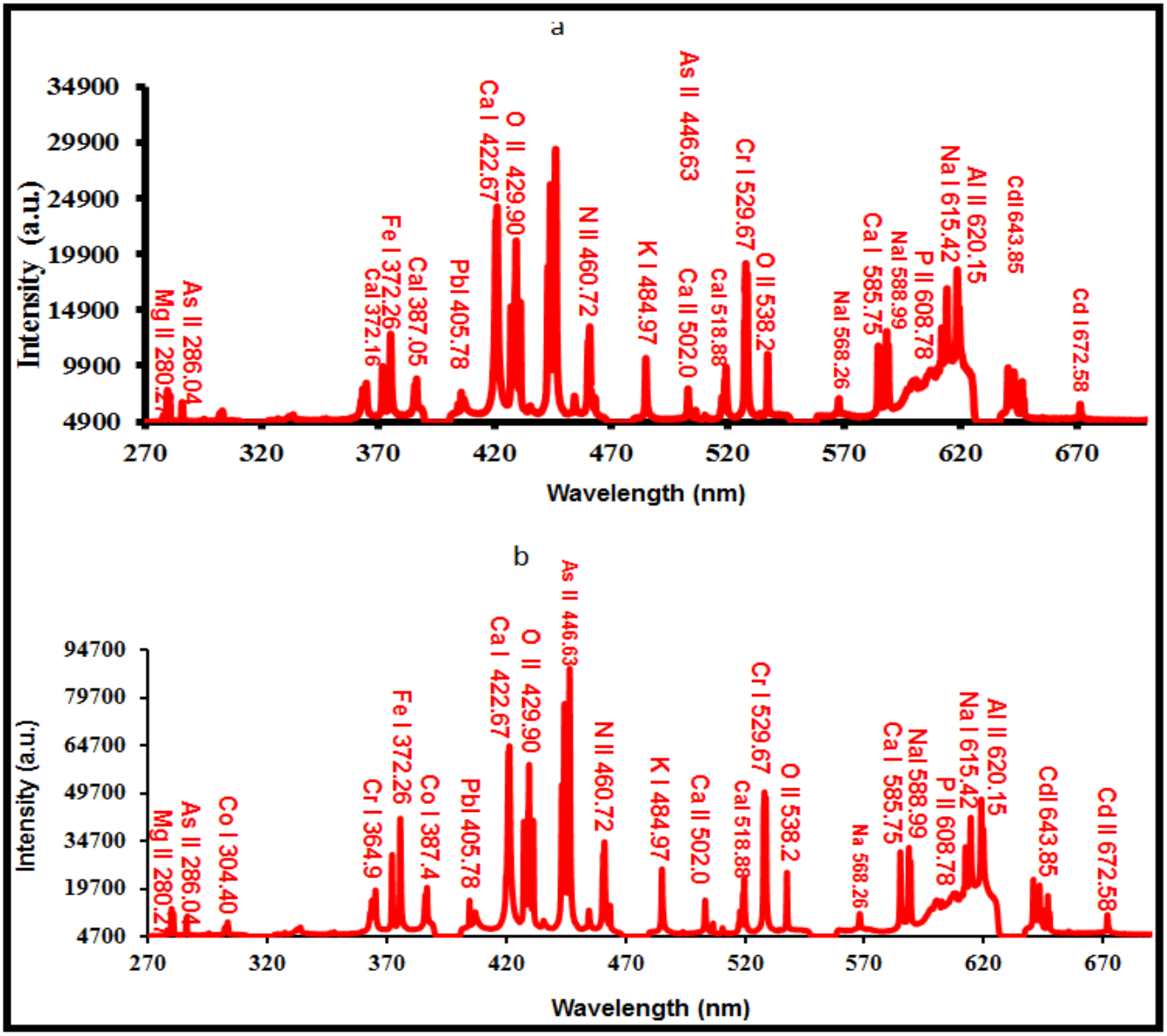

Fig. 4.37 Typical LIBS spectra showing different elements present in the teeth samples of smoker group in the 270 -700 nm wavelength region recorded at laser pulse energy = 40 mJ and wavelength of 266 nm.

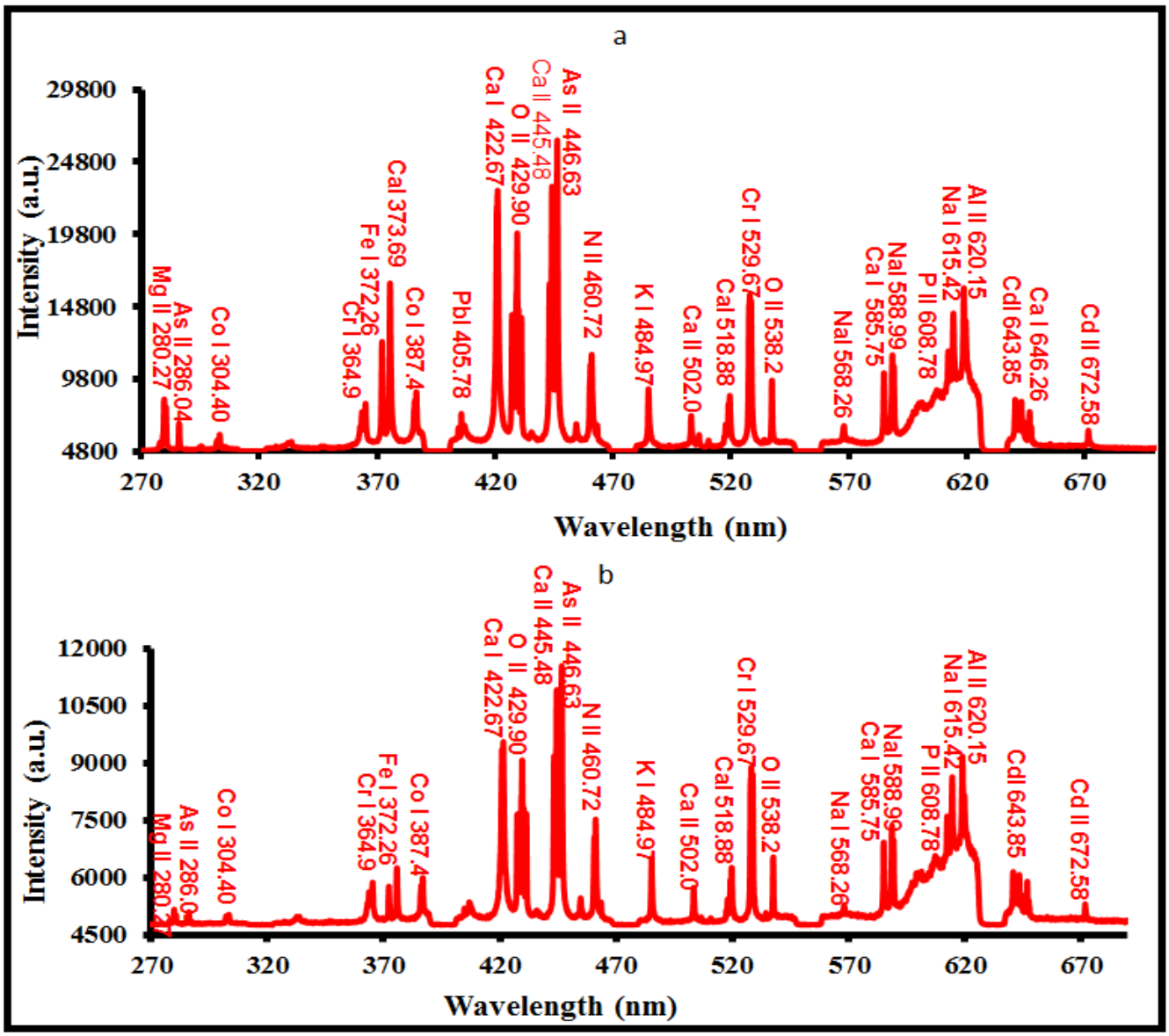

Fig. 4.38 Typical LIBS spectra showing different elements present in the teeth samples of non smoker group in the 270 -700 nm wavelength region recorded at laser pulse energy = 40 mJ and wavelength of 266 nm.

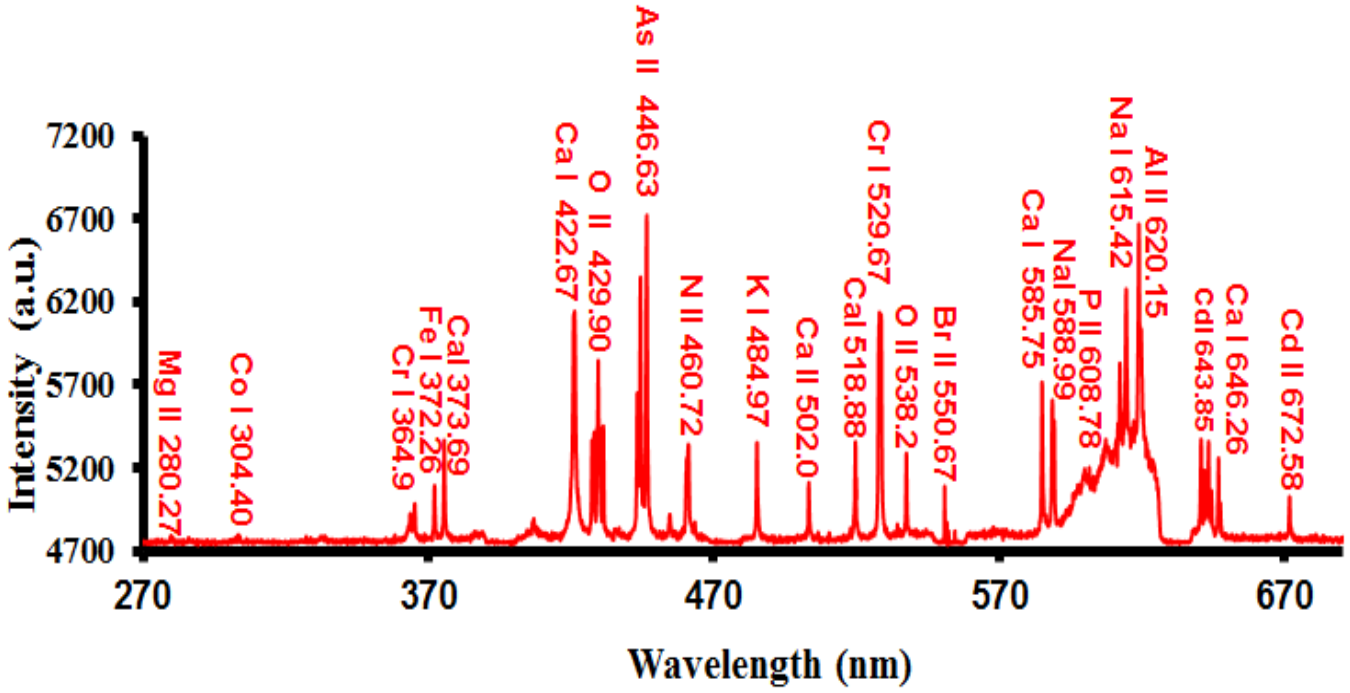

Fig. 4.39 Typical LIBS spectra showing different elements present in the teeth samples of control group in the 270 -700 nm wavelength region recorded at laser pulse energy 40 mJ and wavelength of 266 nm.

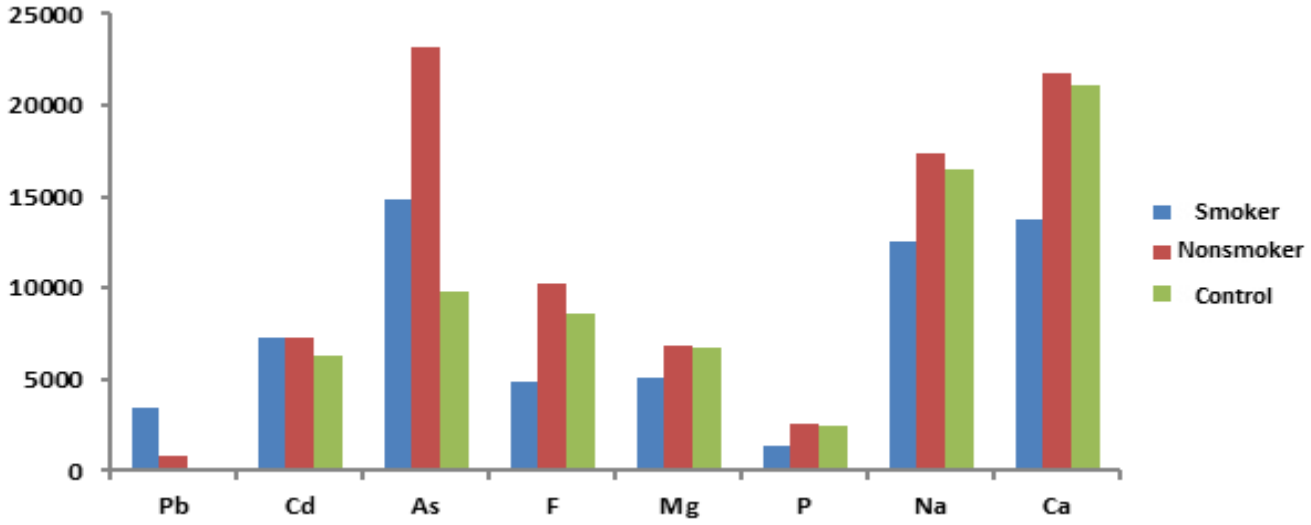

Fig. 4.40: Chart plot of mean LIBS signal intensity of Pb, Cd and As in smoker, non-smoker and control groups.

4.4.4 Clinical Monitoring of Teeth Sample.

Clinical parameters were evaluated for each patient using the following procedures:

1. PD was measured from the gingival margin to thebottom of the pocket.

2. CAL was measured from the cement-enamel junction tothe bottom of the pocket. PD and CAL were recorded using a standard periodontal probe with manual pressure of approximately 25 g at six sites per tooth (mesiobuccal, buccal, distobuccal, mesiolingual, lingual, and distolingual).

3. Plaque index [205] parameter was defined as (0 no plaque; 1 thin plaque layer at the gingival margin only detected by scraping with a probe; 2 moderate layer of plaque along the gingival margin (interdental spaces free but plaque is visible to the naked eye); 3 abundant plaque along the gingival margin (interdental spaces filled with plaque). PI was obtained on four sites (mesiobuccal, buccal, distobuccal, and lingual).

4. Gingival index was defined as 0 normal gingival (no inflammation; no discoloration; no bleeding); 1 mild inflammation (slight erythema; no bleeding); 2 moderate inflammation and bleeding on probing; 3 severe inflammation (severe erythema and tendency to spontaneous bleeding). The GI was obtained on four sites (mesiobuccal, buccal, distobuccal, and lingual). For each one of these above-mentioned variables, the mean value of all recordings was called as mean PD, mean CAL, mean PI, and mean GI, respectively, of the individual[205]. For pocket depth and attachment loss measurements and periodontal index (PDI), the clinical method as proposed by Ramfjord and described in detail in[206] was adopted in this study.

4.4.5 Determination of Toxic Elements Concentration in Teeth Samples.

In order to determine the concentration of toxic elements presented in the teeth samples, small amounts from each teeth sample were carefully extracted to be analysed. The calibration curves

between the analyte concentration in the teeth matrix and its LIBS signal lines intensity were carefully plotted for estimating the limit of detection of our LIBS system.

To draw the calibration curves, 5000 µg/ml solution of Ca, Mg, Na, As, Cd, and Pb was used to prepare standard samples of known concentrations in double distilled water. The standard solutions were having concentrations varying from 50 ppm (parts per million) to 1200 ppm for Ca, Mg, Na, As, Cd, and Pb by weight. These solutions with known concentration were utilized, and the wet paste was dried in the Oven at 350 K temperature during one day for preparation of standard samples to draw the calibration curves.

The maximum Pb concentration measured in smoker group was in 34 - 55 ppm range for non-smokers in 23- 29 ppm range and for the controlled group in 0.17-0.31 ppm range after drawing the calibration curves. It is worth mentioning that these values are higher than the permissible safe limits specified by the world health organization. In addition, the measured concentrations by our LIBS system were counter verified by using a standard method such as inductively coupled plasma spectrometry. Our LIBS results are in good agreement with the results obtained using ICP-MS technique. The recorded LIBS spectra in this study were well identified to the finger wavelengths of 405.7 nm (Pb-I), 643.8 nm (Cd-I), 446.6 nm (As-I), 422.7 nm (Ca-I), 608.78 nm (P-I), 280.27 (Mg-I) and 588.9 nm (Na-I), 538.2 (O II), 460.72 (N II), 372.62 (Fe I) using NIST data base. Emission intensities of Pb, Cd and As corresponding to the lines 405.7, 638.8, 446.6,nm for each teeth were recorded .

Gingival index (GI), plaque index (PI), clinical attachment loss (CAL), and probing pocket depth (PD) were recorded for all three cases. After the extraction of the teeth, spectrochemical analysis was done using the self-assembled LIBS system. The calibration curves between the analyte concentration in teeth matrix and its LIBS signal line intensity were carefully plotted for

estimation of quantitative analysis of teeth samples. The calibration curves for three toxic elements (Pb, Cd, and As) of our interest are depicted in Fig. 4.41. In order to calibrate our LIBS system for quantitative analysis, the compounds of the elements (Pb, Cd, and As, purchased from Sigma Aldrich) were added to the sample matrix (teeth) in various known concentrations, and the pellet was made for eachconcentration. Besides, a straight line calibration curve was established by drawing the LIBS emission intensity versus lead, cadmium, arsenic concentration in part per million (ppm). The estimated concentrations for each teeth sample were compared with the results obtained with ICP-MS and are presented in Table 4.10.

The recorded values obtained by each technique (LIBS, ICP-MS), indicated clearly that the concentration of Pb present in the teeth samples is above the acceptable permissible limit of 3.6 ppm. The concentrations of most of toxic elements were significantly high in smoker group. This could be due to the rise of the clinical attachment loss (CAL) for smoker patients and the nonsmokers who exhibit these toxic elements presence as a result of passive smoking, polluted nutrition and bad dental hygiene. The carcinogenic effects of lead and cadmium are well known besides the existence of arsenic prevents the precipitation of fluorine which could also accelerate teeth decay at faster rate.

Table 4.11 lists toxic elements detected in teeth samples along with their wavelengths, mean intensities and transition probability for smoker, nonsmoker and controlled groups. Results of this study also revealed that the mean gingival index (GI) in smoker group was 1.966 and it was 1.24 in non-smoker group while it was 0.933 in control group.

Our study revealed that for the CAL values, there is a statistically significant difference between the smoker group and the other two groups ($p \leq 0.05$).

CAL concentration was less in the teeth of smoker than other two other group. GI in nonsmokers was less than smokers and the difference was statistically significant ($p \leq 0.05$) and plaque index (PI) was higher in smokers than controlled group and the difference was statistically quite significant ($p \leq 0.05$). An important positive correlation has been found between smoking and clinical attachment loss. In addition, toxic and injurious species such as As, Cd and Pb and other elements like Ca, Na, P and Mg were detected using LIBS technique. The mean of GI for smoker, nonsmoker and control is presented in Table 4.12.

For ICP-MS analysis, the teeth samples were digested in 5% nitric acid of 99.99% purity. Representative 1 gram (dry weight) of teeth sample was digested with repeated additions of nitric acid (HNO_3) and hydrogen peroxide (H_2O_2). The resultant solution was reduced in volume while heating at 95°C for 6 hours and then diluted to a final volume. The resulting solution of the sample was analyzed for Pb, As and Cd using Inductively Coupled Plasma Spectrometer calibrated through the use of reference standards of three levels of accuracy. This procedure has taken care any doubt about the accuracy of the analysis of heterogeneous media such as tooth sample using ICP-MS. The results achieved with LIBS technique are in a perfect agreement with the standard ICP result.

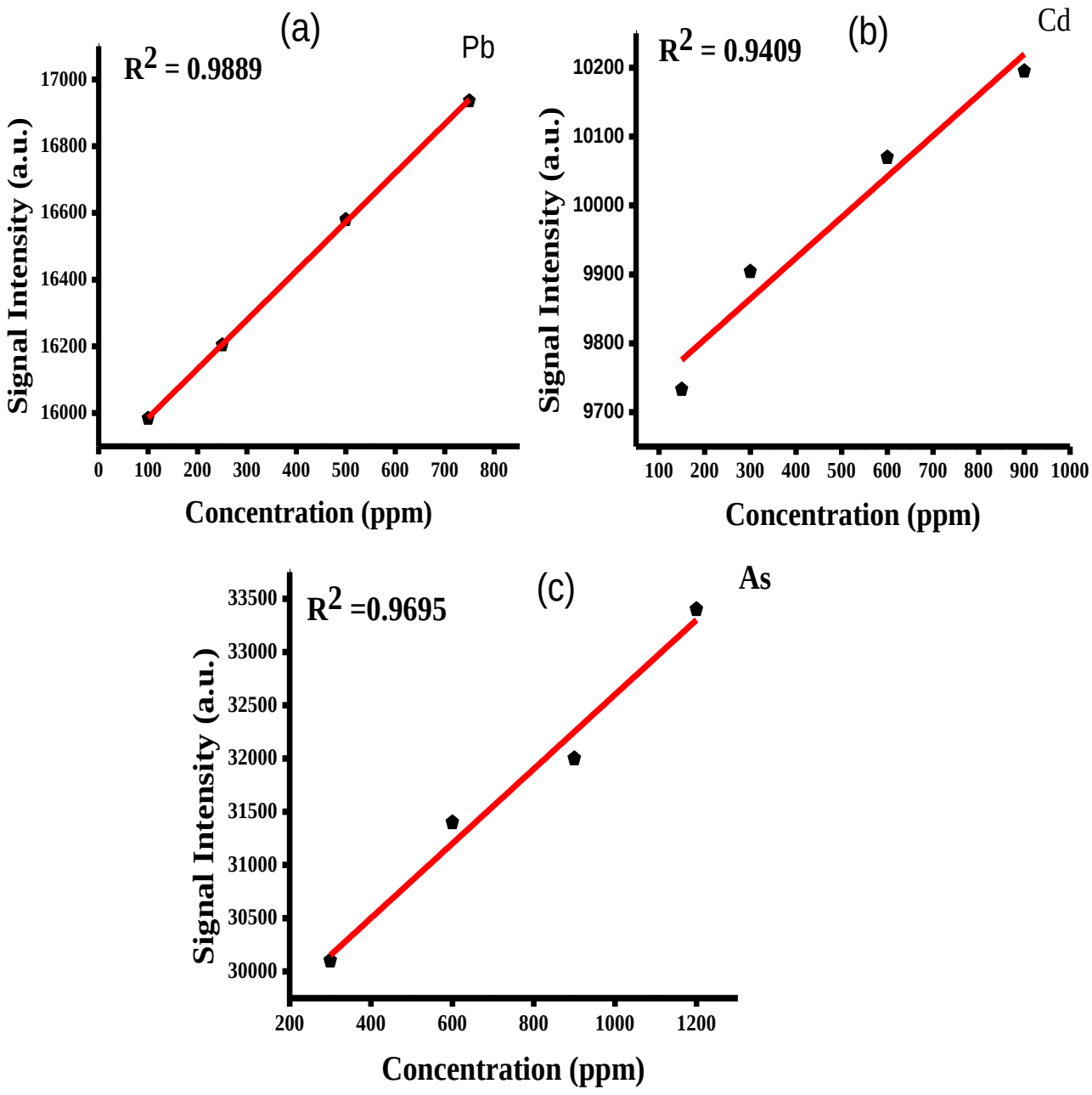

Fig.4.41 LIBS calibration curves of (a) Pb, (b) As and (c) Cd.

Table 4.10. List of toxic elements detected by LIBS and ICP-MS technique and their comparison in smoker, non-smoker and control groups.

Elements detected In Teeth samples	Wavelength (nm)	Sample type	Comparison of LIBS and ICP mean values and relative accuracy (RA)			
			LIBS(ppm)	ICP(ppm)	RA	Standard deviation (S.D.)LIBS
Pb	405.7	Smoker	34.42	35.12	0.98	0.99
		Nonsmoker	23.32	24.41	0.96	0.97
		Control	0.17	0.18	0.94	0.99
Cd	643.85	Smoker	0.33	0.35	0.94	0.99
		Nonsmoker	0.26	0.28	0.93	0.97
		Control	0.01	0.02	0.50	0.99
As	446.63	Smoker	0.91	0.98	0.93	0.99
		Nonsmoker	0.64	0.79	0.81	0.97
		Control	0.05	0.06	0.83	0.99

Table 4.11 Toxic elements detected in teeth samples along with their wavelength, mean LIBS signal intensities and transition probability.

Element	Wavelength (nm)	Mean Intensity For smoker (a.u.)	Mean Intensity For nonsmoker (a.u.)	Transition	Transition probability
Pb	405.8	12334.1	9272.18	$6p_{1/2}\,6p_{3/2} \rightarrow 6p_{1/2}\,7s_{1/2}$	8.9E+07
Cd	643.85	17172.2	10256.4	$5S\ 5p \rightarrow 5s\ 5d$	0.55E+08
As	446.63	54375.5	24156.2	$3d^5\ 4s \rightarrow 3d^5\ 4p$	3.07E+07

Table 4.12. The mean values of gingival index (GI) and standard deviation (SD) for smoker, nonsmoker and control groups.

	Smoker		nonsmoker		control	
GI	mean	SD	mean	SD	mean	SD
	1.57	0.55	1.18	0.31	0.871	0.11

CONCLUSION

A high sensitive spectrometer based on laser induced breakdown spectroscopy was assembled for qualitative and quantitative analysis of various brands of tea samples available in the market. The main elements detected in tea samples were Br, Cr, Fe, K, Ca, Cu, and Si. The spectral assignment was carried out by using the NIST Data base and finger print wavelengths of each element were identified. The temporal behaviors of plasma parameters like electron temperature and electron density were also studied for the plasma generated prior to tea sample analysis for the first time. For quantitative analysis, standard samples were prepared in known concentration and calibrations curves for each element were drawn. The concentration of iron, chromium, potassium, bromine, copper, silicon, and calcium estimated in all the tea samples are between 378-656 ppm, 96-124 ppm, 1421-6785 ppm, 99-1476 ppm, 17-36 ppm, 2-11 ppm and 92-130 ppm respectively. In order to validate our LIBS results, standard technique like ICP-MS was also applied for the analysis of same tea samples and it is worth mentioning that our LIBS results are in excellent agreement with ICP-MS results. The concentration detected by LIBS system was much higher than the safe permissible limit of Br and Cr set by EPA and food drug agencies.

A laser induced breakdown spectrometer was assembled and applied successfully for the spectro-chemical analysis of date fruits samples. The main focus of this study was to evaluate the nutritional value of date fruits by detection of concentration of nutritional element like calcium (Ca) and magnesium (Mg) concentration and chromium (Cr) as a toxic element. The minimum detection limit established after drawing the calibration curves using standard samples for Ca, Mg and Cr was 6, 17 and 1 ppm respectively. In addition, the date plasma parameters such as electron temperature and electron number density was measured which was 5660 k and 3.47 X $10^{16}cm^{-3}$ respectively using the Boltzmann plot. In addition, the Ca, Mg and Cr

concentrations measured using LIBS were confirmed by a standard method like ICP-MS spectrometer and our LIBS results are in excellent agreement with ICP-MS.

A UV-pulsed LIBS system equipped with a highly sensitive gated ICCD camera was developed to detect the toxic species like fluorine in cigarettes. The maximum concentration of fluorine present in various brands of cigarettes was 234, 371, 341, and 360 ppm, respectively. The concentration detected with our setup for the toxic fluorine was higher than the safe permissible limits set by the Saudi Royal commission responsible for environmental standards in the Kingdom of Saudi Arabia. In addition, the sensitive lines for other elements like Ba, Na, Ca, Ni, and Cu were detected and identified in the recorded LIBS spectra of tobacco cigarettes. For the quantitative analysis, the calibration curves were drawn to determine the trace concentration of fluorine in cigarettes. The experience gained through this work can be useful for the development of a portable system for on-line analysis of toxic chemicals present in cigarettes, especially during the manufacturing process of cigarettes. The limits of detection of fluoride were also estimated by using standard samples containing the fluoride in known concentrations in the cigarette tobacco and drawing a calibration curve.

A laser-induced breakdown spectrometer was assembled and tested for the analysis of teeth of various groups of patients having a history of chronic periodontitis, including smokers and nonsmokers; this analysis was compared with that of a controlled group of people who did not have a history of chronic periodontitis. The maximum concentration of Pb, Cd, and As detected using our LIBS spectrometer in the smoker group was in the 34–55, 0.33–0.51, and 0.91–1.5 ppm range; for nonsmokers, 23–29, 0.26–0.31, and 0.64–11 ppm range; and for control group, 0.17–0.31, 0.01–0.05, and 0.05–0.09 ppm range. The system was optimized by achieving optically thin plasma by establishing the local thermodynamic equilibrium by measuring the

electron density and electron temperature, good signal-to-noise ratio, and optimum gate parameters of the ICCD camera. For the quantitative analysis, the calibration curves were drawn to determine the concentration of Pb, Cd, and As by preparing the standard samples in a known concentration. In order to validate our LIBS results, teeth samples were also analyzed using the standard ICP-MS method, and our LIBS results are in excellent agreement with the ICP-MS results. In addition, this study has demonstrated that smoking and passive smoking increases the accumulation of toxic elements such as cadmium, lead, and arsenic on the teeth roots. This could indirectly reduce the gingival inflammatory response that is manifested by reduced gingival bleeding. The increased lead levels detected on root surfaces of periodontal disease teeth in smokers could shed some light and explain the increase of attachment loss and periodontal destruction for such patients. Cadmium and arsenic were also found in nonsmoker root surfaces, which may be due to passive smoking and poor dental hygienic conditions.

Future Recommendation

For future study using LIBS, it is recommended to employed doubled pulsed LIBS, this might enhance the signal to background ratio (SBR), limit of detection (LOD) and the spectral intensity of the LIBS signal. It is also recommended that the sample holder should be enclosed in chamber where ambient condition can be varied; this could improve the spectra obtained from the plasma plume, and thereby improving the qualitative and quantitative analysis of test samples. LIBS study could also be extended to study of toxicity level of soil on farm lands and their composition. Other areas where LIBS study could extend are determination of rock and pebbles composition, and in rock type identification through composition analysis.

BIBLIOGRAPHY

[1] A. Lenk, T. Witke, and G. Granse, "Density and electron temperature of laser induced plasma — a comparison of different investigation methods," *Appl. Surf. Sci.*, vol. 96–98, pp. 195–198, Apr. 1996.

[2] "Editorial Board," *Appl. Surf. Sci.*, vol. 96–98, pp. ii–iii, Apr. 1996.

[3] T. Hughes, *Plasmas and laser light*. New York: Wiley, 1975.

[4] W. Kruer, *The physics of laser plasma interactions*. Redwood City Calif.: Addison-Wesley, 1988.

[5] "Physics of Laser Plasma. (=Handbook of Plasma Physics; Vol. 3)., by Rubenchick, A. / Witkowski, S. (Edts.): North-Holland Publishing Company Amsterdam, 9780444874269 Cloth fest gebunden - Antiquariat Thomas Haker GmbH & Co. KG." [Online]. Available: http://www.abebooks.com/Physics-Laser-Plasma-Handbook-Vol-3/7750571685/bd. [Accessed: 03-Oct-2015].

[6] D. W. Hahn and N. Omenetto, "Laser-Induced Breakdown Spectroscopy (LIBS), Part I: Review of Basic Diagnostics and Plasma–Particle Interactions: Still-Challenging Issues Within the Analytical Plasma Community," *Appl. Spectrosc.*, vol. 64, no. 12, p. 335A–366A, Dec. 2010.

[7] D. W. Hahn and N. Omenetto, "Laser-Induced Breakdown Spectroscopy (LIBS), Part II: Review of Instrumental and Methodological Approaches to Material Analysis and Applications to Different Fields," *Appl. Spectrosc.*, vol. 66, no. 4, pp. 347–419, Apr. 2012.

[8] N. L. Lanza, R. C. Wiens, S. M. Clegg, A. M. Ollila, S. D. Humphries, H. E. Newsom, and J. E. Barefield, "Calibrating the ChemCam laser-induced breakdown spectroscopy instrument for carbonate minerals on Mars," *Appl. Opt.*, vol. 49, no. 13, p. C211, Apr. 2010.

[9] A. K. Knight, N. L. Scherbarth, D. A. Cremers, and M. J. Ferris, "Characterization of Laser-Induced Breakdown Spectroscopy (LIBS) for Application to Space Exploration," *Appl. Spectrosc.*, vol. 54, no. 3, pp. 331–340, Mar. 2000.

[10] S. J. Rehse, H. Salimnia, and A. W. Miziolek, "Laser-induced breakdown spectroscopy (LIBS): an overview of recent progress and future potential for biomedical applications.," *J. Med. Eng. Technol.*, vol. 36, no. 2, pp. 77–89, Feb. 2012.

[11] S. H. Wise and J. R. Almirall, "Chemical taggant detection and analysis by laser-induced breakdown spectroscopy.," *Appl. Opt.*, vol. 47, no. 31, pp. G15–20, Nov. 2008.

[12] S. Musazzi, *Springer Series in Optical Sciences 182 Laser-Induced Breakdown Spectroscopy*. .

[13] L. C. Trevizan, D. Santos, R. E. Samad, N. D. Vieira, L. C. Nunes, I. A. Rufini, and F. J. Krug, "Evaluation of laser induced breakdown spectroscopy for the determination of micronutrients in plant materials," *Spectrochim. Acta Part B At. Spectrosc.*, vol. 64, no. 5,

pp. 369–377, May 2009.

[14] S. Carter, A. S. Fisher, M. W. Hinds, S. Lancaster, and J. Marshall, “Atomic spectrometry update. Review of advances in the analysis of metals, chemicals and materials,” *J. Anal. At. Spectrom.*, vol. 28, p. 1814, 2013.

[15] R. Gaudiuso, M. Dell’Aglio, O. De Pascale, G. S. Senesi, and A. De Giacomo, “Laser induced breakdown spectroscopy for elemental analysis in environmental, cultural heritage and space applications: a review of methods and results.,” *Sensors (Basel).*, vol. 10, no. 8, pp. 7434–68, Jan. 2010.

[16] R. Noll, *Laser-Induced Breakdown Spectroscopy: Fundamentals and Applications*. Springer Science & Business Media, 2012.

[17] *Laser-Induced Breakdown Spectroscopy*. .

[18] M. A. Gondal, Y. W. Maganda, M. A. Dastageer, F. F. Al Adel, A. A. Naqvi, and T. F. Qahtan, “Detection of carcinogenic chromium in synthetic hair dyes using laser induced breakdown spectroscopy.,” *Appl. Opt.*, vol. 53, no. 8, pp. 1636–43, Mar. 2014.

[19] S. Beldjilali, D. Borivent, L. Mercadier, E. Mothe, G. Clair, and J. Hermann, “Evaluation of minor element concentrations in potatoes using laser-induced breakdown spectroscopy,” *Spectrochim. Acta - Part B At. Spectrosc.*, vol. 65, no. 8, pp. 727–733, 2010.

[20] F. Mehari, M. Rohde, C. Knipfer, R. Kanawade, F. Klämpfl, W. Adler, F. Stelzle, and M. Schmidt, “Laser induced breakdown spectroscopy for bone and cartilage differentiation - ex vivo study as a prospect for a laser surgery feedback mechanism,” *Biomed. Opt. Express*, vol. 5, no. 11, p. 4013, 2014.

[21] D. Bulajic, M. Corsi, G. Cristoforetti, S. Legnaioli, V. Palleschi, A. Salvetti, and E. Tognoni, “A procedure for correcting self-absorption in calibration free-laser induced breakdown spectroscopy,” *Spectrochim. Acta Part B At. Spectrosc.*, vol. 57, no. 2, pp. 339–353, Feb. 2002.

[22] M. Corsi, G. Cristoforetti, M. Hidalgo, S. Legnaioli, V. Palleschi, A. Salvetti, E. Tognoni, and C. Vallebona, “Double pulse, calibration-free laser-induced breakdown spectroscopy: A new technique for in situ standard-less analysis of polluted soils,” *Appl. Geochemistry*, vol. 21, no. 5, pp. 748–755, May 2006.

[23] H. Griem, *Spectral Line Broadening by Plasmas*. Elsevier Science, 2012.

[24] B. C. Windom and D. W. Hahn, “Laser ablation—laser induced breakdown spectroscopy (LA-LIBS): A means for overcoming matrix effects leading to improved analyte response,” *J. Anal. At. Spectrom.*, vol. 24, no. 12, p. 1665, 2009.

[25] a. E. Hussein, P. K. Diwakar, S. S. Harilal, and a. Hassanein, “The role of laser wavelength on plasma generation and expansion of ablation plumes in air,” *J. Appl. Phys.*, vol. 113, pp. 1–10, 2013.

[26] J. P. Singh, H. Zhang, F.-Y. Yueh, and K. P. Carney, “Investigation of the Effects of Atmospheric Conditions on the Quantification of Metal Hydrides Using Laser-Induced

Breakdown Spectroscopy," *Appl. Spectrosc.*, vol. 50, no. 6, pp. 764–773, Jun. 1996.

[27] M. Autin, A. Briand, P. Mauchien, and J. M. Mermet, "Characterization by emission spectrometry of a laser-produced plasma from a copper target in air at atmospheric pressure," *Spectrochim. Acta Part B At. Spectrosc.*, vol. 48, no. 6–7, pp. 851–862, May 1993.

[28] R. G. Pinnick, P. Chylek, M. Jarzembski, E. Creegan, V. Srivastava, G. Fernandez, J. D. Pendleton, and A. Biswas, "Aerosol-induced laser breakdown thresholds: wavelength dependence.," *Appl. Opt.*, vol. 27, no. 5, pp. 987–96, Mar. 1988.

[29] *Glow Discharge Spectroscopies*. Springer Science & Business Media, 2013.

[30] D. S. Weiss, B. C. Young, and S. Chu, "Precision measurement of ?/m Cs based on photon recoil using laser-cooled atoms and atomic interferometry," *Appl. Phys. B Lasers Opt.*, vol. 59, no. 3, pp. 217–256, Sep. 1994.

[31] Y.-I. Lee, S. P. Sawan, T. L. Thiem, Y.-Y. Teng, and J. Sneddon, "Interaction of a Laser Beam with Metals. Part II: Space-Resolved Studies of Laser-Ablated Plasma Emission," *Appl. Spectrosc.*, vol. 46, no. 3, pp. 436–441, Mar. 1992.

[32] J. G. Jackson, A. Novichikhin, R. W. Fonseca, and J. A. Holcombe, "Mass spectral studies of thermal decomposition of metal nitrates: an introduction to the discussion of two mechanisms," *Spectrochim. Acta Part B At. Spectrosc.*, vol. 50, no. 12, pp. 1423–1426, Oct. 1995.

[33] K. J. Mason and J. M. Goldberg, "Production and initial characterization of a laser-induced plasma in a pulsed magnetic field for atomic spectrometry," *Anal. Chem.*, vol. 59, no. 9, pp. 1250–1255, May 1987.

[34] X. L. Mao, M. A. Shannon, A. J. Fernandez, and R. E. Russo, "Temperature and Emission Spatial Profiles of Laser-Induced Plasmas during Ablation Using Time-Integrated Emission Spectroscopy," *Appl. Spectrosc.*, vol. 49, no. 7, pp. 1054–1062, Jul. 1995.

[35] M. Kuzuya, H. Matsumoto, H. Takechi, and O. Mikami, "Effect of Laser Energy and Atmosphere on the Emission Characteristics of Laser-Induced Plasmas," *Appl. Spectrosc.*, vol. 47, no. 10, pp. 1659–1664, Oct. 1993.

[36] S. Palanco and J. Laserna, "Spectral Analysis of the Acoustic Emission of Laser-Produced Plasmas," *Appl. Opt.*, vol. 42, no. 30, p. 6078, Oct. 2003.

[37] J. Sneddon, T. L. Thiem, and Y.-I. Lee, *Lasers in Analytical Atomic Spectroscopy*. John Wiley & Sons, 1996.

[38] *Laser-Induced Breakdown Spectroscopy*. Elsevier, 2007.

[39] G. Abdellatif and H. Imam, "A study of the laser plasma parameters at different laser wavelengths," *Spectrochim. Acta Part B At. Spectrosc.*, vol. 57, no. 7, pp. 1155–1165, Jul. 2002.

[40] L. M. Cabalín and J. J. Laserna, "Experimental determination of laser induced breakdown thresholds of metals under nanosecond Q-switched laser operation," *Spectrochim. Acta*

Part B At. Spectrosc., vol. 53, no. 5, pp. 723–730, May 1998.

[41] R. E. Russo, X. L. Mao, O. V. Borisov, and H. Liu, "Influence of wavelength on fractionation in laser ablation ICP-MS," *J. Anal. At. Spectrom.*, vol. 15, no. 9, pp. 1115–1120, Jan. 2000.

[42] X. Mao, W.-T. Chan, M. Caetano, M. A. Shannon, and R. E. Russo, "Preferential vaporization and plasma shielding during nano-second laser ablation," *Appl. Surf. Sci.*, vol. 96–98, pp. 126–130, Apr. 1996.

[43] *Solid-State Laser Engineering*, vol. 1. New York, NY: Springer New York, 2006.

[44] M. J. Myers, J. D. Myers, and A. G. Myers, "Lasers Induced Breakdown SPectroscopy (LIBS)," *Lasers in Chemestry*, p. 1554, 2008.

[45] J. S. Huang, H. T. Liu, and K. C. Lin, "Laser-induced breakdown spectroscopy in analysis of Al3+ liquid droplets: On-line preconcentration by use of flow-injection manifold," *Anal. Chim. Acta*, vol. 581, pp. 303–308, 2007.

[46] X. . Mao, A. . Ciocan, O. . Borisov, and R. . Russo, "Laser ablation processes investigated using inductively coupled plasma–atomic emission spectroscopy (ICP–AES)," *Appl. Surf. Sci.*, vol. 127–129, pp. 262–268, May 1998.

[47] F. Anabitarte and A. Cobo, "Laser-Induced Breakdown Spectroscopy : Fundamentals , Applications , and Challenges," vol. 2012, 2012.

[48] A. S. Eppler, D. A. Cremers, D. D. Hickmott, M. J. Ferris, and A. C. Koskelo, "Matrix Effects in the Detection of Pb and Ba in Soils Using Laser-Induced Breakdown Spectroscopy," *Appl. Spectrosc.*, vol. 50, no. 9, pp. 1175–1181, Sep. 1996.

[49] C. Aragon, J. A. Aguilera, and F. Penalba, "Improvements in Quantitative Analysis of Steel Composition by Laser-Induced Breakdown Spectroscopy at Atmospheric Pressure Using an Infrared Nd:YAG Laser," *Appl. Spectrosc.*, vol. 53, no. 10, pp. 1259–1267, Oct. 1999.

[50] R. Wisbrun, I. Schechter, R. Niessner, H. Schroeder, and K. L. Kompa, "Detector for Trace Elemental Analysis of Solid Environmental Samples by Laser Plasma Spectroscopy," *Anal. Chem.*, vol. 66, no. 18, pp. 2964–2975, Sep. 1994.

[51] R. Krasniker, V. Bulatov, and I. Schechter, "Study of matrix effects in laser plasma spectroscopy by shock wave propagation," *Spectrochim. Acta Part B At. Spectrosc.*, vol. 56, no. 6, pp. 609–618, Jun. 2001.

[52] J. A. Bolger, "Semi-quantitative Laser-Induced Breakdown Spectroscopy for Analysis of Mineral Drill Core," *Appl. Spectrosc.*, vol. 54, no. 2, pp. 181–189, Feb. 2000.

[53] R. Noll, H. Bette, A. Brysch, M. Kraushaar, I. Mönch, L. Peter, and V. Sturm, "Laser-induced breakdown spectrometry — applications for production control and quality assurance in the steel industry," *Spectrochim. Acta Part B At. Spectrosc.*, vol. 56, no. 6, pp. 637–649, Jun. 2001.

[54] M. a. Gondal, T. Hussain, Z. H. Yamani, and M. a. Baig, "The role of various binding

materials for trace elemental analysis of powder samples using laser-induced breakdown spectroscopy," *Talanta*, vol. 72, pp. 642–649, 2007.

[55] Ş. YALÇIN, D. R. CROSLEY, G. P. SMITH, and G. W. FARIS, "Spectroscopic Characterization of Laser-Produced Plasmas for In Situ Toxic Metal Monitoring," *Hazard. Waste Hazard. Mater.*, vol. 13, no. 1, pp. 51–61, Jan. 1996.

[56] D. a Cremers and L. J. Radziemski, "Basics of the LIBS plasma," *Handb. Laser-Induced Break. Spectrosc.*, pp. 23–65, 2006.

[57] R. Agrawal, R. Kumar, S. Rai, A. K. Pathak, A. K. Rai, and G. K. Rai, "LIBS: A Quality Control Tool for Food Supplements," *Food Biophys.*, vol. 6, pp. 527–533, 2011.

[58] S. Zhang, X. Wang, M. He, Y. Jiang, B. Zhang, W. Hang, and B. Huang, "Laser-induced plasma temperature," *Spectrochim. Acta - Part B At. Spectrosc.*, vol. 97, pp. 13–33, 2014.

[59] T. Hussain and M. a Gondal, "Laser induced breakdown spectroscopy (LIBS) as a rapid tool for material analysis," *J. Phys. Conf. Ser.*, vol. 439, p. 13, 2013.

[60] P. Stavropoulos, C. Palagas, G. N. Angelopoulos, D. N. Papamantellos, and S. Couris, "Calibration Measurements in laser-induced breakdown spectroscopy using nanosecond and picosecond lasers," *Spectrochim. Acta Part B At. Spectrosc.*, vol. 59, no. 12, pp. 1885–1892, Dec. 2004.

[61] H. Hegazy, H. A. Abd El-Ghany, S. H. Allam, and T. M. El-Sherbini, "Spectral evolution of nano-second laser interaction with Ti target in Air," *Appl. Phys. B*, vol. 110, no. 4, pp. 509–518, Jan. 2013.

[62] J. . Aguilera and C. Aragón, "Multi-element Saha–Boltzmann and Boltzmann plots in laser-induced plasmas," *Spectrochim. Acta Part B At. Spectrosc.*, vol. 62, no. 4, pp. 378–385, Apr. 2007.

[63] D. A. Cremers and L. J. Radziemski, *Handbook of Laser-Induced Breakdown Spectroscopy*. Chichester, UK: John Wiley & Sons, Ltd, 2006.

[64] M. A. Gondal and T. Hussain, "Determination of poisonous metals in wastewater collected from paint manufacturing plant using laser-induced breakdown spectroscopy.," *Talanta*, vol. 71, no. 1, pp. 73–80, Jan. 2007.

[65] S. S. Harilal, C. V Bindhu, and V. P. N. Nampoori, "Tem per atu re in a Laser -Prod u ced Plasm a fr om YBa 2 Cu 3 O 7," vol. 52, no. 3, pp. 449–455, 1998.

[66] K. Y. Yamamoto, D. A. Cremers, M. J. Ferris, and L. E. Foster, "Detection of Metals in the Environment Using a Portable Laser-Induced Breakdown Spectroscopy Instrument," *Appl. Spectrosc.*, vol. 50, no. 2, pp. 222–233, 1996.

[67] F. Colao, R. Fantoni, V. Lazic, a. Morone, a. Santagata, and a. Giardini, "LIBS used as a diagnostic tool during the laser cleaning of ancient marble from Mediterranean areas," *Appl. Phys. A Mater. Sci. Process.*, vol. 79, no. 2, pp. 213–219, Jul. 2004.

[68] V. K. Unnikrishnan, K. Alti, V. B. Kartha, C. Santhosh, G. P. Gupta, and B. M. Suri, "Measurements of plasma temperature and electron density in laser-induced copper

plasma by time-resolved spectroscopy of neutral atom and ion emissions," *Pramana*, vol. 74, no. 6, pp. 983–993, Sep. 2010.

[69] N. Ozbek and S. Akman, "Method Development for t he De termination o f Fluorine in Water Samples via Molecular Absorption of CaF Using A High - Resolution Continuum Source Electrothermal Atomic Absorption Spectrophotometer," vol. 05006, pp. 2–5, 2012.

[70] T. Frömel, S. Münster-müller, and P. T. P. Knepper, "Fluorine analysis using molecular absorption spectroscopy," pp. 1–2, 2014.

[71] O. Samek, D. C. S. Beddows, H. H. Telle, G. W. Morris, M. Liska, and J. Kaiser, "Quantitative analysis of trace metal accumulation in teeth using laser-induced breakdown spectroscopy," vol. 182, pp. 179–182, 1999.

[72] B. Le Drogoff, J. Margot, M. Chaker, M. Sabsabi, O. Barthelemy, T. W. Johnston, S. Laville, F. Vidal, and Y. von Kaenel, "Temporal characterization of femtosecond laser pulses induced plasma for spectrochemical analysis of aluminum alloys," *Spectrochim. Acta Part B-Atomic Spectrosc.*, vol. 56, no. October 2000, pp. 987–1002, 2001.

[73] Y. J. Hong, G. C. Kwon, G. Cho, H. M. Shin, and E. H. Choi, "Measurement of electron temperature and density using stark broadening of the coaxial focused plasma for extreme ultraviolet lithography," *IEEE Trans. Plasma Sci.*, vol. 38, no. 5, pp. 1111–1117, 2010.

[74] C. Colón, A. Alonso-Medina, and C. Herrán-Martínez, "Spectroscopic study of a laser-produced lead plasma: experimental atomic transition probabilities for Pb III lines," *J. Phys. B At. Mol. Opt. Phys.*, vol. 32, no. 15, pp. 3887–3897, Aug. 1999.

[75] G. Bekefi, "Principles of laser plasmas," *New York*, 1976.

[76] M. Baudelet and B. W. Smith, "The first years of laser-induced breakdown spectroscopy," *J. Anal. At. Spectrom.*, vol. 28, p. 624, 2013.

[77] L. J. Radziemski, "From LASER to LIBS, the path of technology development," *Spectrochim. Acta Part B At. Spectrosc.*, vol. 57, no. 7, pp. 1109–1113, Jul. 2002.

[78] R. Fantoni, L. Caneve, F. Colao, L. Fornarini, V. Lazic, and V. Spizzichino, "Methodologies for laboratory Laser Induced Breakdown Spectroscopy semi-quantitative and quantitative analysis—A review," *Spectrochim. Acta Part B At. Spectrosc.*, vol. 63, no. 10, pp. 1097–1108, Oct. 2008.

[79] T. Hussain and M. a. Gondal, "Detection of toxic metals in waste water from dairy products plant using laser induced breakdown spectroscopy," *Bull. Environ. Contam. Toxicol.*, vol. 80, pp. 561–565, 2008.

[80] M. a. Gondal, Y. W. Maganda, M. a. Dastageer, F. F. Al Adel, a. a. Naqvi, and T. F. Qahtan, "Detection of the level of fluoride in the commercially available toothpaste using laser induced breakdown spectroscopy with the marker atomic transition line of neutral fluorine at 731.1 nm," *Opt. Laser Technol.*, vol. 57, pp. 32–38, 2014.

[81] E. Tognoni, V. Palleschi, M. Corsi, and G. Cristoforetti, "Quantitative micro-analysis by laser-induced breakdown spectroscopy: a review of the experimental approaches," *Spectrochim. Acta Part B At. Spectrosc.*, vol. 57, no. 7, pp. 1115–1130, Jul. 2002.

[82] M. Noda, Y. Deguchi, S. Iwasaki, and N. Yoshikawa, “Detection of carbon content in a high-temperature and high-pressure environment using laser-induced breakdown spectroscopy,” *Spectrochim. Acta Part B At. Spectrosc.*, vol. 57, no. 4, pp. 701–709, Apr. 2002.

[83] C. E. McManus, N. J. McMillan, R. S. Harmon, R. C. Whitmore, F. C. De Lucia, Jr., and A. W. Miziolek, “Use of laser induced breakdown spectroscopy in the determination of gem provenance: beryls,” *Appl. Opt.*, vol. 47, no. 31, p. G72, Sep. 2008.

[84] J. Goujon, A. Giakoumaki, V. Piñon, O. Musset, D. Anglos, E. Georgiou, and J. P. Boquillon, “A compact and portable laser-induced breakdown spectroscopy instrument for single and double pulse applications,” *Spectrochim. Acta Part B At. Spectrosc.*, vol. 63, no. 10, pp. 1091–1096, Oct. 2008.

[85] C.-Y. Pan, X.-W. Du, N. An, Z.-Y. Han, S.-B. Wang, W. Wei, and Q.-P. Wang, “[Laser-induced breakdown spectroscopy system for elements analysis in high-temperature and vacuum environment].,” *Guang Pu Xue Yu Guang Pu Fen Xi*, vol. 33, no. 12, pp. 3388–91, Dec. 2013.

[86] J. Gruber, J. Heitz, N. Arnold, D. Bäuerle, N. Ramaseder, W. Meyer, J. Hochörtler, and F. Koch, “In Situ Analysis of Metal Melts in Metallurgic Vacuum Devices by Laser-Induced Breakdown Spectroscopy,” *Appl. Spectrosc.*, vol. 58, no. 4, pp. 457–462, 2004.

[87] J. K. Antony, N. J. Vasa, V. L. N. S. Raja, and A. S. Laxmiprasad, “Laser induced breakdown spectroscopy analysis of lunar simulants under high vacuum conditions,” in *TENCON 2010 - 2010 IEEE Region 10 Conference*, 2010, pp. 449–453.

[88] G. Kim, J. Kwak, K.-R. Kim, H. Lee, K.-W. Kim, H. Yang, and K. Park, “Rapid detection of soils contaminated with heavy metals and oils by laser induced breakdown spectroscopy (LIBS),” *J. Hazard. Mater.*, vol. 263, pp. 754–760, 2013.

[89] M. Yao, L. Huang, J. Zheng, S. Fan, and M. Liu, “Assessment of feasibility in determining of Cr in Gannan Navel Orange treated in controlled conditions by laser induced breakdown spectroscopy,” *Opt. Laser Technol.*, vol. 52, pp. 70–74, 2013.

[90] Q. Godoi, F. O. Leme, L. C. Trevizan, E. R. Pereira Filho, I. a. Rufini, D. Santos, and F. J. Krug, “Laser-induced breakdown spectroscopy and chemometrics for classification of toys relying on toxic elements,” *Spectrochim. Acta - Part B At. Spectrosc.*, vol. 66, pp. 138–143, 2011.

[91] G. S. Senesi, M. Dell’Aglio, R. Gaudiuso, a. De Giacomo, C. Zaccone, O. De Pascale, T. M. Miano, and M. Capitelli, “Heavy metal concentrations in soils as determined by laser-induced breakdown spectroscopy (LIBS), with special emphasis on chromium,” *Environ. Res.*, vol. 109, pp. 413–420, 2009.

[92] V. Juvé, R. Portelli, M. Boueri, M. Baudelet, and J. Yu, “Space-resolved analysis of trace elements in fresh vegetables using ultraviolet nanosecond laser-induced breakdown spectroscopy,” *Spectrochim. Acta - Part B At. Spectrosc.*, vol. 63, no. 10, pp. 1047–1053, 2008.

[93] E. C. Ferreira, E. a. Menezes, W. O. Matos, D. M. B. P. Milori, A. R. a Nogueira, and L.

Martin-Neto, “Determination of Ca in breakfast cereals by laser induced breakdown spectroscopy,” *Food Control*, vol. 21, no. 10, pp. 1327–1330, 2010.

[94] L. Peng, D. Sun, M. Su, J. Han, and C. Dong, “Optics & Laser Technology Rapid analysis on the heavy metal content of spent zinc – manganese batteries by laser-induced breakdown spectroscopy,” *Opt. Laser Technol.*, vol. 44, no. 8, pp. 2469–2475, 2012.

[95] M. a. Gondal, Z. S. Seddigi, M. M. Nasr, and B. Gondal, “Spectroscopic detection of health hazardous contaminants in lipstick using Laser Induced Breakdown Spectroscopy,” *J. Hazard. Mater.*, vol. 175, pp. 726–732, 2010.

[96] H. Horie and K. Kohata, “Analysis of tea components by high-performance liquid chromatography and high-performance capillary electrophoresis,” *J. Chromatogr. A*, vol. 881, pp. 425–438, 2000.

[97] T. Karak and R. M. Bhagat, “Trace elements in tea leaves, made tea and tea infusion: A review,” *Food Res. Int.*, vol. 43, no. 9, pp. 2234–2252, 2010.

[98] R. N. Gallaher, K. Gallaher, a. J. Marshall, and a. C. Marshall, “Mineral analysis of ten types of commercially available tea,” *J. Food Compos. Anal.*, vol. 19, pp. 53–57, 2006.

[99] R. C. Reed, *The Superalloys: Fundamentals and Applications*. .

[100] D. A. Cremers and L. J. Radziemski, *Handbook of Laser-Induced Breakdown Spectroscopy*. .

[101] *Laser-Induced Breakdown Spectroscopy*. Elsevier, 2007.

[102] D. A. Cremers and L. J. Radziemski, *Handbook of Laser-Induced Breakdown Spectroscopy*. John Wiley & Sons, 2013.

[103] W. Demtröder, *Laser Spectroscopy 1: Basic Principles*. Springer, 2014.

[104] D. E. Kim, K. J. Yoo, H. K. Park, K. J. Oh, and D. W. Kim, “Quantitative Analysis of Aluminum Impurities in Zinc Alloy by Laser-Induced Breakdown Spectroscopy,” *Appl. Spectrosc.*, vol. 51, no. 1, pp. 22–29, Jan. 1997.

[105] X. Hou and B. T. Jones, “Inductively Coupled Plasma / Optical Emission Spectrometry,” pp. 9468–9485, 2000.

[106] H. Greenfield, “CHAPTER 3 Inductively Coupled Plasma — Atomic Emission Spectrometry,” 1964.

[107] S. Liao, Y. H. Kao, and R. A. Hiipakka, “Green tea: biochemical and biological basis for health benefits.,” *Vitam. Horm.*, vol. 62, pp. 1–94, Jan. 2001.

[108] A. Absorption, “Analysis of Pb , Cd and As in Tea Leaves Using Graphite Furnace Atomic Absorption Spectrophotometry.”

[109] S. R. Ambadekar, S. Parab, and A. Bachankar, “Determination of Cadmium , Copper , Nickel , Lead in some tea samples in India,” *Int. J. Res. Pharm. Biomed. Sci.*, vol. 3, no. 2, pp. 943–946, 2012.

[110] F.-M. Shen and H.-W. Chen, “Element composition of tea leaves and tea infusions and its

impact on health.," *Bull. Environ. Contam. Toxicol.*, vol. 80, no. 3, pp. 300–4, Mar. 2008.

[111] O. Sadeghi, N. Tavassoli, M. M. Amini, H. Ebrahimzadeh, and N. Daei, "Pyridine-functionalized mesoporous silica as an adsorbent material for the determination of nickel and lead in vegetables grown in close proximity by electrothermal atomic adsorption spectroscopy," *Food Chem.*, vol. 127, no. 1, pp. 364–368, 2011.

[112] R. F. Milani, L. I. Peron, E. S. Saron, M. A. Morgano, and F. F. Silva, "A Validated Method for Direct Analysis : 13 Trace Elements Determination in Tea Infusions using the Agilent 7700x ICP-MS with Integrated Sample Introduction System in Discrete Sampling (ISIS-DS)."

[113] Z. Naeem, I; Mubeen, H; Taskeen, A; and Saddiqe, "Investigations of Heavy metals In Commercial Spices Brands," *New York Sci. J.*, vol. 2, no. 5, pp. 20–26, 2009.

[114] R. Robinson, "Green tea extract may have neuroprotective effects in Parkinson's disease," *Lancet*, vol. 358, no. 9279, p. 391, Aug. 2001.

[115] T. O. Cheng, "Why did green tea not protect against coronary artery disease but protect against myocardial infarction?," *Am. J. Cardiol.*, vol. 91, no. 10, pp. 1290–1291, May 2003.

[116] A. Dabbagh, F. Esmailian, and S. F. Aranki, *Postoperative Critical Care for Cardiac Surgical Patients*, vol. 29. Springer Science & Business Media, 2013.

[117] G. Karimi, M. K. Hasanzadeh, A. Nili, and Z. Khashayarmanesh, "Concentrations and Health Risk of Heavy Metals inTea Samples Marketed in IRAN," vol. 174, pp. 164–174, 2008.

[118] S. Seenivasan, N. Manikandan, N. N. Muraleedharan, and R. Selvasundaram, "Heavy metal content of black teas from south India," *Food Control*, vol. 19, no. 8, pp. 746–749, Aug. 2008.

[119] D. Desideri, M. a. Meli, C. Roselli, and L. Feduzi, "Polarized X ray fluorescence spectrometer (EDPXRF) for the determination of essential and non essential elements in tea," *Microchem. J.*, vol. 98, no. 2, pp. 186–189, 2011.

[120] P. T. Lieu, M. Heiskala, P. A. Peterson, and Y. Yang, "The roles of iron in health and disease," *Mol. Aspects Med.*, vol. 22, no. 1–2, pp. 1–87, Feb. 2001.

[121] H. P. Corporation, "Preconcentration of Copper Using 1 , 5-Diphenyl Carbazide as the Complexing Agent via Dispersive Liquid-Liquid Microextraction and Determination by Flame Atomic Absorption Spectrometry," vol. 2013, 2013.

[122] B. Peng, Y. Shen, Z. Gao, M. Zhou, Y. Ma, and S. Zhao, "Determination of total iron in water and foods by dispersive liquid-liquid microextraction coupled with microvolume UV-vis spectrophotometry," *Food Chem.*, vol. 176, pp. 288–293, 2015.

[123] A. B. B. Torino, M. D. F. P. Gilberti, E. da Costa, G. A. F. de Lima, and H. Z. W. Grotto, "Evaluation of erythrocyte and reticulocyte parameters as indicative of iron deficiency in patients with anemia of chronic disease," *Rev. Bras. Hematol. Hemoter.*, vol. 37, no. 2, pp. 77–81, 2015.

[124] N. N. Al Hassan, “The prevalence of iron deficiency anemia in a Saudi University female students,” *J. Microsc. Ultrastruct.*, vol. 3, no. 1, pp. 25–28, 2015.

[125] K. Schlesier, B. Kühn, M. Kiehntopf, K. Winnefeld, M. Roskos, R. Bitsch, and V. Böhm, “Comparative evaluation of green and black tea consumption on the iron status of omnivorous and vegetarian people,” *Food Res. Int.*, vol. 46, no. 2, pp. 522–527, 2012.

[126] F. J. He and G. A. MacGregor, “Fortnightly review: Beneficial effects of potassium,” *BMJ*, vol. 323, no. 7311, pp. 497–501, Sep. 2001.

[127] C. M. Tanase, P. Griffin, K. G. Koski, M. J. Cooper, and K. a. Cockell, “Sodium and potassium in composite food samples from the Canadian Total Diet Study,” *J. Food Compos. Anal.*, vol. 24, no. 2, pp. 237–243, 2011.

[128] F. H. Nielsen, “Ultratrace elements in nutrition: Current knowledge and speculation,” *J. Trace Elem. Exp. Med.*, vol. 11, no. 2–3, pp. 251–274, 1998.

[129] M. Låg, E. J. Søderlund, J. G. Omichinski, G. Brunborg, J. A. Holme, J. E. Dahl, S. D. Nelson, and E. Dybing, “Effect of bromine and chlorine positioning in the induction of renal and testicular toxicity by halogenated propanes.,” *Chem. Res. Toxicol.*, vol. 4, no. 5, pp. 528–34, Jan. .

[130] M. Korolczuk, “Voltammetric Determination of Cr(VI) in Natural Water in the Presence of Bipyridine Following Its Deposition to the Metallic State,” *Electroanalysis*, vol. 11, no. 16, pp. 1218–1221, Nov. 1999.

[131] A. Manova, S. Humenikova, M. Strelec, and E. Beinrohr, “Determination of chromium(VI) and total chromium in water by in-electrode coulometric titration in a porous glassy carbon electrode,” *Microchim. Acta*, vol. 159, no. 1–2, pp. 41–47, Apr. 2007.

[132] A. CARLOSENA, M. GALLEGO, and M. VALC�RCEL, “Evaluation of Various Sample Preparation Procedures for the Determination of Chromium, Cobalt and Nickel in Vegetables,” *J. Anal. At. Spectrom.*, vol. 12, no. 4, pp. 479–486, Jan. 1997.

[133] M. Y. Thor, L. Harnack, D. King, B. Jasthi, and J. Pettit, “Evaluation of the comprehensiveness and reliability of the chromium composition of foods in the literature,” *J. Food Compos. Anal.*, vol. 24, no. 8, pp. 1147–1152, 2011.

[134] A. Bobrowski, A. Królicka, and J. Zarębski, “Characteristics of Voltammetric Determination and Speciation of Chromium - A Review,” *Electroanalysis*, vol. 21, no. 13, pp. 1449–1458, Jul. 2009.

[135] R. Gaudiuso, M. Dell’Aglio, O. de Pascale, G. S. Senesi, and A. de Giacomo, “Laser induced breakdown spectroscopy for elemental analysis in environmental, cultural heritage and space applications: A review of methods and results,” *Sensors*, vol. 10, pp. 7434–7468, 2010.

[136] M. A. Gondal, Y. W. Maganda, M. A. Dastageer, F. F. Al Adel, A. A. Naqvi, and T. F. Qahtan, “Detection of carcinogenic chromium in synthetic hair dyes using laser induced breakdown spectroscopy.,” *Appl. Opt.*, vol. 53, no. 8, pp. 1636–43, Mar. 2014.

[137] Y.-I. Lee, S. P. Sawan, T. L. Thiem, Y.-Y. Teng, and J. Sneddon, "Interaction of a Laser Beam with Metals. Part II: Space-Resolved Studies of Laser-Ablated Plasma Emission," *Appl. Spectrosc.*, vol. 46, no. 3, pp. 436–441, 1992.

[138] Y.-I. Lee, K. Song, H.-K. Cha, J.-M. Lee, M.-C. Park, G.-H. Lee, and J. Sneddon, "Influence of Atmosphere and Irradiation Wavelength on Copper Plasma Emission Induced by Excimer and Q-switched Nd:YAG Laser Ablation," *Appl. Spectrosc.*, vol. 51, no. 7, pp. 959–964, 1997.

[139] G. Cristoforetti, G. Lorenzetti, S. Legnaioli, and V. Palleschi, "Investigation on the role of air in the dynamical evolution and thermodynamic state of a laser-induced aluminium plasma by spatial- and time-resolved spectroscopy," *Spectrochim. Acta Part B At. Spectrosc.*, vol. 65, no. 9–10, pp. 787–796, Sep. 2010.

[140] S. S. Harilal, B. O'Shay, M. S. Tillack, and M. V. Mathew, "Spectroscopic characterization of laser-induced tin plasma," *J. Appl. Phys.*, vol. 98, pp. 1–7, 2005.

[141] J. B. Simeonsson and A. W. Miziolek, "Time-resolved emission studies of ArF-laser-produced microplasmas.," *Appl. Opt.*, vol. 32, no. 6, pp. 939–47, Feb. 1993.

[142] J. B. Simeonsson and A. W. Miziolek, "Spectroscopic studies of laser-produced plasmas formed in CO and CO2 using 193, 266, 355, 532 and 1064 nm laser radiation," *Appl. Phys. B Laser Opt.*, vol. 59, no. 1, pp. 1–9, Jul. 1994.

[143] G. Cristoforetti, A. De Giacomo, M. Dell'Aglio, S. Legnaioli, E. Tognoni, V. Palleschi, and N. Omenetto, "Local Thermodynamic Equilibrium in Laser-Induced Breakdown Spectroscopy: Beyond the McWhirter criterion," *Spectrochim. Acta Part B At. Spectrosc.*, vol. 65, no. 1, pp. 86–95, Jan. 2010.

[144] R. E. Russo, X. Mao, and S. S. Mao, "Peer Reviewed: The Physics of Laser Ablation in Microchemical Analysis," *Anal. Chem.*, vol. 74, no. 3, p. 70 A–77 A, Feb. 2002.

[145] B. C. Castle, K. Visser, B. W. Smith, and J. D. Winefordner, "Level populations in a laser-induced plasma on a lead target," *Spectrochim. Acta Part B At. Spectrosc.*, vol. 52, no. 13, pp. 1995–2009, Nov. 1997.

[146] X. Zeng, S. S. Mao, C. Liu, X. Mao, R. Greif, and R. E. Russo, "Plasma diagnostics during laser ablation in a cavity," *Spectrochim. Acta - Part B At. Spectrosc.*, vol. 58, pp. 867–877, 2003.

[147] W. Ashraf and A. a. Mian, "Levels of selected heavy metals in black tea varieties consumed in Saudi Arabia," *Bull. Environ. Contam. Toxicol.*, vol. 81, pp. 101–104, 2008.

[148] B. Ismail, J. Henry, I. Haffar, and R. Baalbaki, "Date consumption and dietary significance in the United Arab Emirates," *J. Sci. Food Agric.*, vol. 86, no. 8, pp. 1196–1201, Jun. 2006.

[149] I. A. Ahmed, A. W. K. Ahmed, and R. K. Robinson, "Chemical composition of date varieties as influenced by the stage of ripening," vol. 54, pp. 305–309, 1995.

[150] R. M. Myhara, J. Karkalas, and M. S. Taylor, "The composition of maturing Omani dates," *J. Sci. Food Agric.*, vol. 79, no. 11, pp. 1345–1350, Aug. 1999.

[151] M. Elleuch, S. Besbes, O. Roiseux, C. Blecker, C. Deroanne, N.-E. Drira, and H. Attia, "Date flesh: Chemical composition and characteristics of the dietary fibre," *Food Chem.*, vol. 111, no. 3, pp. 676–682, Dec. 2008.

[152] M. A. Al-Farsi and C. Y. Lee, "Nutritional and functional properties of dates: a review.," *Crit. Rev. Food Sci. Nutr.*, vol. 48, no. 10, pp. 877–87, Nov. 2008.

[153] A. Y. Ali-Mohamed and A. S. H. Khamis, "Mineral ion content of the seeds of six cultivars of Bahraini date palm (Phoenix dactylifera).," *J. Agric. Food Chem.*, vol. 52, no. 21, pp. 6522–5, Oct. 2004.

[154] P. Di Mascio, M. Murphy, and H. Sies, "Antioxidant defense systems: the role of carotenoids, tocopherols, and thiols," *Am J Clin Nutr*, vol. 53, no. 1, p. 194S–200, Jan. 1991.

[155] A. Tapas, D. Sakarkar, and R. Kakde, "Flavonoids as Nutraceuticals: A Review," *Trop. J. Pharm. Res.*, vol. 7, no. 3, pp. 1089–1099, Sep. 2008.

[156] M. B. Petrovich, V. R. A. Filho, and J. A. G. Neto, "Direct determination of calcium in milk by atomic absorption spectrometry using flow-injection analysis," *Eclética Química*, vol. 32, no. 3, pp. 25–30, 2007.

[157] A. Rosanoff, "The high heart health value of drinking-water magnesium.," *Med. Hypotheses*, vol. 81, no. 6, pp. 1063–5, Dec. 2013.

[158] S. Chen, S. Zhu, Y. He, and D. Lu, "Speciation of chromium and its distribution in tea leaves and tea infusion using titanium dioxide nanotubes packed microcolumn coupled with inductively coupled plasma mass spectrometry.," *Food Chem.*, vol. 150, pp. 254–9, May 2014.

[159] M. Galiová, J. Kaiser, K. Novotný, J. Novotný, T. Vaculovič, M. Liška, R. Malina, K. Stejskal, V. Adam, and R. Kizek, "Investigation of heavy-metal accumulation in selected plant samples using laser induced breakdown spectroscopy and laser ablation inductively coupled plasma mass spectrometry," *Appl. Phys. A*, vol. 93, no. 4, pp. 917–922, 2008.

[160] P. Dhar, I. Gembitsky, P. K. Rai, N. K. Rai, A. K. Rai, and G. Watal, "A Possible Connection Between Antidiabetic & Antilipemic Properties of Psoralea corylifolia Seeds and the Trace Elements Present: A LIBS Based Study," *Food Biophys.*, vol. 8, no. 2, pp. 95–103, 2012.

[161] M. Yao, M. Liu, L. Huang, and J. Zhao, "Rapid Detection of Heavy Metal Contents in Fruits by Laser Induced Breakdown Spectroscopy," vol. 7, pp. 98–101, 2009.

[162] T. A. Perfetti and A. Rodgman, "The Complexity of Tobacco and Tobacco Smoke *," vol. 24, no. 5, 2011.

[163] A. L. H. Müller, C. C. Müller, F. G. Antes, J. S. Barin, V. L. Dressler, E. M. M. Flores, and E. I. Müller, "Determination of Bromide, Chloride, and Fluoride in Cigarette Tobacco by Ion Chromatography after Microwave-Induced Combustion," *Anal. Lett.*, vol. 45, no. 9, pp. 1004–1015, Jun. 2012.

[164] A. R. Al-shammery, E. E. Guile, and M. El Backly, "Original Articles T HE P

REVALENCE OF D ENTAL F LUOROSIS IN S AUDI A RABIA ‡," vol. 9, no. 2, pp. 11–14, 1997.

[165] A. A. Zahvoronkov and L. S. Strochkova, "Fluorosis: Geographical pathology and some experimental findings," *Fluoride - Quarterly Reports*, vol. 14, no. 4. pp. 182–191, 1981.

[166] R. D. Kaul and A. K. Susheela, "Evidence of muscle fiber degeneration in rabbits treated with sodium fluoride," *Fluoride - Quarterly Reports*, vol. 7, no. 4. pp. 177–181, 1974.

[167] N. J. Chinoy and E. Sequeira, "Reversible fluoride induced fertility impairment in male mice," *Fluoride - Q. Reports*, vol. 25, no. 2, pp. 71–76, 1992.

[168] J. Marinus, G. L. Moseley, F. Birklein, R. Baron, C. Maihöfner, W. S. Kingery, and J. J. van Hilten, "Clinical features and pathophysiology of complex regional pain syndrome," *Lancet Neurol.*, vol. 10, no. 7, pp. 637–648, 2011.

[169] H. Services, "TOXICOLOGICAL PROFILE FOR FLUORIDES , HYDROGEN FLUORIDE , AND FLUORINE," no. September, 2003.

[170] T. Attin, A. M. Lennon, M. Yakin, K. Becker, W. Buchalla, R. Attin, and A. Wiegand, "Deposition of fluoride on enamel surfaces released from varnishes is limited to vicinity of fluoridation site.," *Clin. Oral Investig.*, vol. 11, no. 1, pp. 83–8, Mar. 2007.

[171] Q. Wang, A. Makishima, and E. Nakamura, "Determination of Fluorine and Chlorine by Pyrohydrolysis and Ion Chromatography: Comparison with Alkaline Fusion Digestion and Ion Chromatography," *Geostand. Geoanalytical Res.*, vol. 34, no. 2, pp. 175–183, Sep. 2010.

[172] P. Blatn and F. Kvasni, "Determination of fluoride in feed mixtures by capillary isotachophoresis," vol. 670, pp. 223–228, 1994.

[173] N. Ozbek and S. Akman, "Method development for the determination of fluorine in toothpaste via molecular absorption of aluminum mono fluoride using a high-resolution continuum source nitrous oxide/acetylene flame atomic absorption spectrophotometer.," *Talanta*, vol. 94, pp. 246–50, May 2012.

[174] H. Gleisner, B. Welz, and J. W. Einax, "Optimization of fluorine determination via the molecular absorption of gallium mono-fluoride in a graphite furnace using a high-resolution continuum source spectrometer," *Spectrochim. Acta - Part B At. Spectrosc.*, vol. 65, no. 9–10, pp. 864–869, 2010.

[175] H. Gleisner, J. W. Einax, S. Morés, B. Welz, and E. Carasek, "A fast and accurate method for the determination of total and soluble fluorine in toothpaste using high-resolution graphite furnace molecular absorption spectrometry and its comparison with established techniques," *J. Pharm. Biomed. Anal.*, vol. 54, no. 5, pp. 1040–1046, 2011.

[176] N. US Department of Commerce, "NIST Physical Reference Data."

[177] A. L. Osterheld, "Principles of Plasma Spectroscopy," *Nucl. Fusion*, vol. 38, no. 8, pp. 1255–1255, Aug. 1998.

[178] N. (Institute of P. Konjević, a. (Observatoire D. P.-M. Lesage, J. R. (National I. of S. and

T. Fuhr, and W. L. (National I. of S. and T. Wiese, “Experimental Stark Widths and Shifts for Spectral Lines of Neutral and Ionized Atoms,” *J. Phys. Chem. Ref. Data*, vol. 31, no. 3, pp. 819–927, 2002.

[179] M. A. Gondal, Y. W. Maganda, M. A. Dastageer, F. F. Al-Adel, A. A. Naqvi, and T. F. Qahtan, “Development of a laser induced breakdown sensor for detection of carcinogenic chemicals in cosmetic products,” in *2013 High Capacity Optical Networks and Emerging/Enabling Technologies*, 2013, pp. 84–87.

[180] Meenakshi and R. C. Maheshwari, “Fluoride in drinking water and its removal,” *J. Hazard. Mater.*, vol. 137, no. February, pp. 456–463, 2006.

[181] S. S. Harilal, C. V. Bindhu, R. C. Issac, V. P. N. Nampoori, and C. P. G. Vallabhan, “Electron density and temperature measurements in a laser produced carbon plasma,” *J. Appl. Phys.*, vol. 82, no. 5, p. 2140, Sep. 1997.

[182] M. A. Gondal, Y. W. Maganda, M. A. Dastageer, F. F. Al Adel, A. A. Naqvi, and T. F. Qahtan, “Detection of the level of fluoride in the commercially available toothpaste using laser induced breakdown spectroscopy with the marker atomic transition line of neutral fluorine at 731.1nm,” *Opt. Laser Technol.*, vol. 57, pp. 32–38, Apr. 2014.

[183] R. J. Genco, “Host responses in periodontal diseases: current concepts.,” *J. Periodontol.*, vol. 63, no. 4 Suppl, pp. 338–55, Apr. 1992.

[184] R. F. Gerlach, J. A. Cury, F. J. Krug, and S. R. P. Line, “Effect of lead on dental enamel formation.,” *Toxicology*, vol. 175, no. 1–3, pp. 27–34, Jun. 2002.

[185] R. F. Gerlach, A. P. de Souza, J. A. Cury, and S. R. Line, “Effect of lead, cadmium and zinc on the activity of enamel matrix proteinases in vitro.,” *Eur. J. Oral Sci.*, vol. 108, no. 4, pp. 327–34, Aug. 2000.

[186] S. G. GROSSI, J. ZAMBON, E. E. MACHTEI, R. SCHIFFERLE, S. ANDREANA, R. J. GENCO, D. CUMMINS, and G. HARRAP, “EFFECTS OF SMOKING AND SMOKING CESSATION ON HEALING AFTER MECHANICAL PERIODONTAL THERAPY,” *J. Am. Dent. Assoc.*, vol. 128, no. 5, pp. 599–607, May 1997.

[187] P. A. Bhusari and R. Chopra, “A morphological survey of root grooves and their influence on periodontal attachment loss.,” *Saudi Dent. J.*, vol. 23, no. 2, pp. 91–7, Apr. 2011.

[188] C. Babür, G. Ozcan, D. U. Cebi, B. Pervane, B. Ozdemir, A. Yücel, A. A. Biri, and C. Babür, “Gingival crevicular fluid levels of osteoprotegerin (OPG) in premenopausal and postmenopausal women with or without chronic periodontitis.,” *J. Dent.*, vol. 40, no. 5, pp. 364–71, May 2012.

[189] N. Waszkiewicz, S. Chojnowska, A. Zalewska, K. Zwierz, A. Szulc, and S. D. Szajda, “Salivary hexosaminidase in smoking alcoholics with bad periodontal and dental states.,” *Drug Alcohol Depend.*, vol. 129, no. 1–2, pp. 33–40, Apr. 2013.

[190] L. Kardeşler, N. Buduneli, B. Biyikoğlu, S. Cetinkalp, and N. Kütükçüler, “Gingival crevicular fluid PGE2, IL-1beta, t-PA, PAI-2 levels in type 2 diabetes and relationship with periodontal disease.,” *Clin. Biochem.*, vol. 41, no. 10–11, pp. 863–8, Jul. 2008.

[191] C. Rutsatz, S. G. Baumhardt, C. A. Feldens, C. K. Rösing, R. Grazziotin-Soares, and F. B. Barletta, "Response of pulp sensibility test is strongly influenced by periodontal attachment loss and gingival recession.," *J. Endod.*, vol. 38, no. 5, pp. 580–3, May 2012.

[192] E. Guzeldemir, H. U. Toygar, C. Boga, and U. Cilasun, "Dental and periodontal health status of subjects with sickle cell disease," *J. Dent. Sci.*, vol. 6, no. 4, pp. 227–234, Dec. 2011.

[193] H. LOE and J. SILNESS, "PERIODONTAL DISEASE IN PREGNANCY. I. PREVALENCE AND SEVERITY.," *Acta Odontol. Scand.*, vol. 21, pp. 533–51, Dec. 1963.

[194] S. G. Grossi, J. Zambon, E. E. Machtei, R. Schifferle, S. Andreana, R. J. Genco, D. Cummins, and G. Harrap, "Effects of smoking and smoking cessation on healing after mechanical periodontal therapy.," *J. Am. Dent. Assoc.*, vol. 128, no. 5, pp. 599–607, May 1997.

[195] S. S. Hakki, G. Berk, N. Dundar, M. Saglam, and N. Berk, "Effects of root planing procedures with hand instrument or erbium, chromium:yttrium-scandium-gallium-garnet laser irradiation on the root surfaces: a comparative scanning electron microscopy study.," *Lasers Med. Sci.*, vol. 25, no. 3, pp. 345–53, May 2010.

[196] D. A. Scott, R. M. Palmer, and J. A. Stapleton, "Validation of smoking status in clinical research into inflammatory periodontal disease.," *J. Clin. Periodontol.*, vol. 28, no. 8, pp. 715–22, Aug. 2001.

[197] A. Akpinar, H. Toker, H. Ozdemir, V. Bostanci, and H. Aydin, "The effects of non-surgical periodontal therapy on oxidant and anti-oxidant status in smokers with chronic periodontitis.," *Arch. Oral Biol.*, vol. 58, no. 6, pp. 717–23, Jun. 2013.

[198] S. Thorat Manojkumar, A. R. Pradeep, G. Garg, and A. Raju, "Gingival crevicular fluid levels of oncostatin M in periodontal conditions.," *Cytokine*, vol. 50, no. 3, pp. 248–52, Jun. 2010.

[199] G. Colombo, I. Dalle-Donne, M. Orioli, D. Giustarini, R. Rossi, M. Clerici, L. Regazzoni, G. Aldini, A. Milzani, D. A. Butterfield, and N. Gagliano, "Oxidative damage in human gingival fibroblasts exposed to cigarette smoke.," *Free Radic. Biol. Med.*, vol. 52, no. 9, pp. 1584–96, May 2012.

[200] J. E. Sansonetti, "Wavelengths, Transition Probabilities, and Energy Levels for the Spectra of Sodium (Na I–Na XI)," *J. Phys. Chem. Ref. Data*, vol. 37, no. 4, p. 1659, Dec. 2008.

[201] P. Parvin, S. Z. Shoursheini, F. Khalilinejad, A. Bavali, M. Moshgel Gosha, and B. Mansouri, "Simultaneous fluorescence and breakdown spectroscopy of fresh and aging transformer oil immersed in paper using ArF excimer laser," *Opt. Lasers Eng.*, vol. 50, no. 11, pp. 1672–1676, Nov. 2012.

[202] S. Z. Mortazavi, P. Parvin, A. Reyhani, A. N. Golikand, and S. Mirershadi, "Effect of Laser Wavelength at IR (1064 nm) and UV (193 nm) on the Structural Formation of Palladium Nanoparticles in Deionized Water," *J. Phys. Chem. C*, vol. 115, no. 12, pp.

5049–5057, Mar. 2011.

[203] S. Z. Shoursheini, P. Parvin, B. Sajad, and M. A. Bassam, "Dual-Laser-Beam-Induced Breakdown Spectroscopy of Copper Using Simultaneous Continuous Wave CO_2 and Q-Switched Nd:YAG Lasers," *Appl. Spectrosc.*, vol. 63, no. 4, pp. 423–429, Apr. 2009.

[204] P. Parvin, F. Hadavand Mirzaee, M. Keraji, A. Bavali, and H. Mehravaran, "Laser Induced Fluorescence and Breakdown Spectroscopy and Acoustic Response, to Discriminate Malignant and Normal Tissues," *Opt. Photonics Soc. Iran*, vol. 20, no. 6, pp. 1009–1012, Feb. 2014.

[205] J. Silness and H. Löe, "Periodontal Disease in Pregnancy II. Correlation Between Oral Hygiene and Periodontal Condition," *Acta Odontol. Scand.*, vol. 22, no. 1, pp. 121–135, Jan. 1964.

[206] S. P. Ramfjord, "Indices for Prevalence and Incidence of Periodontal Disease," *J. Periodontol.*, vol. 30, no. 1, pp. 51–59, Jan. 1959.

Vitae

Name :Habibullah Yusuf Babanagairi

Nationality :Nigerian

Date of Birth :15/05/1987

Email :habyeb@yahoo.com

Address :King Fahd University of petroleum and minerals, 31261 Dhahran Saudi Arabia

Academic Background :From August/2013 to May/2016

Masters of Science in Physics, King Fahd University of petroleum and minerals, Dhahran Saudi Arabia.

: From December/2006 to October/2011

Bachelor of Technology in physics, Federal University of Technology Minna, Niger State, Nigeria.

Publication

1. M. A. Gondal, **Yusuf. B. Habibullah,** L. E 0loore, M. A. Iqbal**,** Determination of carcinogenic Fluorine in cigarettes using pulsed UV laser induced breakdown spectroscopy. **Applied Optics Journal, 54, 5560-5567 (2015).**
2. M. A. Gondal, M. A. Dastageer, F.F. Al-Adel, A.A. Naqvi, **Y. B. Habibullah**, Detection of highly toxic elements (Lead and Chromium) in Commercially available eyeliner (Kohl) Using Laser Induced Break down Spectroscopy, **Optics and Laser technology, 75, 99-104 (2015).**
3. Abdul M. Alhasmi1, Mohammed A. Gondal, Mohamed M. Nasr, Sami Shafik, **Yusuf B. Habibullah,** Detection of toxic elements using Laser Induced Breakdown Spectroscopy in smoker and nonsmoker's teeth and investigation of periodontal parameters, **Applied Optics Journal Vol. 54, No. 24 / August 20 2015. (2015).**
4. A. O. Mehder , M. A. Gondal, M. A. Dastageer , M. A. Iqbal , **Y. B. Habibullah**, L. E. Oloore, Direct spectral analysis and determination of high content of carcinogenic bromine in bread using UV pulsed laser induced breakdown spectroscopy. **Accepted in Journal of environmental science and health: Part B (2015).**
5. M. A. Gondal, **Y. B. Habibullah**, Umair Baig, L. E. Oloore , Direct Spectral Analysis of Tea Samples using 266 nm UV pulsed Laser-induced Breakdown Spectroscopy and Cross Validation of LIBS Results with ICP-MS. **Talanta 152 341–352 (2016).**
6. A.O. Mehder, Mohammed A. Gondal, **Yusuf B. Habibullah**, Umair Baig, and Luqman E. Oloore, "Spectro-chemical analysis of date palm fruits using UV-pulsed LIBS". **Submitted to Talanta (Under review).**